EXPERIMENTAL INVESTIGATION INTO

MICROSTRUCTURES OF AIRCRAFT GRADE

BALSA SHEAR WEBS

By

Taylor Michelle Matlock

Bachelor of Science in Aerospace Engineering

Bachelor of Science in Mechanical Engineering

Oklahoma State University

Stillwater, Oklahoma

2020

Submitted to the Faculty of the
Graduate College of the
Oklahoma State University
in partial fulfillment of
the requirements for
the Degree of
MASTER OF SCIENCE
May 2023

EXPERIMENTAL INVESTIGATION INTO

MICROSTRUCTURES OF AIRCRAFT GRADE

BALSA SHEAR WEBS

Thesis Approved

Dr. Andy Arena
_____
Thesis Adviser

Dr. Joseph Conner
_____

Dr. Aurelie Azoug
_____

ACKNOWLEDGEMENTS

First, I must thank my advisor Dr. Andy Arena. I also must thank Randy Ho, my best friend for helping to keep me motivated throughout the years. Next, I must give a final thanks to my amazing husband, Braden. He has been a constant supporter, listener, and editor when I need him. Since starting on the journey of graduate school he has always been on my side, even when it can cause life to be hard at home. I cannot express how much his support means to me; I love you Braden.

Name: Taylor Michelle Matlock

Date of Degree: MAY 2023

Title of Study: EXPERIMENTAL INVESTIGATION INTO MICROSTRUCTURE OF

AIRCRAFT GRADE BALSA SHEAR WEBS

Major Field: MECHANICAL AND AEROSPACE ENGINEERING

Abstract: Unmanned aerial vehicles (UAVs) typically rely on balsa wood as the primary material for their aircraft structure. While previous research at Oklahoma State University had established basic material properties of aircraft grade balsa wood, it has also yielded some counterintuitive findings. Specifically, thicker, higher density balsa wood was observed to have a lower force to failure than the thinner, less dense balsa wood. Furthermore, it was hypothesized that this was due to an increase in microstructural defects as thickness increased [1]. This prompted an extensive investigation into balsa wood failure characteristics, with a particular focus on the possible correlation between microstructural defects and the unexpected failure of thicker, more dense balsa wood. To test this hypothesis, four experiments were conducted. The first two experiments involved tensile tests with the force applied perpendicular to the grain direction. The first experiment resulted in trends like the previously mentioned research. However, the second experiments, conducted with balsa wood sourced from a distributor with more rigorous selection standards, showed that ultimate tensile strength increased proportionally to density and remains within the bounds of found uncertainty until reaching the "heavy" density classification (greater than $14\frac{lb}{ft^3}$). The third experiment focused on tensile testing with the force applied parallel to the grain direction to obtain data for different plane directions, but this test set was inconclusive due to the load cell of the testing apparatus having a maximum loading of 1000N. Finally, visual experimentation was performed. This revealed that increasing the density of balsa wood correlates to an increase in the number and size of ray cells which contributes to the increase in the modulus of elasticity and misalignment of fibers of the cell. This was ultimately determined to be the cause of the ultimate failure at higher density for thicker balsa wood. In conclusion, heavy and extra heavy density of balsa wood were found to be unsuitable for use aircraft shear webs. Additionally, the groundwork for visual inspection of balsa wood was laid through these experiments.

Table of Contents

List of Tables

List of Figures

x

CHAPTER I

INTRODUCTION

With unmanned aerial vehicles (UAVs) becoming increasingly integral in today's world, so is the manufacturing of those vehicles. Most UAVs are composed of composite materials, such as fiberglass, epoxy resin, and balsa wood. Epoxy and fiberglass or other fibrous material typically make up the skin of the airframe while balsa wood makes up structural components such as ribs, bulkheads, shears webs, spars, and the core of the skin. Some of these components can be seen in Figure 1. Research on these composite materials has increased in recent years but the amount of data present pales in comparison to other more well-known homogeneous materials such as aluminum and steel. With Dr. Andy Arenas, Graduate Student Design lab (GSD), and his capstone projects, SpeedFest and Design Built Fly (DBF) actively working with composite aircraft for over 25 years, there is a great interest in the properties of the materials that go into designing and creating a composite aircraft. Before, there was little research focused on balsa wood. However, the GSD lab recently investigated the material properties of balsa wood with the release of a thesis by Zachary Watkins, "MODELING AND FAILURE ANALYSIS OF COMPOSITE I-BEAMS FOR UAV WING SPAR DESIGN" [1].

1
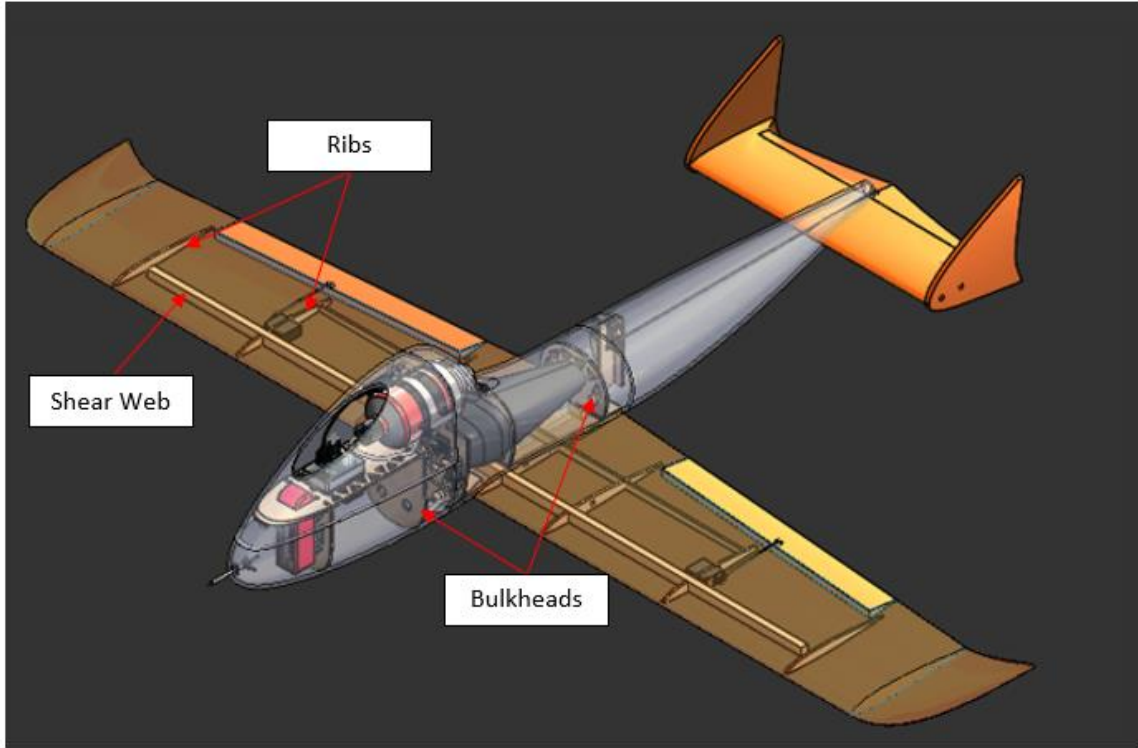
Figure 1: Structural Call Out of Black Teams SpeedFest Plane, 2020
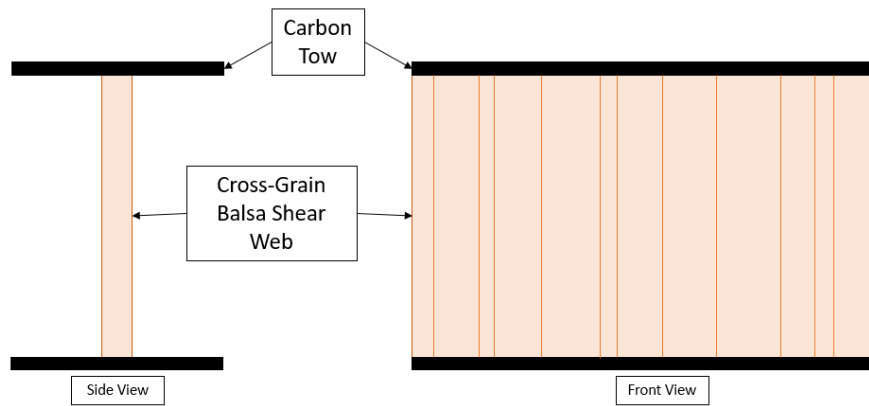
Figure 2: Side and Front View of Cross-Grain Balsa with Carbon Tow Cap

UAV spars are commonly I-beam's made from composite materials, with the carbon spar cap taking the bending load and the cross-grain balsa taking the shear loading of the wing. This

specific design can be seen in Figure 2. While previous research laid the groundwork for further investigation into balsa wood it was primarily used to develop an analysis tool for shear webs of different geometries and explained failure analysis of balsa shear web spar designs.

While this is helpful in an overall view, the question was raised whether the thicker balsa wood that would be used in larger-scale aircraft would be able to perform the same as thinner balsa shear webs. This is due to the findings of thicker shear webs being weaker in comparison to thinner balsa shear webs. It is speculated that thicker balsa has a higher probability of failure than its thin counterpart due to the larger frequency and size of fibers, and vessels [1].

With balsa wood itself considered a composite material having inherent inhomogeneous properties, in the aerospace field it is commonly laminated between fiberglass or reinforced to add extra rigidity to the material–creating a sandwiched composite material. With past methods of trial and error when referencing composite materials, specifically balsa spars, there is less implementation of engineering tactics and more testing till failure. While this can be manageable with small-scale aircraft that take minimal time to build, once outside of the group 1 range of UAVs, with a max gross takeoff weight of 0-20lb, it becomes more strenuous on the design and manhours to rely on only this method. The thesis mentioned above created a spar analysis program that helped with this, but there were interesting trends with the balsa material properties that were theorized to occur due to defects on the cellular level. There is a desire to understand more about the structure-property relationships of balsa wood to help better design the structural makeup of UAVs.

With the research that went into creating the analysis tool that was previously developed by the GSD lab, showing inconsistent results for the balsa wood, there began another potential explanation for the findings. That greater care is taken upon inspection of thinner lighter balsa sheets due to the more common use in aerospace fields, this is what has been deemed 'unintentional quality control'. This is otherwise defined as an inherent bias that occurs. The material properties

3

of balsa were investigated, and an analysis tool was created and validated and found that the "balsa wood is highly dependent on thickness, where thicker balsa wood samples have a higher probability for defects and failure" [1].

Due to these findings, there is an apparent desire to understand why these counterintuitive properties are exhibited. Since it was hypothesized that defects increased as the thickness of balsa increased, the need for investigation of the microstructure of balsa wood as well as the visual defects in the microstructure arose. This information could be beneficial to correlating failures to the microstructure of the material in hopes to start accurately predicting future failure. If it is found true that the thicker selections of balsa wood have a larger abundance of defects, the selection process of structural members will change to reflect the findings. Overall, giving the option to quality check materials more accurately and to further optimize the thickness of the balsa shear web. This would allow for greater safety measures in future shear webs that are to be designed and built in the GSD lab.

The research shown in this thesis will help better understand and justify the previous findings as mentioned above. The work done by Dr. Andy Arena and I will help to further our understanding of the microstructure of balsa wood, gain a better idea of the best size of balsa sheets to use for shear web applications, and how to inspect for defects. This will allow for "QC", quality check, sheets that are in inventory and to predict sheets that will have a lower force required for failure. Once the research has been found valid, the optimum thickness, density, and potential layering of shear webs can be found.

Goals & Objectives

Goals:

1. Investigate the microstructure of balsa shear webs in composite wing spars and how it may affect failure.

2. Determine if predicting failure through visual inspection of balsa sheets is possible.

Objectives:

1. Conduct an extensive literature review of balsa material properties, the microstructure of balsa wood and how it relates to the strength properties, previous failure findings on balsa, and how to visually inspect balsa.

2. Investigate the phenomenon of lesser force to failure in thicker higher density sheets of balsa wood.

3. Develop a test bench to better examine the microstructure of balsa wood.

4. Find a method to predict and find failure due to the microstructure of balsa wood.

5. Manufacture test samples of varying thicknesses and predict failure.

6. Conduct tensile experiments.

7. Compare data to previous research and theoretical data.

CHAPTER II

REVIEW OF LITERATURE

Before starting experimentation, it is important to investigate past failure analyses of balsa wood and to overview the current material properties that are known. This overall information is the foundation needed before progressing into testing the mesostructure/microstructure of balsa wood. Therefore, the first section of this chapter will cover an overview of balsa wood to lay the groundwork for what is to come. Next, there will be an investigation into the meso/microstructure of balsa wood. Balsa has had some research into its material properties in the past, although not every grain direction is accurately portrayed. So, the next section will be looking into what material properties are known and their overall strength characteristics. Finally, an investigation of any previous research done on visual inspection techniques and/or quality control will be done.

Overview of Balsa Wood

Balsa wood, *Ochroma Pyramidal*, is a desired material in the aircraft world due to its high strength-to-weight ratio. Other common uses for balsa wood are boats, rafts, musical instruments, and composite sandwiches [2]. Balsa wood is softer than other woods even though it is classified as a hardwood, so it is easy to work with no matter what project is at hand. It is also very adaptable depending on the grain direction and cut that is being used. Traditionally, in the GSD lab, there are only two-grain direction types referenced, and those are with-the-grain or against-the-grain.

This only takes into consideration the visible grains pattern. Looking further at grain direction, it can be seen that it can be classified into three sections: A, B, and C grain directions [3].
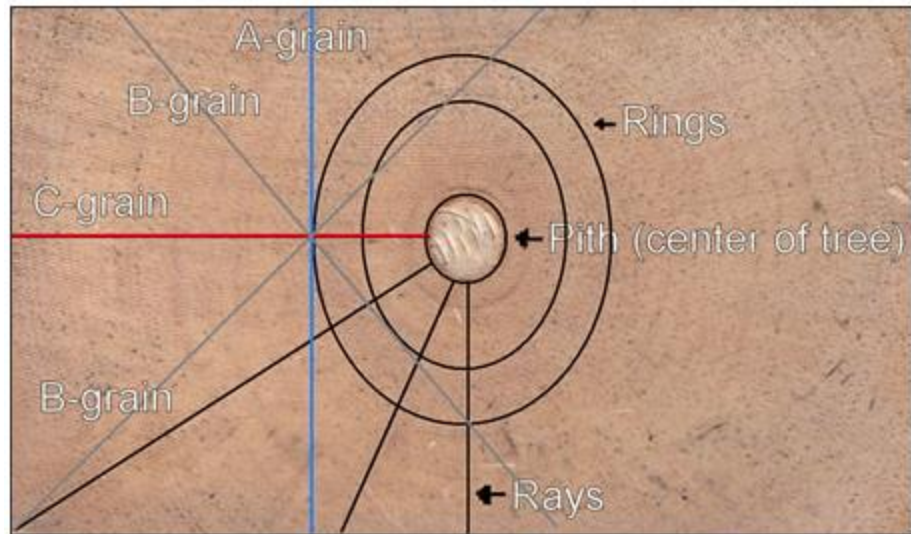
Figure 3: Grain Direction Cut Shown in Trunk [3]

Figure 4: Grain Direction Shown on Broadside of Sheet [3]

Above in Figure 3 it can be seen where in the trunk each type of grain is cut, as well as what each grain type looks like from the broad side of the sheet, Figure 4. Each grain type is useful for different projects. A grain is the most flexible grain type due to the cut being along the fibers or a tangent cut to the growth rings, this is a good cut for forming balsa core to fuselage curves or

forming other curved shapes. B grain is a mixture between both A and C grain directions, it retains

some of the flexibility of the fibers from the A grain but also utilizes rays to stiffen up the sheets

similarly to C grain. B grain is a good cut for flat sides or shear webs. C grain is the stiffest grain

direction, and it will not conform easily to curvatures like the previous 2-grain directions and is

more likely to fracture when handling. C grain maintains this stiffness due to the grains being

sandwiched between rays which allows one side to be in tension while the other is in compression.

Therefore, C grain is a good option for wing ribs and trailing edges [3], [4].

While grain direction is important in deciding where to use different balsa sheets it is not

the only deciding factor. Another major factor in deciding what type of balsa is required is density.

Balsa wood can vary greatly in density, and this is mainly attributed to the age of the wood when

collected [5]. The density of balsa wood is between $4\frac{lb}{ft^3}. - 24\frac{lb}{ft^3}$, with the most common densities

between 8 - $16\frac{lb}{ft^3}$. [4]. Below a table breaking down balsa density and its classification can be

seen. Moving forward, when discussing the density of balsa, the classifications shown in Table 1

will be used. As the grain direction of balsa wood comes with preferred uses so does density.

Lower-density balsa is most useful for forming a core for skins, leading edges, and potentially wing

ribs, it is recommended to use higher-density balsa for large spars or bulkheads [4].

Table 1: Balsa Density and Classification

Density (lb-cu. ft)	Classification
less than 6	Extra Light / Contest Grade
6-10	Light
10-14	Medium
14-19	Heavy
greater than 19	Extra Heavy

When comparing the aspect of balsa specimens of varying density there are some major visual differences between the extremes, extra light, and extra heavy. Looking at Figure 5, it can be noted that the heavier the balsa the darker the wood becomes, and the vessels can be seen darkening as well from an almost yellow to an amber color. Looking further at the balsa samples another visual difference can be seen, as previously stated vessels increase as density increases, but in Figure 6 that fact can be seen. The progression of densities can be seen through just this fact alone, where the extra light density has lighter colored and fewer vessels, and as the density increases to medium and to extra heavy the vessels become increasingly dark and more prevalent.

Figure 5: Visual Comparison of Densities

Figure 6: Visual Comparison of Densities, Side View

Balsa Wood Meso/Micro/Nano Structure

As seen in the previous section both the grain direction and the density of balsa wood are important to consult when deciding what type of wood to use in different applications. To further the research into balsa wood, this section will investigate balsa wood meso, micro, and nanostructure.

With that it is important to understand each direction and what components make up and strengthen each direction.
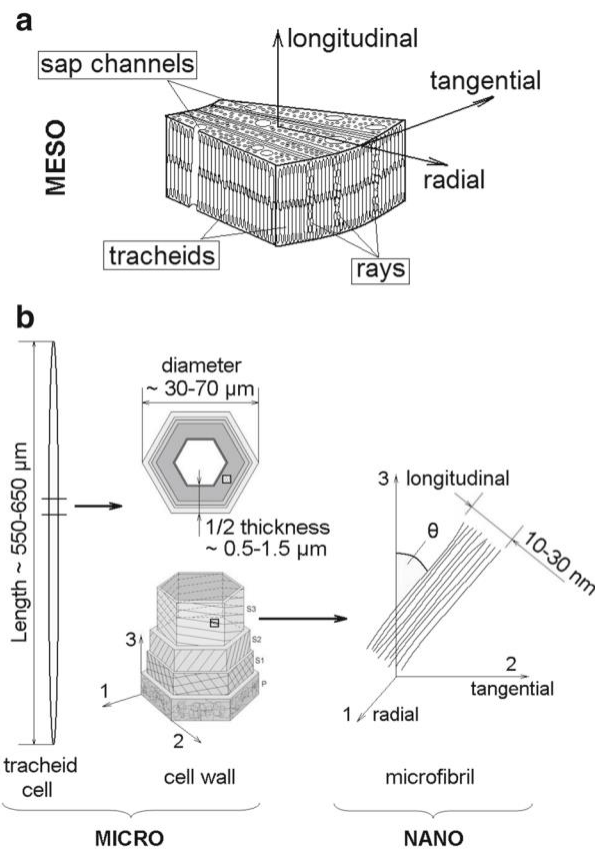
Figure 7: Meso, Micro, and Nano Structure of Balsa Wood [5]

Breaking down balsa wood structure into 3 scales, meso, micro, and nano. Above you can see in Figure 7 the breakdown of these levels of structure. [5] The GSD lab is limited to a microscope that can zoom 100X therefore, it is not possible to visually investigate micro and nanostructures firsthand. It is hoped that the previous research found into the microstructure and nanostructure of balsa wood will supply the knowledge needed.

The overarching substructure is the mesostructure, this is when visually looking at balsa wood the three types of cells can be identified. These cells are rays, fiber, and vessels, all of which reinforce the wood. In some papers, fibers are labeled as tracheids, and vessels are labeled as sap channels. For clarity in this paper the terms rays, fibers, and vessels will be used when discussing the different cell types.
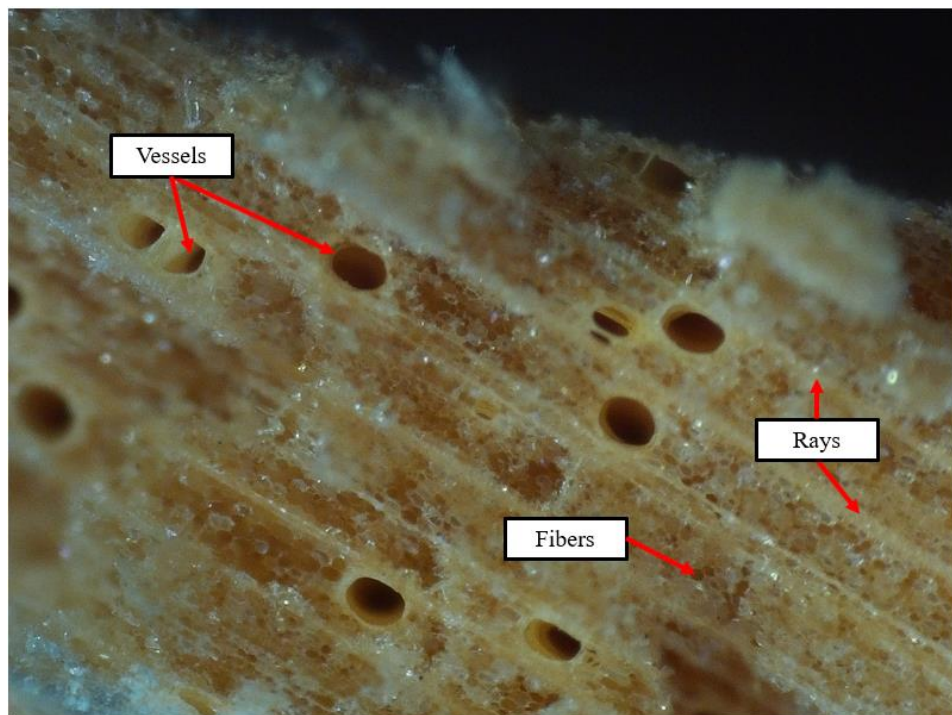
Figure 8: Vessels, Fibers, and Rays Labeled on Balsa Wood Cross Section
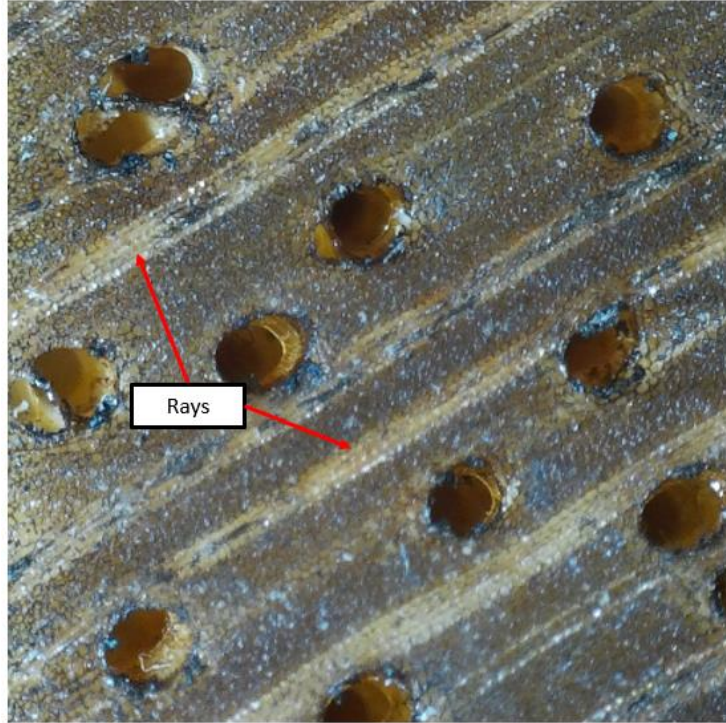
Figure 9: Closer View of Rays
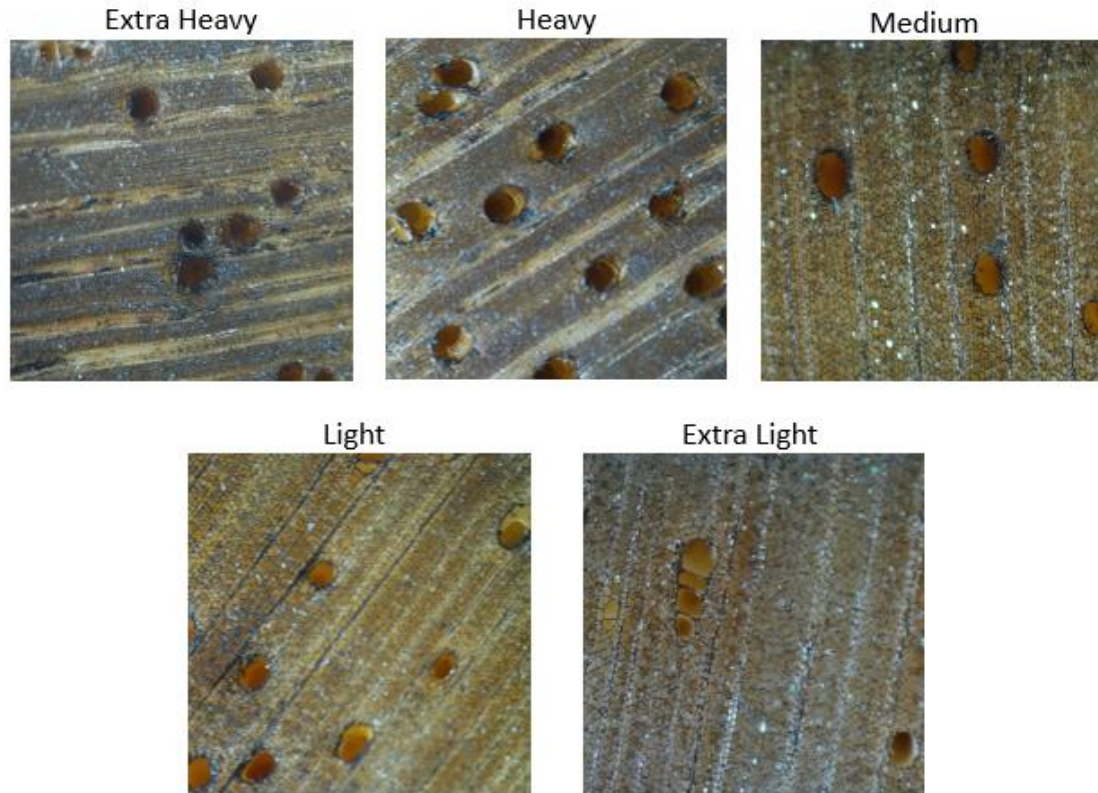
Figure 10: Zoomed-in View of Balsa Cross Section at Multiple Densities

Looking closer at Figure 10, the 3 cell types are labeled on a cross-section of balsa wood. Firstly, looking at vessels they appear like large voids in the cross-sectional area of the wood, fibers run longitudinally through the wood, and rays align radially. Next in Figure 9 a closer view of the rays can be seen; they are rectangular cells that run in a line together breaking up the fibers. When investigating further it is seen that fibers are the main makeup of the structure at around 66-76% [6]. But as fiber volume decreases, the amount will increase as there is an increase in density. This is because "high-density latewood fibers are smaller and have a thicker cell wall than low-density early wood fibers" [6] Rays, which account for 20-25%, act as reinforcements when loaded in the radial direction in light-density balsa and appear to be slightly larger in the heavy-density balsa [6]. Rays have a large influence on the radial tensile strength of wood. Rays are the driving factor of

the misalignment of fibers- mostly in the axial-tangential plan, this is due to rays penetrating the wood structure where the fibers are [7], a visual of this can be seen in Figure 9. Vessels, which are the smallest group and only account for 3-9% of the cellular structure, are what transport water through the cell, interestingly there are more in the higher density which is thought to help transport more water required [8]. This can be seen in Figure 10, where the higher density balsa has larger vessels appearing, additionally the rays become more noticeable in the heavier density balsa wood due to a greater contrast in the wood.

Table 2: Breakdown of Vessels, Rays, and Fibers [6]

	LD balsa	MD balsa	HD balsa
Air-dry density (kg/m^3)	64	163	274
Vessels			
D (μm)	220.4 ± 31.0 (14)	320.8 ± 31.1 (23)	258.8 ± 38.6 (39)
d (μm)	156.6 ± 21.5 (14)	251.0 ± 18.5 (23)	206.6 ± 24.0 (39)
L (μm)	n.d.	382.1 ± 121.1 (19)	n.d.
t (μm)	n.d.	4.0 ± 1.1 (99)	n.d.
T (μm)	n.d.	9.5 ± 1.5 (70)	n.d.
Volume fraction (%)	2.8 ± 0.5 (4)	6.6 ± 1.1 (4)	8.8 ± 2.1 (8)
Solid fraction (%)	6.8	4.5	5.5
Rays			
a (μm)	49.6 ± 8.4 (23)	35.8 ± 6.1 (34)	32.5 ± 3.5 (34)
b (μm)	19.4 ± 3.3 (23)	18.2 ± 3.1 (34)	15.8 ± 1.7 (34)
L (μm)	n.d.	30.7 ± 6.0 (60)	n.d.
t (μm)	n.d.	0.9 ± 0.3 (97)	n.d.
Volume fraction (%)	20.9 ± 2.1 (4)	19.9 ± 0.8 (3)	24.8 ± 1.9 (7)
Solid fraction (%)	6.5	7.4	8.3
Fibers			
h (μm)	21.8 ± 4.5 (57)	18.0 ± 4.8 (105)	9.8 ± 3.0 (270)
t (μm)	0.8 ± 0.2 (50)	1.8 ± 0.5 (125)	2.2 ± 0.8 (250)
L (μm)	n.d.	755.3 ± 122.2 (38)	n.d.
θ (°)	n.d.	6.1 ± 2.0 (30)	n.d.
Volume fraction (%)	76.3	73.5	66.4
Solid fraction (%)	4.3	10.8	21.5

The next substructure is the microstructure, this is where with a microscope the primary wall (P), secondary wall (S), and tertiary wall (T) or also known as secondary wall 3 can be seen.

This is shown in a closer image in Figure 11. The secondary wall, being the largest, further breaks down into S1, S2, and S3.
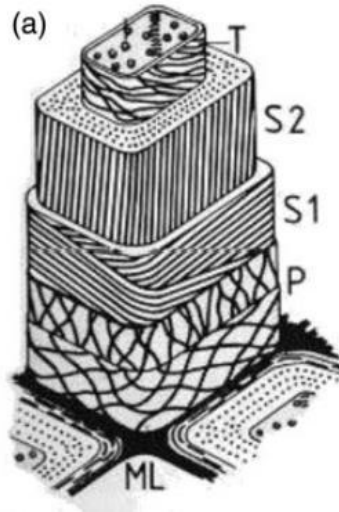
Figure 11: Balsa Wood Cell Wall [9]

Below in Table 3 the properties of, cell types, shapes, and sizes, as well as cell wall layers and typical MFA, can be seen [5]. The S wall is responsible for the mechanical properties of the cell. With the S2 layer being the largest and where most research has been investigated. It is also known that in higher-density balsa the S2 layer is about 73% of the secondary layer compared to when it is lower density the S2 is around 30%, or about the same as the other 2 sections in the second layer [8]. The S2 layer impacts the stiffness and the S1 and S3 are impacted in the transverse direction [6].

Table 3: Cell Properties List [5]

Cell type	Fraction of the total porosity (%)	Shape of the cross section	Length (μm)	Diameter (μm)	Aspect ratio
Tracheids	80–90 [3]	Hexagonal	550–650 [3]	30–70 [2]	16–25 [2,46]
Rays	8–15 [3]	Rectangular	76 [4]	13 [4]	6 Calculated based on data from [4]
Sap channels	The rest of the volume	Circular	–	150–250 [3]	–

Cell wall layer	Thickness (μm) [20]	MFA (°) [6,20]
P (several layers)	0.1	Random
S1	0.1–0.35	60–80
S2	1–10	0–30
S3	0.5–1.1	60–90

And the last sub-structure shown is the nanostructure, which will be mentioned in this section briefly. This is an even more zoomed-in view of the cells, mainly focusing on microfibrils. This substructure will be mostly discussed regarding the MFA (mean microfibril angle) and could be classified as a part of the micro substructure. The MFA of the S1 and S3 layers have microfibrils
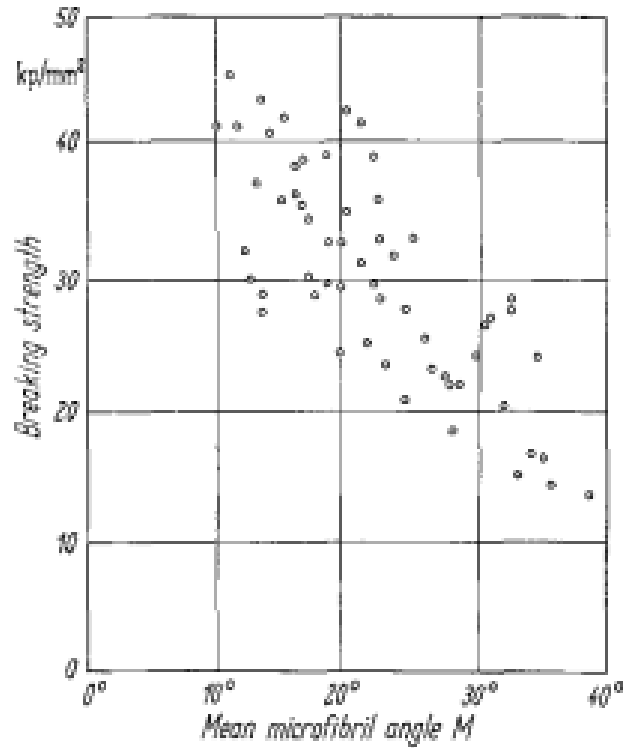
that are 90°, while in S2 there is a variance of 10-30° or aligned with the longitudinal axis [8]. A higher MFA correlates to a lower modulus, and balsa having a lower MFA in the S2 layer is a large factor in the stiffness of the wood [10]. An investigation into *Pinus Radiata*, Pinewood, attempted to find a relationship between MFA and breaking strength. Overall, it was found that after an MFA of around 25°, the breaking strength decreases significantly. Looking at Figure 12, the trend is linear. While this information is useful it is important to note that *Pinus Radiata* is a softwood and may not behave exactly like balsa wood.

Figure 12: MFA Vs. Breaking Strength [10]

With this section, it is seen that the structure of balsa wood also plays a significant role in the overall strength of the wood, along with the grain direction and density of balsa. With that knowledge, the strength characteristics of balsa can be better understood.

Strength Characteristics

Balsa is an anisotropic material, more specifically an orthotropic material. Because of this, its properties will vary depending on the axial direction [11]. Stress, $\sigma = F/A$ will translate into stresses in each plane direction, longitudinal, radial, and tangential respectively, σ_L, σ_R, and σ_T. With the force being in the direction normal to the face of the axis plane, this can be seen in Figure 13. While discussing the results of the balsa wood it is good to note the plane and axes direction of specific strength properties that will be tested. For example, if using a B-grain and tensile testing, and the force is perpendicular to the grain direction, the tensile stress will be in the radial direction or, σ_R and if forces are parallel to the grain direction, it would be in reference to the longitude plane, σ_L.
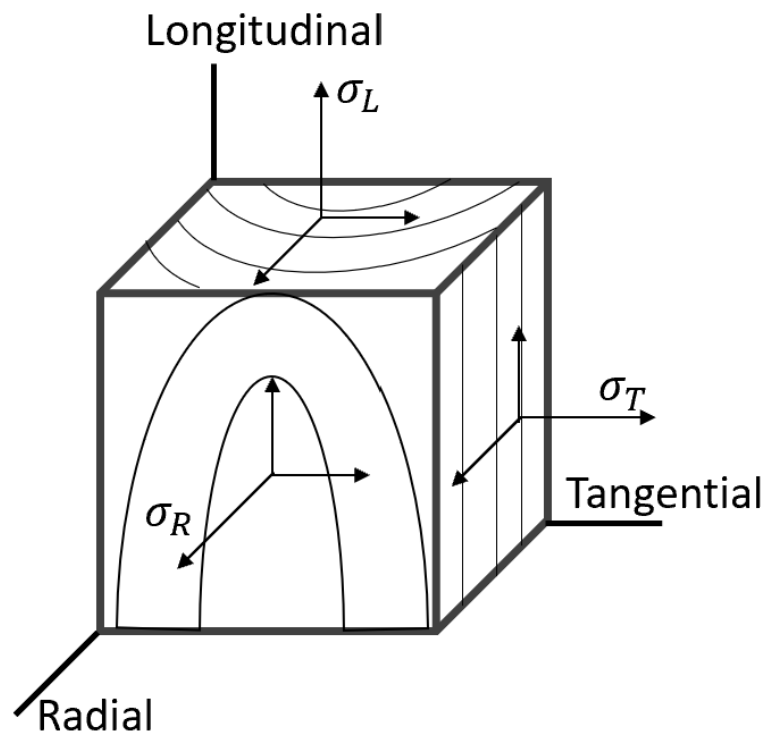
Figure 13: Stress Tensor

It is known that the strength properties parallel to the grain are higher than the properties perpendicular to the grain due to the primary bonds of the cell wall being in the same direction as the grain. [12]. To better understand the following information, it is important to have a grasp on where these axes lie on the wood itself. Below in Figure 14, it can be seen visually where each axial plane is in reference to the trunk of the wood. The longitudinal axis, sometimes referenced as the axial direction, is in the direction of growth for the tree trunk, the radial axis runs through the center of the tree but perpendicular to the longitudinal axis, and finally, the tangential axis is tangent to the growth rings [13]
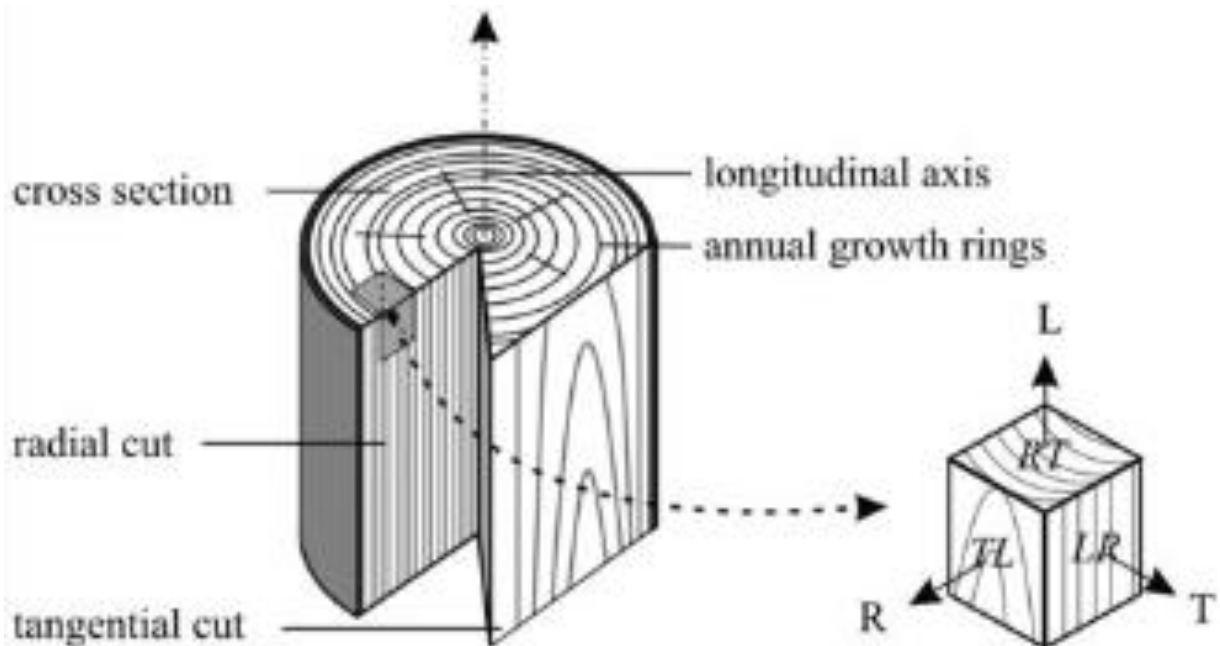
Figure 14: Tree Trunk Cut, and Axes Labeled [13]

First, an overall view of balsa was investigated. From Figure 15, it can be seen that in total balsa wood is not as widely investigated in compression, shear, or tension in comparison to other species of wood [12]. Therefore, a more focused approach in researching the properties of balsa

wood arose. This is to investigate the possibility of a correlation between the failure of balsa wood

to density, as well as the direction of the wood's axes.

Mechanical properties for five wood species at 12% moisture content.[a]

	Bending		Compression		Shear	Tension		
Species	Modulus of rupture (MPa)	Modulus of elasticity (GPa)	Parallel to grain (MPa)	Perpendicular to grain (MPa)	Parallel to grain (MPa)	Parallel to grain (MPa)	Perpendicular to grain (MPa)	Side hardness (kN)[a]
Loblolly pine	88.0	12.3	49.2	5.4	9.6	88.0	3.2	3.1
Sitka spruce	70.0	10.8	38.7	4.0	7.9	75.8	2.6	2.4
Red oak	99.0	12.5	46.6	7.0	12.3	101.4	5.5	5.7
Yellow poplar	70.0	10.9	38.2	3.4	8.2	154.4	3.7	2.4
Balsa	21.6	3.4	14.9	—	2.1	—	—	—

a Force at 5.6 mm indention.

Figure 15: Overview of Multiple Species of Wood Strength Properties [12]

Another journal article related the 3 orthogonal axes to load response and then found the

modulus of each axis [14]. Below the young modulus of each axis, the axial, radial, and tangential,

in relation to density can be seen in Figure 16. From the image, each axes modulus can be related

linearly to the density.
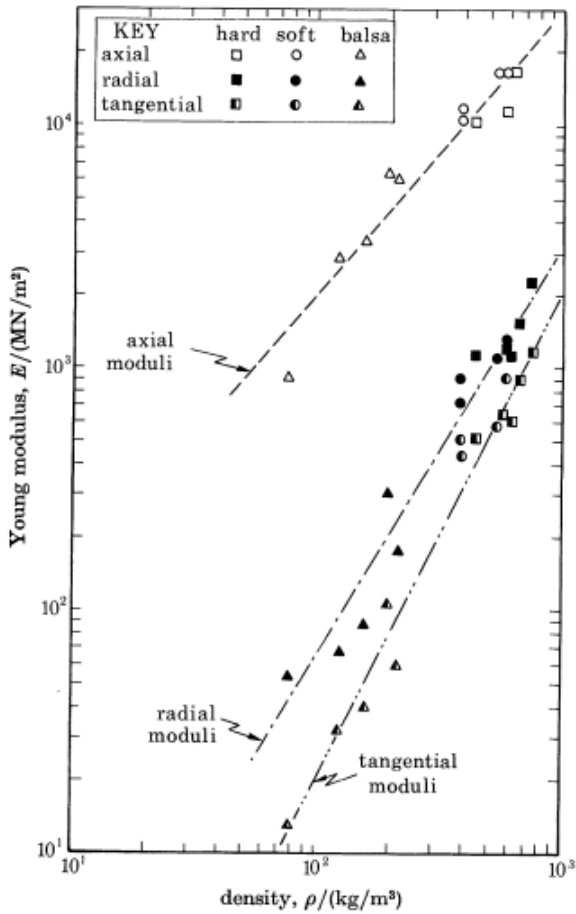
Figure 16: Density vs Young Modulus [14]

An investigation into the strength characteristics of balsa in relation to the density and direction of axes was discovered. This investigated compression, bending, torsion, and elastic modulus in both the axial and radial directions [8]. A linear trend was found in the axial direction for the compressive strength as well as Young's modulus. But the results found showed more scatter as density increased and at the higher density side, it showed around 9 GPa for Young's modulus and 43MPa compressive strength. The radial direction did not have a linear trend line, but it still correlated with density and Young's modulus, and the compressive strength of 72-81%

23

respectively. It was found that for Youngs' modulus values of 0.5 GPa were noted and 3.8MPa for compressive strength. Noticing the significant lower values in the radial direction, but it is common to see the lower values when testing outside of the axial direction due to the material being orthogonal. [8]. In Figure 17 the graphs for both axial and radial results of young's modulus and compressive strengths can be seen.
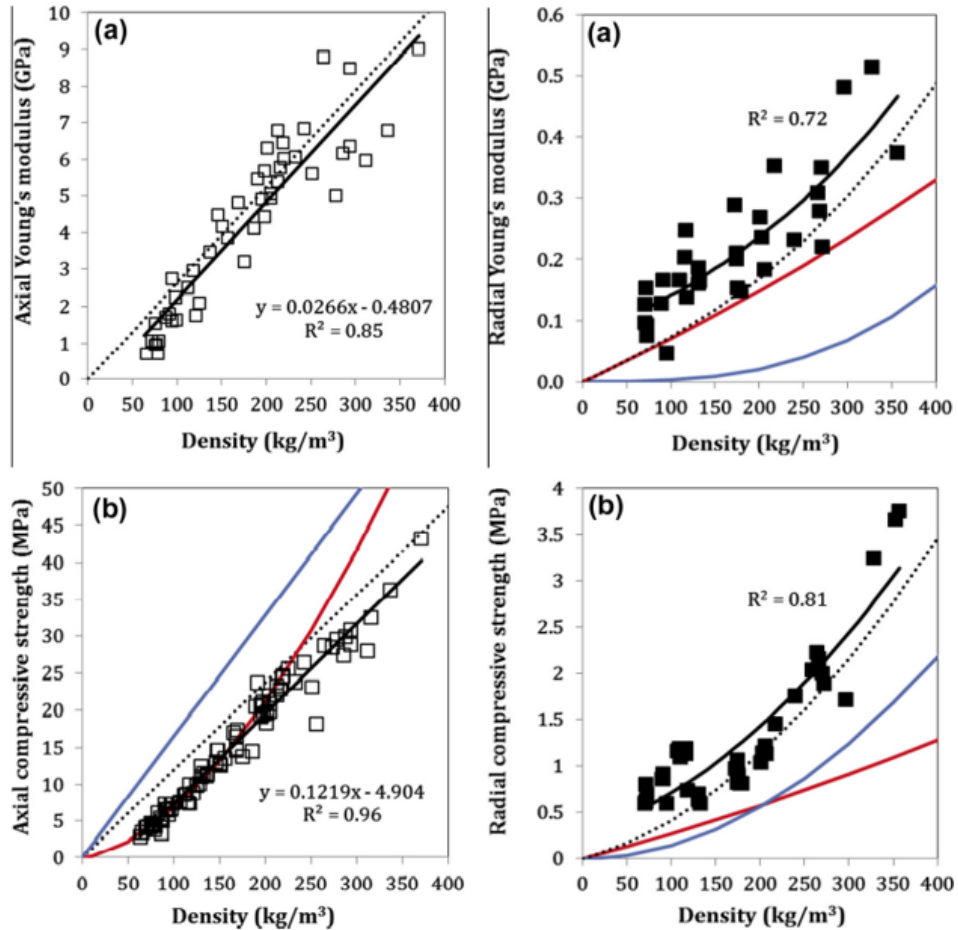
Figure 17: Axial and Radial comparison of Young's Modulus and Compressive Strength. [8].

Looking at the axial direction further and focusing on compressive testing, it was again found that the compressive strength increased as density increased. Also noting that when looking

24

at lower density samples tended to fail by buckling vs kink band formation for the higher density samples. All the samples were loaded in the axial direction and found that in their experiment the average misalignment in the LT (longitudinal – tangential) plane was around 7°. It was found at the highest density the compressive strength was to be around 45MPa [7]. Continuing with compressive testing, on all axes, another source was found. Similarly, to the previous findings the failure was started by kinking that was mainly in the AT (axial-tangential) plane or the radial axis.
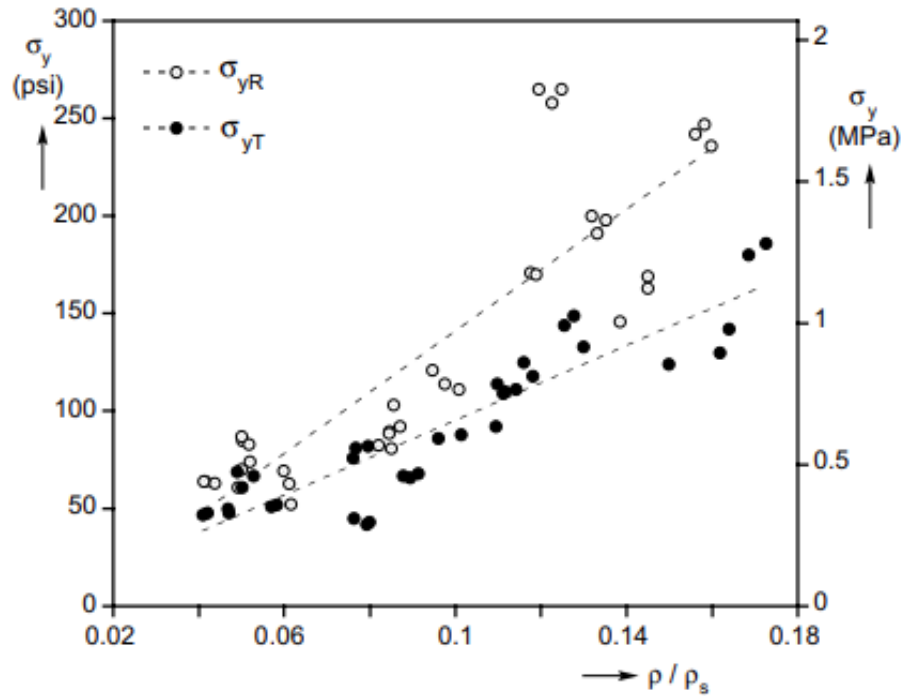
Figure 18: Radial and tangential yield stress [15]

It was explained that the kinking in AT has to do with a higher value of fibers that are misaligned. The measured misalignment was on average 6°. Also, it was noted that lower density failed in folding of a combination of stresses while higher density was kinking. [15] In Figure 18 a graph can be seen showing the compressive yield stresses for both the radial and tangential axis in relation to density. In Figure 19, the shear moduli and shear strength of the AR and AT planes can be seen

25

in relation to the density of the balsa wood Most notable is that the tangential plane is lower in compressive stress, as well as in the shear modulus and shear strength. Also, a larger spread or scatter of values is noted as density increases, this is most apparent in reference to the compressive strength of the tangential plane. [15]
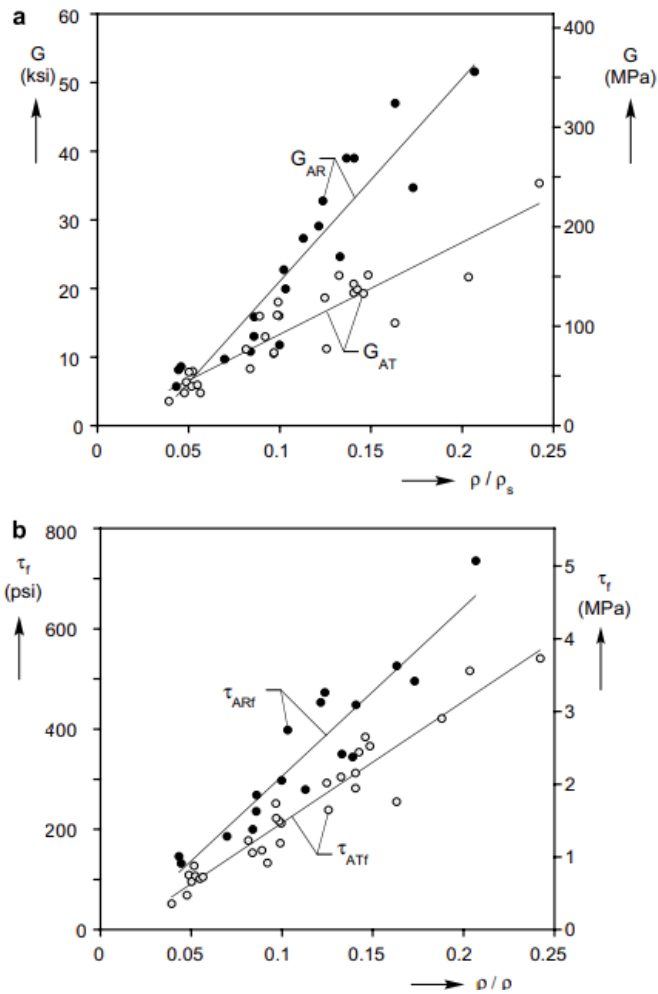
Figure 19: Shear moduli and shear strength for AR and AT planes [15]

Finally, looking into properties that were found from the GSD lab, will show results for tensile and shear tests. It is noted that there is a large difference in both the ultimate shear and

26

tensile strength for the thickness of balsa wood. As previously mentioned, it was found that as density increases and thickness changes from 0.125" to 0.25", both the ultimate tensile and shear strength decrease. Looking at the results closer, in Figure 20, the results for ultimate tensile strength versus density can be seen. It is noted that the extra light and light are clumped together for both thicknesses and are behaving as expected. Once density is increased to medium or greater there becomes more of a spread in results. In Figure 21, the trends are similar to those above in the sense that there is a separation as density increases, but this happens lower in density than previously seen, this spread happens closer to the middle of the light density classification versus with the ultimate tensile strength results starting to show scatter around the medium density classification.

For the two tests ran it is also notable that the 0.125" thick samples had a higher ultimate tensile and shear strength [1].
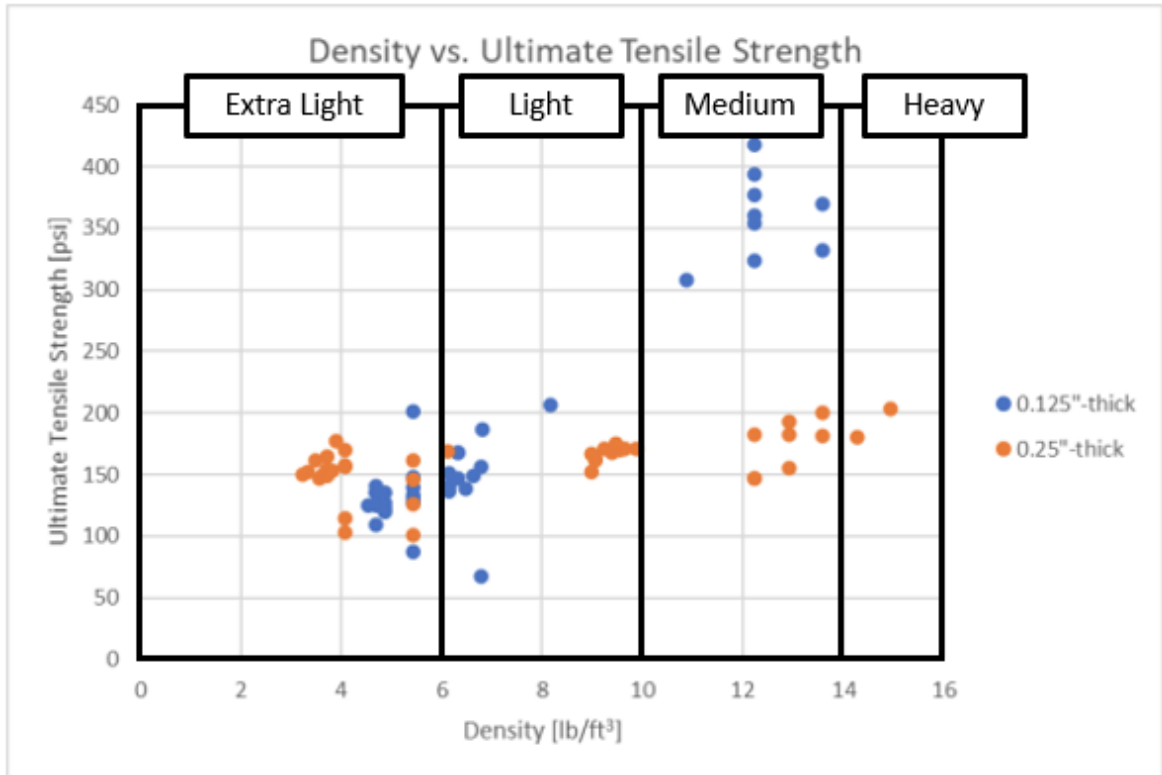
Figure 20: Density Vs. Ultimate Tensile Strength [1]

In Figure 21, the ultimate tensile strength verse density graph is seen with the density grouping marked on the graph. This is tensile tests ran with the force perpendicular to the grain direction. The first thing to note is that this test has the largest density range for the research out of the GSD lab, with the density range falling between extra light and heavy. With that being said, the heavy group has only two test samples for that section. With the results, the extra light grouping behaved as expected with the densities in that section also having relatively the same ultimate tensile strength. However once in the medium to heavy groups the 0.125" thick test samples while

having the same density as the 0.25" thick samples had almost doubled the ultimate tensile strength found [1].
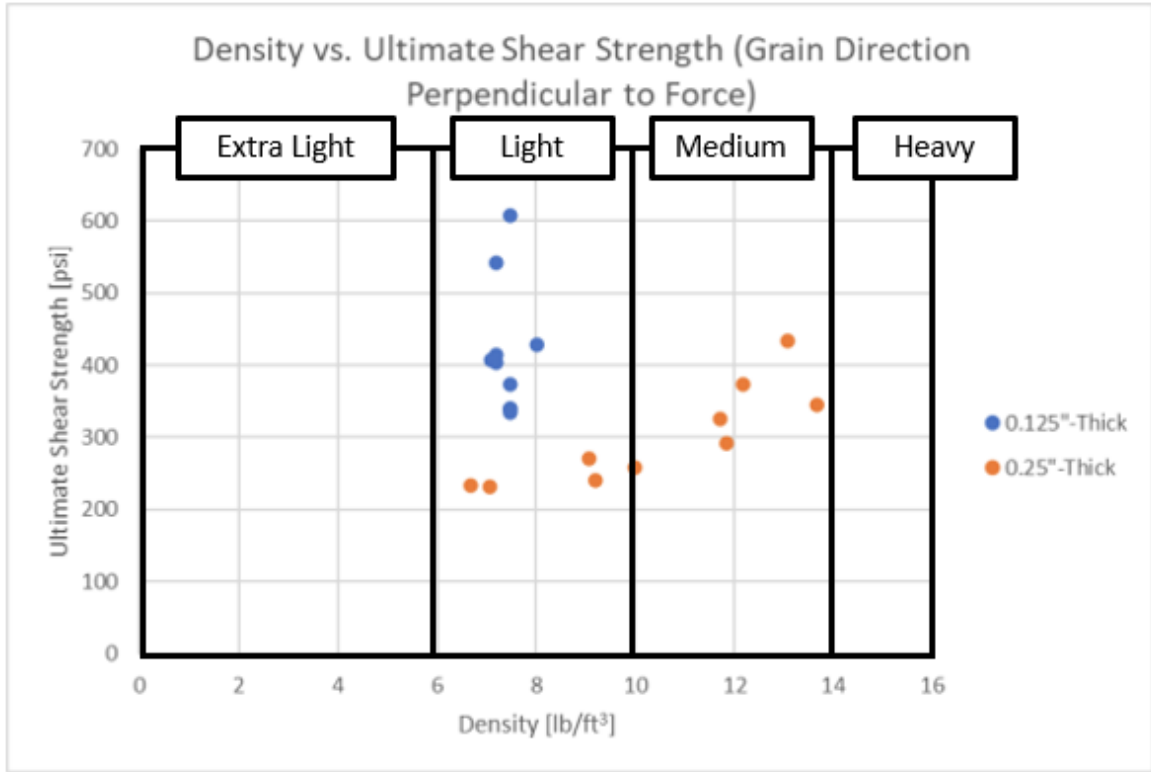
Figure 21: Density Vs. Shear Strength, Force Perpendicular to Grain [1]

In Figure 21, the results from the ultimate shear strength testing with the grain direction is perpendicular to the force can be seen. It can be noted that there is a very small range in the densities for the 0.125" thick samples tested, with only about a range of $1\frac{lb}{ft^3}$. Additionally, there is a difference in the ultimate shear strength of about 52% in that section. Furthermore, as density increases the ultimate shear strength of those values do not increase proportionally as a whole for

this set of data, making the less dense 0.125" thick samples have a higher ultimate shear strength in comparison to the denser 0.25" [1].
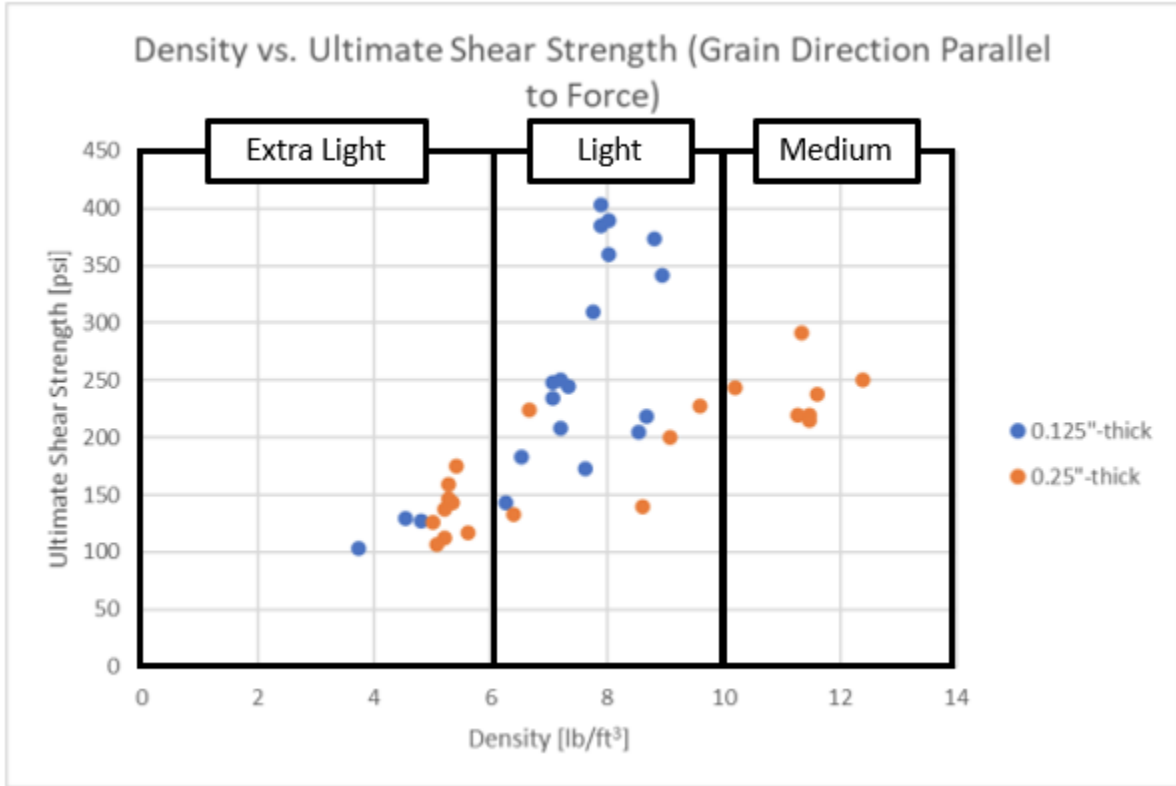
Figure 22: Density Vs. Shear Strength, Force Parallel to the Grain [1]

The results for density verse ultimate shear strength of force parallel to the grain direction can be seen in Figure 22. It can be seen from this graph that the test samples behave as expected for the density range between 4-7$\frac{lb}{ft^3}$. However, after this there is a discrepancy between the 0.125" thick and the 0.25" thick samples. Similarly, to what was seen above in the shear testing with the force being perpendicular to the grain direction, the thinner samples have a recorded ultimate shear strength almost double what the thicker samples are recorded at [1].

While the results are seen above, an overview of balsa material characteristics can be seen below. While their results are shown it is important to note that there is some variation in some of the numbers recorded. Furthermore, the results for the ultimate shear and tensile strengths are from the previous thesis from the GSD lab that was looked at above, and the values that were pulled where the average of that density group and does not take into consideration the thickness, which as stated before was found to change the ultimate strength values. Additionally, the higher ends of the density classifications are not as studied so there are no results in some of the categories.

Table 4: Found Balsa Wood Strength Characteristic [8, 1]

	Density				
	Extra Light	Light	Medium	Heavy	Extra Heavy
Direction	Compressive Stress, (PSI)[8]				
Axial	725	1450	2900	3900	5075
Radial	110	110	145	290	500
	Ultimate Shear Strength (PSI) [1]				
Axial	150	250	275	~	~
Radial	~	400	375	~	~
	Ultimate Tensile Strength (PSI) [1]				
Axial	~	~	~	~	~
Radial	150	175	250	200	~

Investigation into Material Inspection

Currently, there are multiple ways to inspect wood whether that is visual inspection or using imaging systems. This section will briefly mention each method of inspection, first there will be a discussion of what the inspection process is and what to look for.

There are steps that are involved in the process, the first being classifying the wood type. This can become a challenge if you are in a very biodiverse area. Next, will be finding and logging wood defects. Below in Figure 23, the defects can be seen. Each defect and then the number of defects per sheet of lumber will be logged [16]. While it is important to log each defect, some do not hinder the mechanical properties, those classified defects are the sound knots (a), (b), and pin

31

knots (d) while everything else is considered to reduce the quality of the wood [16]. Next is deciding what is the limit for defects, this can vary depending on the application.

Human inspection is the most historically common way to decide the quality of wood, and with 70% reliability, it is easy to see why it is still used today [16]. A downside of human inspection is a strain on the eye as well as fatigue. For larger quality control facilities human inspection can be time-consuming and end up costing more in labor in the life of the projects. Additionally, the abundance of skilled workers is decreasing with the increase in technology [16].
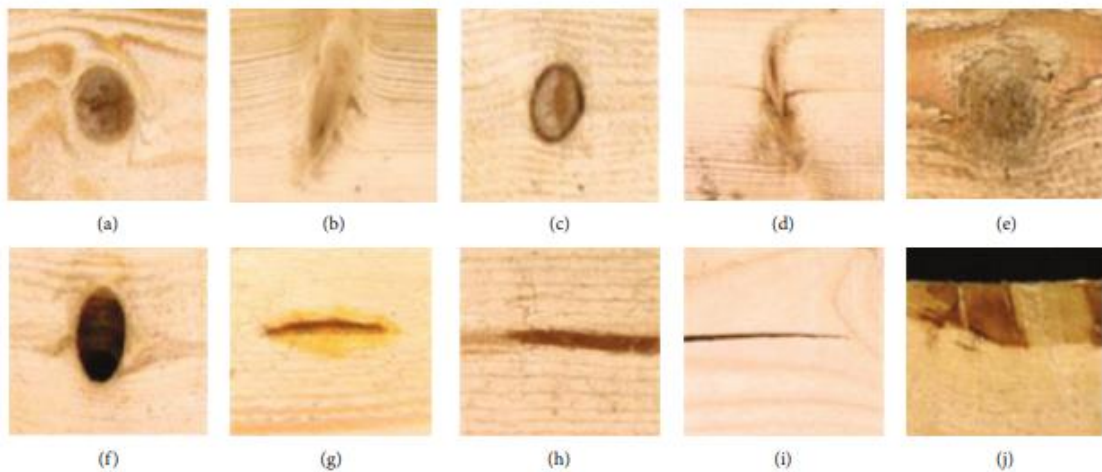
Figure 23: Classified Defects: (a) sound knot, (b) sound knot in the radial plane, (c) black knot, (d) pin knots, (e) decayed knot, (f) knot hole, (g) resin pocket, (h) core stripe, (i) split, and (j) wane [16].

Imaging systems started to become more popular with the increase in the lumber industry but a decrease in inspectors. An added benefit is researchers are seeing a higher detection percentage compared to the human eye, with some researchers even stating an almost 98% accuracy. This process typically involves visual recognition from machines, then running the results through a learning-based categorization system, below in Figure 24, a block diagram that visually describes the process can be seen [16]. Another common issue with this method is errors

in the classification or misclassification of defects. For example, knots can look like one another and can be misclassified. Below a table showing a confusion matrix of classifying detected areas is shown. It can be seen with this system, the confusion that the classifier machine had with accurately detecting and labeling certain defects. A common difficultly was with pitch pockets the most shakes, and it was common for the types of knots to get confused with one another [17].

Table 5: Confusion Matrix for Classifying Defects [17]

	Sound wood	Shake	Dry knot	Sound knot	Black knot	Pitch pocket	Rest	Error (%)
Sound wood	617	32	31	19	4			12.2%
Shake	52	68	2	1				44.7%
Dry knot	23	1	449	10	16			10.0%
Sound knot	14		30	195				18.4%
Black knot			10		18			35.7%
Pitch pocket	7	1	8	5		13		61.8%
Rest	4		9	3	2	1	7	73.1%
Total error	13.9%	33.3%	16.7%	16.3%	55.0%	7.1%	0.0%	17.3%
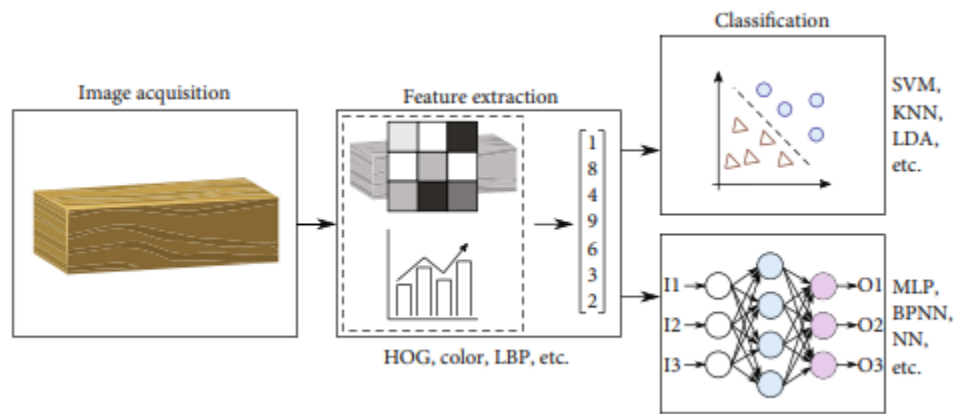
Figure 24: Feature-based classifier block diagram [16]

Overall, this section was useful in comparing human visual inspection with a computerized visual inspection. This also does a good job of describing some of the steps that are needed to accurately follow each inspection method.

CHAPTER III

DEVELOPMENT OF TENSILE TESTING METHOD

When in the preliminary stage of test development finding the best testing method was critical for the research. The material properties seen in the literature review of balsa wood utilize multiple testing types, for example, shear, tensile, bending, and compressive testing to get the results recorded. With the knowledge that the previous results from the GSD lab relied on tensile and shear testing which both followed the same trends – it was decided to move forward with either of those testing methods. After further discussion, it was decided to proceed with tensile testing, due to one of the objectives of this thesis being to investigate the findings found previously at the GSD lab of thinner less dense balsa wood having a higher ultimate shear and tensile strengths in comparison to the thicker denser balsa wood samples tested [1]. Additionally, there is an ease of manufacturing the test samples and implementation of the testing procedures. Tensile testing is a valuable test to consider when testing strength properties, traditionally with wood the strongest tensile strength will be performed with the force in the direction of the grain, or the axial direction, but due to the previous results from the GSD lab tensile testing with the force being applied perpendicular to the grain direction. It was decided to move forward with tensile testing with the force being perpendicular to the grain, or in the same direction as the tangential axis.
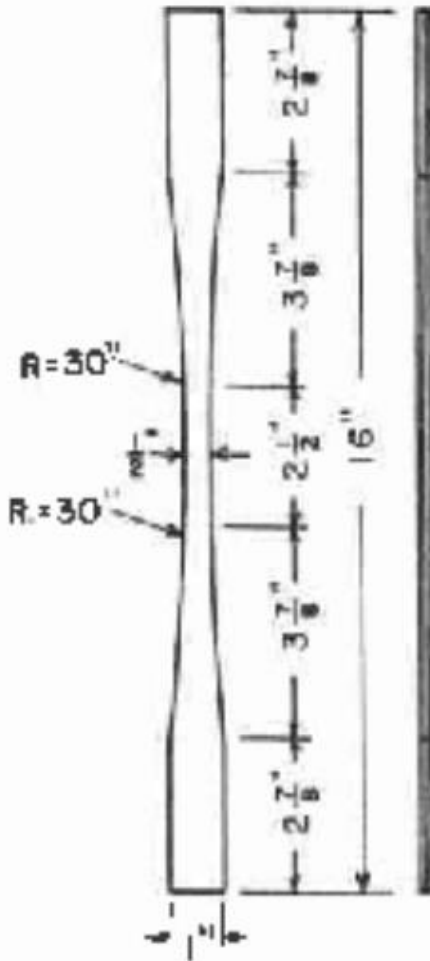
Figure 25: Standard Tensile Test for thicknesses of ¼" or less [18]

During the design and development of an acceptable tensile test sample a few things needed to be decided. First, was what the best test sample would look like. From previous research, it is known that there are standards for tensile testing. A standard tensile test sample for wood that is ¼" thick or less can be seen in Figure 25, [18]. Due to the testing apparatus, the Vernier Structures & Materials Testers, having a displacement area of around 6", which is too small for the 16" length that the standard test shown above, modifications of the standard tensile test sample were needed to be made. The testing apparatus can be seen in Figure 26. This testing apparatus was selected due to its convenience in size and availability for use in the GSD lab.
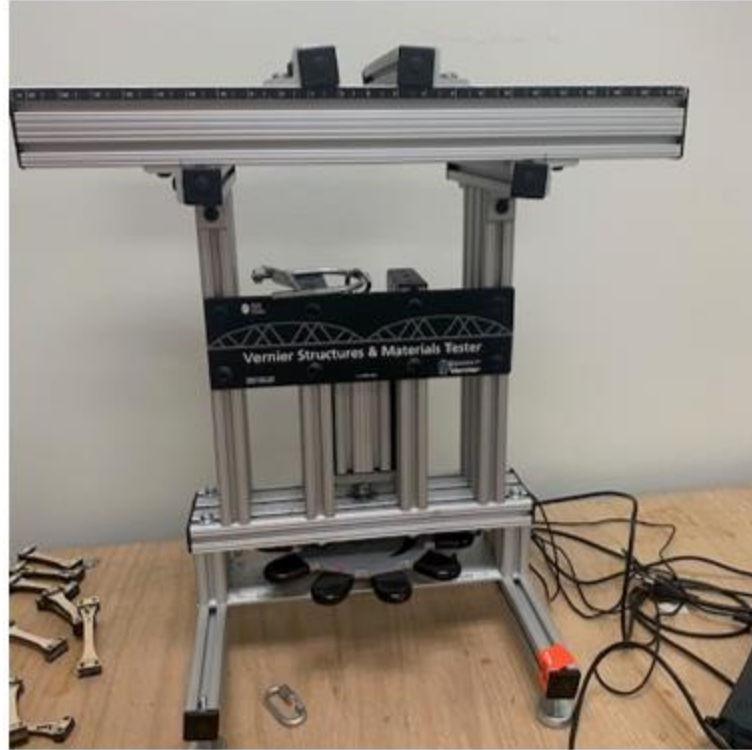
Figure 26:Vernier Structures & Materials Tester

Looking into other past tensile test setups, gave some guidelines on what was needed. The main idea was a smaller gage area and a smooth transition up the shoulders. Below is a layout for the basic design criteria that need to be met for tensile testing. The main criterion is a shoulder length that is greater or equal to the diameter of the gage area [19]. The limiting factor that was not due to guidelines of tensile testing was the maximum sheet width before lamination happens. Most distributors will sell balsa wood in sheets that are 4" wide but will also sell larger widths.
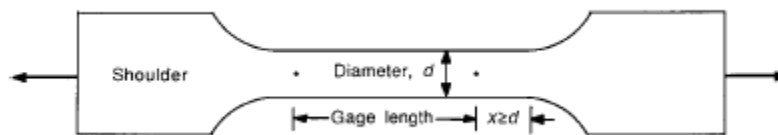
Figure 27: Guide for Tensile Test [19]

37

However, when buying a larger width of balsa wood these sheets of wood must be laminated together to achieve this overall width. Since this paper is focusing on the properties and failure characteristics of balsa itself, laminated balsa sheets were not desired. So, a design was created that followed the criteria of appropriate gage sizing and limiting the test specimen to no more than 4" long.
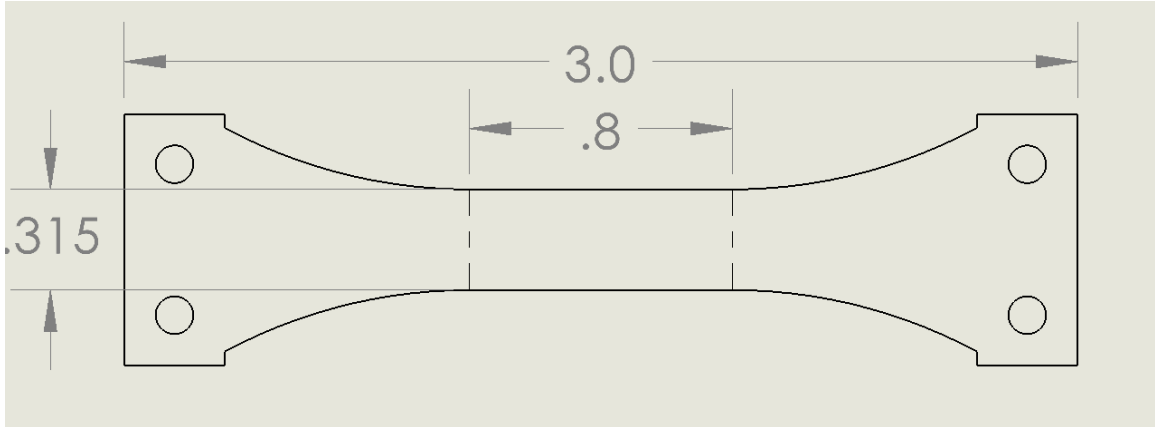
Figure 28: Tensile Test Sets 1 and 2 Sample Design

Statistical Analysis and Sample Number

Initially, when deciding to do this testing methodology. There was a desire to get a better idea of how much balsa wood to buy and how many samples to test to give a more accurate testing pool. This was for cost but also due to wanting a larger sample size to verify that the results that have been found previously are not skewed due to insufficient sample size. When looking at other research and statistical analysis, it was decided to use a sample size equation seen below. The equation is a mean sample size equation. With n, being the sample size, σ being the variability and MOE being the margin of error. Traditionally in research, a confidence level of 95% is used and a variability of 50%, or 0.5 is used to give the maximum variability option [20].

$$n = \frac{z^2 x \sigma^2}{MOE^2}$$

38

Below in Table 6: Sample Size Calculations a few scenarios were investigated. Initially, trying to maintain a 95% confidence level as well as a 50% variability produced a large sample size number. It was decided to continue with a variability of 50%, so lower confidence levels were investigated to see if a more obtainable sample size number is possible. After some discussion it was decided to move forward with a confidence level of 90% and a margin of error of 12%, giving a sample size of 47. This was due to a few reasons, the first being that with the research in this paper testing a hypothesis and not the characteristics of balsa wood, a lower confidence level is still valid; additionally, the maximum number of samples that can be laser cut out of the 36" long balsa sheets are 50. Therefore, most of the test samples are in groups of around 45-50.

Table 6: Sample Size Calculations

Sample Size Calculations				
Confidence Level	Z-Value	Variablitiy, σ	Margin of Error	Sample Size, n
95%	1.96	0.5	0.1	96
90%	1.645	0.5	0.1	68
90%	1.645	0.5	0.12	47

Test Set Up and Procedures

Before starting to test some preliminary procedures need to take place to insure a successful round of testing. To start, all the test samples must be laser cut, weighed, labeled, and doublers glued on. To create ease of annotating, the system of labeling each sample based on density characterization and the number of samples per thickness was created. For example, and 1/8" extra heavy sample that had its weight recorded 15th, the sample will be labeled XH_15 and placed in a folder labeled XH_.125. In Figure 29 a completed test sample with doublers glued on can be seen.

Figure 29: 0.125" Medium, Sample #9

Following the procedures below for testing.

1. Open Logger Pro software on the laptop

2. Verify sensor is connected and recording data.

3. Take a test sample and attach 3D-printed mounts with 4-40 screws.

Figure 30: 3D Printed Mounts

4. With the load cell unloaded attach u bolt connection to the bottom 3D print mount

5. Place the top mount on the 8020 beams.

6. Center the sample to be centered with the load cell.

7. Slowly load the sample by twisting the actuator on the bottom of the vernier tester

8. Once Logger Pro reads a positive number slightly de-load

9. Zero the reading

10. Click record data.

11. Slowly load the vernier tester maintaining a consistent speed

12. Once the sample breaks click stop recording.

13. Save the file as a logger lite to the respective folder.

14. Export the file as .txt to the respective folder

Visually Testing

While imaging systems and other detection systems are great for large-scale detection, for the application at the hand of quality checking one species of wood, it is not a necessary feature. Along with the potential for miss detection that can come along with preliminary stages of learning software, human quality checking is the best option for the current project. Previous research into this topic has helped to lay a foundation for our standards for quality checking and defect detection.

Procedures with Visual Inspection

Due to this testing being up to the human eye, there was a lot of room for improvement. To verify that each test is being conducted the same way procedures have been created. This is to help keep a uniform test group. Below the inspection procedures can be seen.

Follow these procedures when visually testing balsa wood.
1. Inspect all sides of the sample.
2. Note where each defect is by manually marking and taking a picture.
3. Run a tensile test on the balsa sample.
4. Record where the break occurred and if near a defect, either found during inspection or found posttest.

This test is a bit different than the previous test that will be done, starting with preliminary testing to look for trends. With that, there will be samples investigated but not recorded during this

42

learning period. Furthermore, that will mean that the number of samples tested will not be as large as the other tests.

CHAPTER IV

TESTING AND RESULTS

This section will summarize each testing set. A discussion of results will be had as well as an analysis of trends formed, experimentation as well as a comparison of experimental trends to previous research. There are 2 test types and a total of 4 test sections. With the tests being–

Tensile Testing,

- Set #1: force loaded perpendicular to the direction of the grain.

- Set #2: force loaded perpendicular to the direction of the grain, with a larger range of density and set grain direction.

- Set #3: force is parallel to the grain, full density range, and set grain direction,

Visual Testing

- Visual Inspection of Defects and Failure Location

Tensile Test

This section will discuss each test that was run. Along with any modifications that had to be implemented and the results that came out of each test.

Tensile Test Set #1

Tensile test set 1, was tensile tests done with the force perpendicular to the grain direction. However, these test samples were created from balsa sheets that were from the initial balsa wood distributer the GSD lab used. Therefore, the grain direction is not truly known. Additionally, this distributor does not have a wide variety of balsa densities. There was a choice between "aero light" and "regular balsa", with aero light being classified as "wood that is extremely lightweight ($4\frac{lb}{ft^3}$)" but said to not have any better grain structure [21]. Furthermore, there is no known range of densities when buying regular balsa sheets.

With that, there was only about a $7.6\frac{lb}{ft^3}$ variance of density recorded between all the tests that were run during this batch of balsa. With $5\frac{lb}{ft^3}$ being the lowest and $9\frac{lb}{ft^3}$ being the highest. According to Table 1, shown in the Overview of Balsa Wood section above, this group of balsa would be classified between extra light to light density. While it may cover the lower sections of density groupings it fails to account for the groupings, medium - extra heavy.

Table 7: Density Classification Spread for Test Set #1

# of Samples	Classification
23	XL
83	L
0	M
0	H
0	XH

Above in Table 7, this trend of pronominally light-density test samples is shown. While useful information was gathered from this test set, there is a large percentage of balsa wood

45

densities that are not being represented, namely the most common grouping, 8-16$\frac{lb}{ft^3}$, which is the top portion of the light to the lower heavy density classification of balsa wood.

      With that, both test results can be seen on one graph in Figure 31. The density classification is labeled on the graph along with both Aerolight and regular balsa being labeled as A and R, respectively. While at the same density value, some of the test results had a discrepancy between the ultimate stresses, for instance, the 0.25" regular balsa samples had around the same density as the 0.25" Aerolight balsa samples, but the Aerolight samples on average had almost a 10% difference higher in ultimate tensile stress values. With the largest difference being around 23% for the ultimate tensile strength for balsa of the same density. Additionally, it is noted that the range of density was around 5 $\frac{lb}{ft^3}$ to 9.5 $\frac{lb}{ft^3}$. While there is a lot of data there is not a huge trend that can be seen with the data. It can be noted that the Aerolight data overall had a constantly higher ultimate tensile strength in comparison to the regular balsa wood. Due to this, the data will be broken down further.
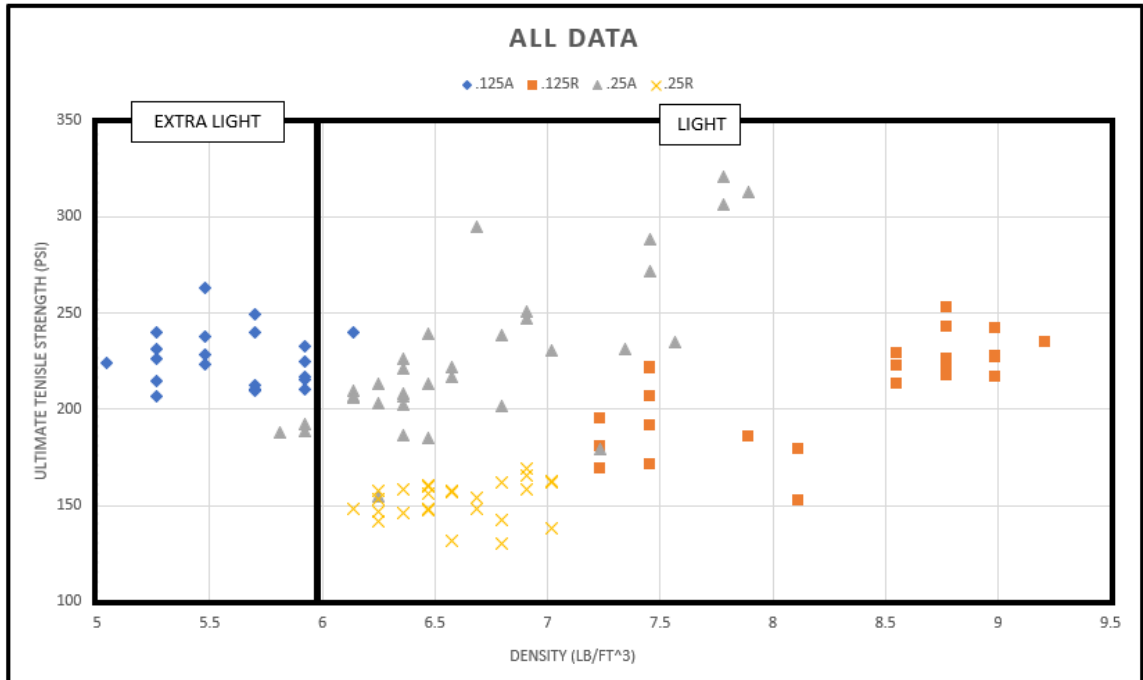
Figure 31: Tensile Test 1, Ultimate Tensile Stress Vs Density

Table 8: Regression Analysis for All Test Data for Set 1

All Data	
Regression Statistics	
Multiple R	0.171769
R Square	0.029505
Adjusted R Square	0.020173
Standard Error	40.36871
Observations	106

Looking closer at the tests that were run as well as running a regression analysis. Below shows the output of the regression analysis that was run on the aero light and regular balsa sheets at both ¼" and 1/8" thick sheets. To further this a regression analysis was run on all data points for the regular balsa sheets as well as for the aero light sheets as well as all the data. This shows that

each sub-test group does not have that great of a correlation between density and stress. That is not too surprising due to the small density changes for each grouping.

Table 9: Regression Analysis for Regular 0.125" and 0.25"; Aerolight 0.125" and 0.25"

1/4 Inch Regular		1/8 Inch Regular	
Regression Statistics		*Regression Statistics*	
Multiple R	0.201408	Multiple R	0.677121
R Square	0.040565	R Square	0.458493
Adjusted R Square	-0.00115	Adjusted R Square	0.433879
Standard Error	265.3378	Standard Error	255.017
Observations	25	Observations	24
1/4 Inch Aerolight		1/8 Inch Aerolight	
Regression Statistics		*Regression Statistics*	
Multiple R	0.766907	Multiple R	0.056348
R Square	0.588146	R Square	0.003175
Adjusted R Square	0.574861	Adjusted R Square	-0.0522
Standard Error	650.5683	Standard Error	196.9657
Observations	33	Observations	20

When breaking this down further to regular balsa and Aerolight balsa a better trend can be seen. Below in Figure 32 the graph of Regular Balsa with the thickness groups noted on the graph can be seen. With the regular balsa wood, all the test samples were classified as light balsa and had no variation in density classifications. The regular balsa then shows about an 80% correlation between density and stress. While there is some scattering noticed it is not large enough to raise concerns since this is a natural material and some variance is to be expected. Also, it is important to note that this set of data is behaving similarly to what is seen in previous research from the GSD lab, with the thinner samples having a higher ultimate tensile strength compared to the thicker test samples.
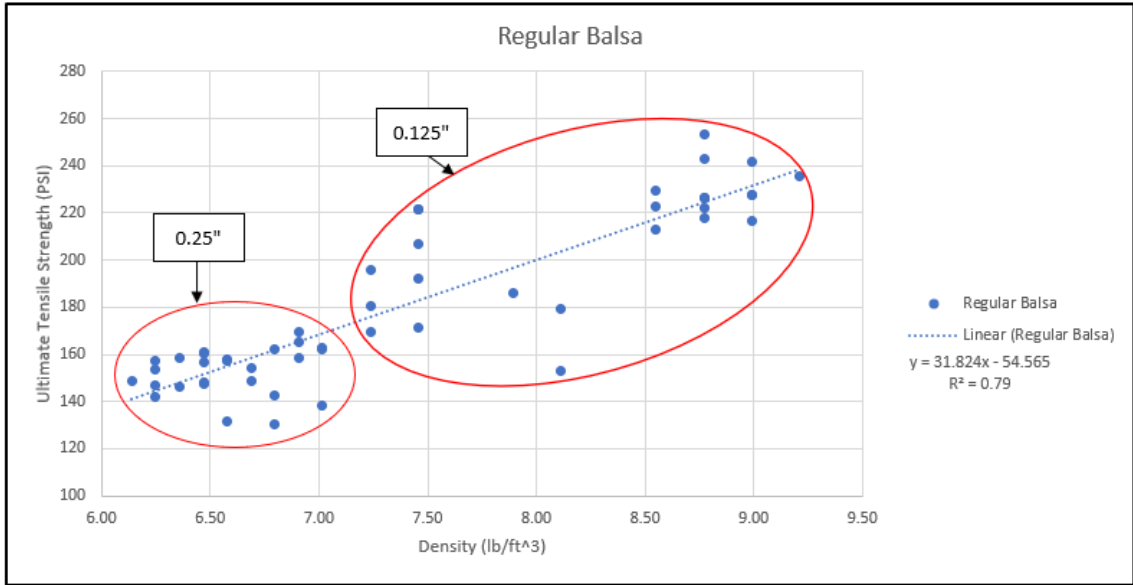
Figure 32: Density vs Ultimate Tensile Strength for Regular Balsa
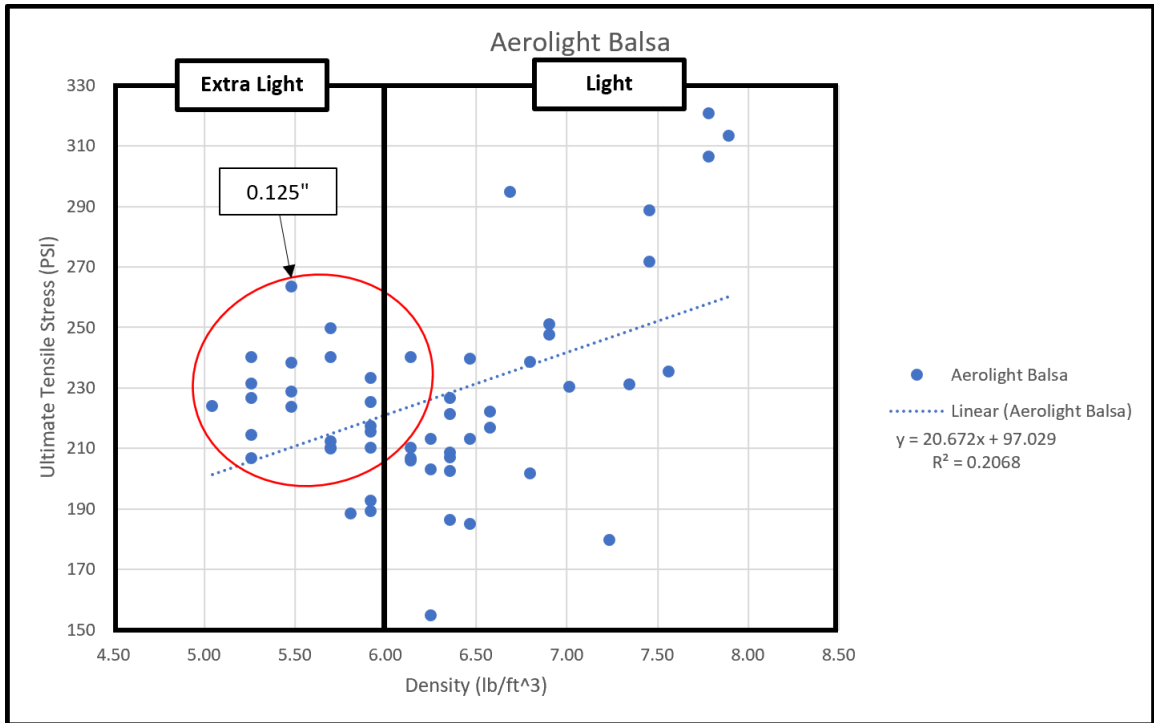
Figure 33: Aerolight Balsa, Ultimate Tensile Stress Vs. Density

49

Next, looking into the Aerolight group of balsa sheets, which can be seen in Figure 33. The graph of Aerolight balsa sheets in terms of density vs ultimate tensile stress is shown and, on the graph, it is noted where the 0.125" thick samples are, and the non-circled points will be the 0.25" thick samples that were tested. Comparing this to the previous graph it is noted that there is a larger scattering and a few more outliers. As well as it is noted that this grouping only has about a 20% correlation of density to stress.

After analyzing the data and noting in some cases double the stress for the same density of balsa, it was decided to change to a balsa distributor that had more rigorous selection processes. It is believed that due to the small density selection and lack of ability to request certain grains, nonintuitive results were found. With the desire to be able to limit grain direction, density, and defects more accurately, the distributor Specialized Balsa was found [3]. This new distributor can meticulously produce a wide range of densities and select the grain cut and direction that was desired.

Tensile Test Set #2

The second set of tests utilized the same method for testing as before. But going through a different distributor was able to be more selective in the process. A new distributor will allow for a density range for extra light to extra heavy – as well as choosing a grain direction. With the knowledge found from the literature review on balsa wood above, an evaluation of different grain directions was useful. It is known that the A grain's flexibility is useful for curvatures, C grain being the stiffest and least likely to conform to shapes, and B grain maintains some characteristics of the flexibility of A grain but also the stiffness of C grain [3]. Therefore, with this information a single grain direction, B grain was selected. This would have the force loaded in the radial direction, this can be seen in Figure 34. Next, it was decided to use all the density variants offered in both ¼ and

1/8-inch sheets to get the largest test data spread. The weight breakdown of each sheet is shown. Noticing that the ¼" light and medium had little variation in weight and the 1/8" extra light and light had very little variance.
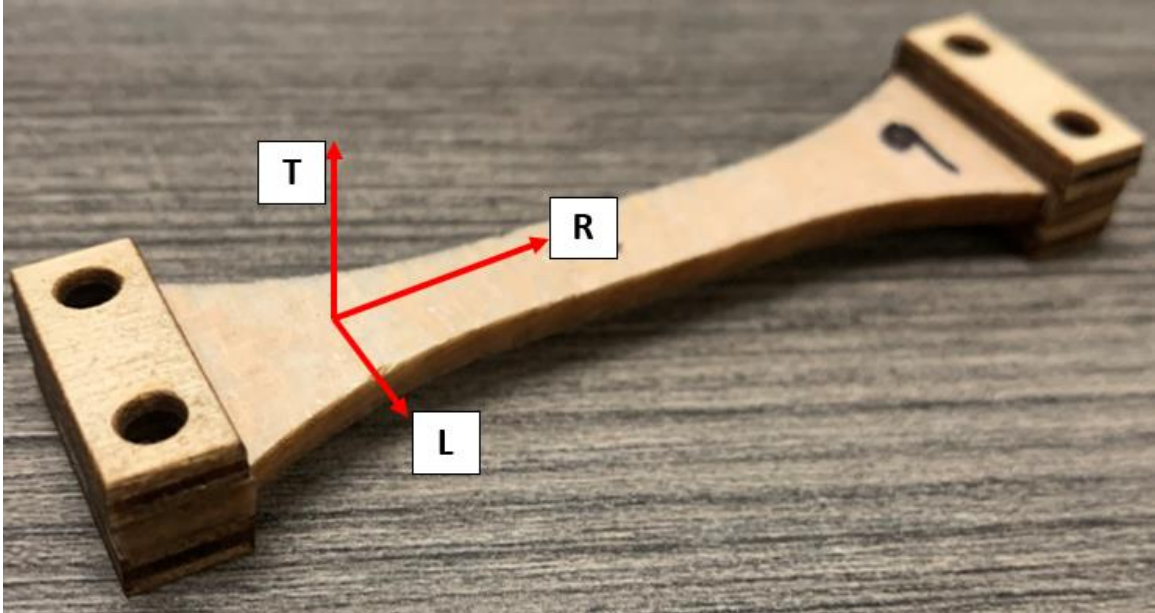
Figure 34: Tensile Test with Loading in the Radial Direction

Table 10: Test Matrix for Test Set #2

	Density Classifications	Thickness (in)
	Extra Light	0.125, 0.25
	Light	0.125, 0.25
B-Grain Direction	Medium	0.125, 0.25
	Heavy	0.125, 0.25
	Extra Heavy	0.125, 0.25

Table 11: Balsa Sheet Information

Balsa Sheet Preliminary Info					
Balsa sheet classification	weight(g)	area (in^2)	thickness(in)	density (g/in^3)	tested (Y/N)
extra light	68.68	196	0.25	1.402	Y
Light	125	196	0.25	2.551	Y
Medium	132	196	0.25	2.694	Y
Heavy	187	196	0.25	3.816	Y
Extra Heavy	253	196	0.25	5.163	Y
extra light	37	196	0.125	1.510	Y
Light	42	196	0.125	1.714	Y
Medium	72	196	0.125	2.939	Y
Heavy	97	196	0.125	3.959	Y
Extra Heavy	133	196	0.125	5.429	Y

In the below table, Table 12, the breakdown of density classifications and the number of samples tested in each group can be seen. With this breakdown of samples vs classification, the average number of test samples per density group was 85, but there is a steep drop off number between heavy and extra heavy, while initially it was planned to test roughly the same number of samples – the extra heavy was so brittle and easy to fracture that some broke before the testing came about. With that in mind, the recorded variance of density in this section of tests is $4\frac{lb}{ft^3}$ - $21\frac{lb}{ft^3}$.

Table 12: Test Set #2 Balsa Density Classification Spread.

# of Samples	Classification
103	Extra Light
93	Light
103	Medium
83	Heavy
42	Extra Heavy
424	Total Tested

One thing to note in this test set is that as the density increased there was more fracturing outside of the gauge area in the ¼-inch thick samples. Due to this the sample size for the group - extra heavy, ¼ inch dwindled to approximately half of the original sample count. With this noted for ¼" thick balsa test samples, it causes the R^2 value to be around 0.47, or a 47% correlation between the density and stress. If the XH group is omitted, it indicates a better correlation of ultimate tensile strength to density of around 73%.

Below in Figure 35 is the graph of all the .25" test samples. Even with the natural scatter that would be excepted from a natural material, once in the extra heavy density, the scatter is extreme. While initially, this was confusing, and trying to find a correlation between this failure was not straight forward, after some discussion a few theories were found. It is believed that the extra heavy balsa sheet may have had a fracture initially in the sheet before manufacturing.
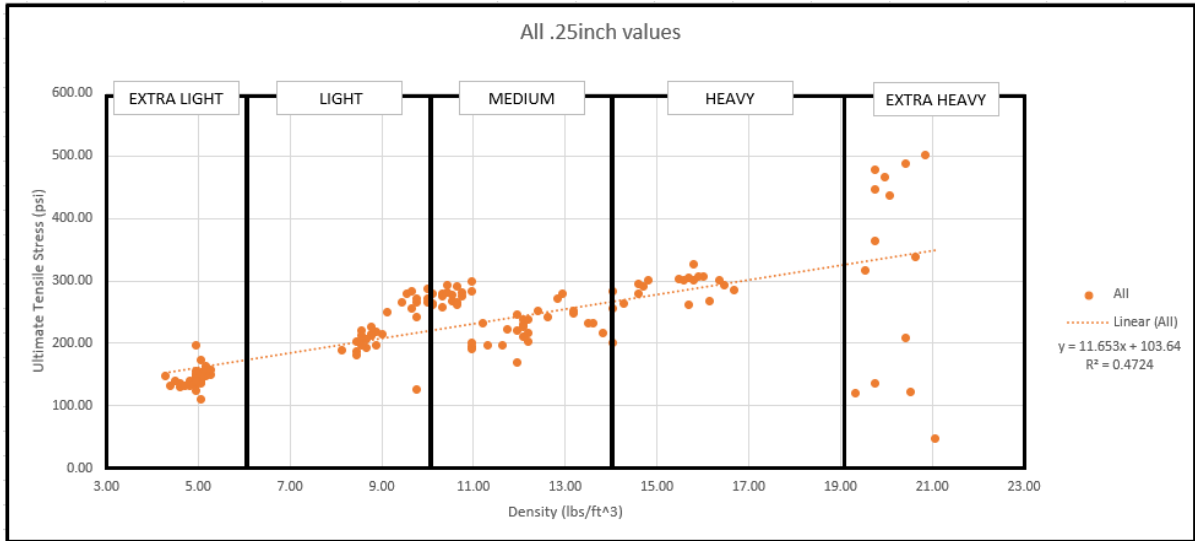
Figure 35: 0.25" Balsa, Ultimate Tensile Stress Vs. Density

Another theory is that laser cutting and assembling of the doublers and 3D printed attachments caused fatigue in the already more brittle material. It is also interesting to note that for density classification of light, medium, heavy, and extra heavy, there was a considerable number of tests that had to be omitted due to failure outside of the gage area. For instance, the light grouping had almost half of the test samples failed outside of that region, the medium had 16, heavy had 9, and extra heavy had 5 samples failed outside of the gage area. This type of failure can be noted in Figure 36, this is any failure that happens outside of the red gage area. Due to this, the tests that failed outside of the gage area were thrown out of the calculations of ultimate tensile stress.
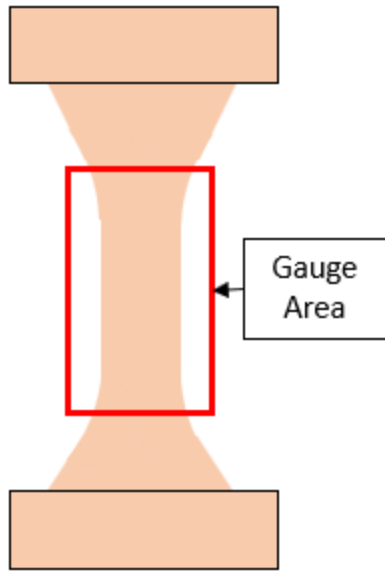
Figure 36: Tensile Test Sample with Gage Area Shown

Figure 37: Failure Inside Gage Area (Left), Failure Outside Gage Area (Right)

For the 0.125" data set, there was a similar trend of the lower section of density classifications behaving as expected, then once past the heavy densities large scattering became apparent. However, even with the scattering this set of data was able to maintain around an 84% correlation of density in relation to ultimate tensile strength.
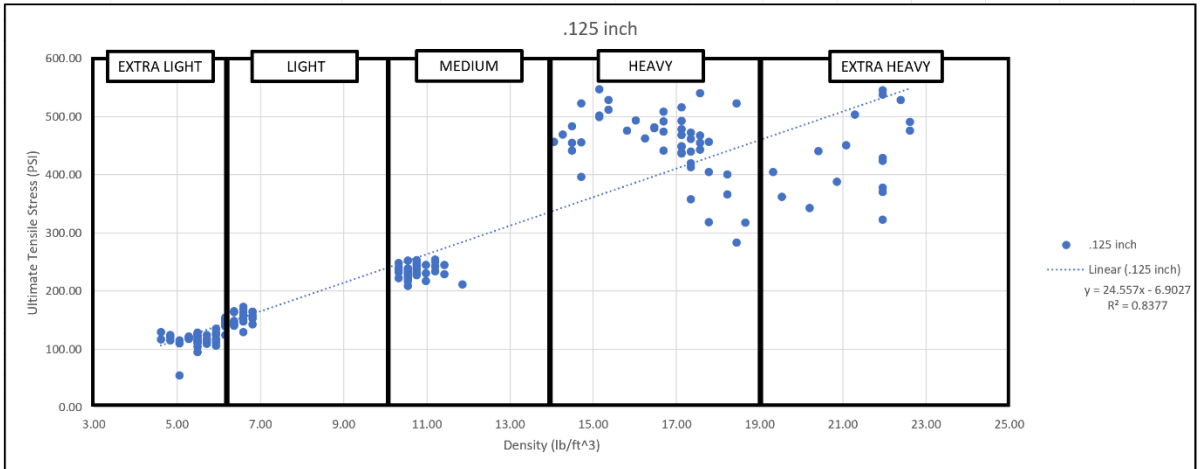
Figure 38: Density Verses Ultimate Tensile Strength for 0.125" Test Group
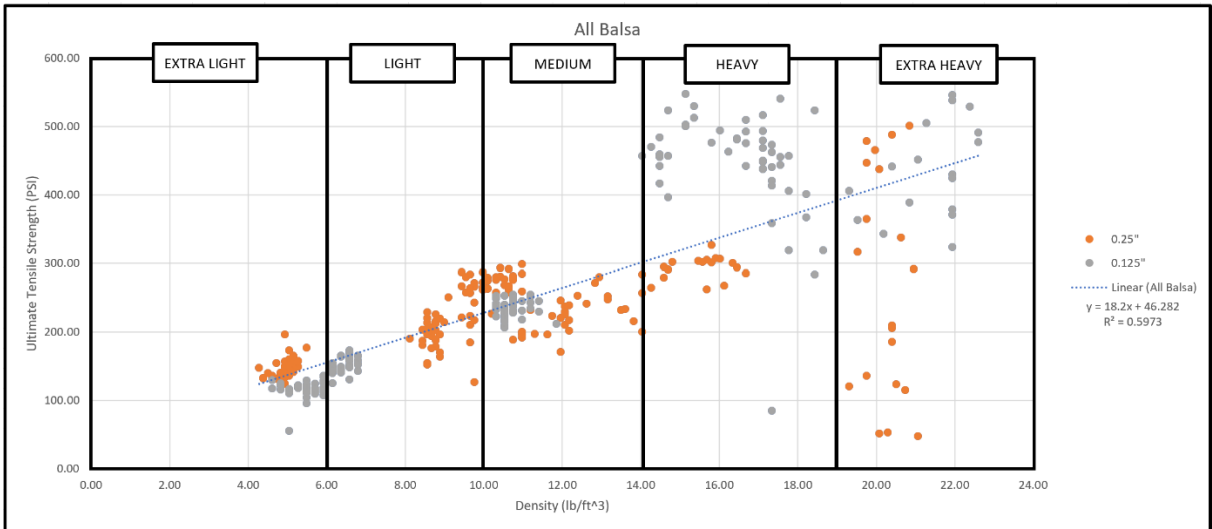
Figure 39: Density verse Ultimate Tensile Strength for All Test Set #2 Samples

The most interesting thing to note is that while the higher densities can have a higher ultimate tensile strength, there is less precision in the failure at the higher densities. While it may be compelling to utilize a denser piece of balsa wood, the variable of failure makes it impossible to justify using. It is believed that this is due to the balsa wood becoming increasingly brittle as the density increases and the thinner test samples being more ductile. This is thought to be because

57

during testing the 0.25" thick specimens were more difficult to handle compared to the 0.125" thick specimens that had more flexure to them. This is when density increases the S2 layer increases which in turn increases the stiffness, as discussed in the Review of Literature section.

Additionally, it can be seen from Table 13: Standard Deviation of Tensile Test #2, that heavy and extra heavy had a very large standard deviation. While the lower densities still had a larger than desired standard deviation those subgroups had a significantly lower value. This shows again that as density increases the variance in results also increases.

Table 13: Standard Deviation of Tensile Test #2

Density	Standard Deviation
XL	18
L	30
M	26
H	123
XH	99

With the results above it was also important to understand the different failure modes of this type of testing. Below in Figure 40 and Figure 41, the difference in failure types can be seen with force parallel and perpendicular to the grain direction. Since most testing was done with the force perpendicular to the grain direction those failure modes will be discussed first. (a) tension failure of earlywood, (b) shearing along a growth ring, (c) tension failure of wood rays, for force parallel to the grain you will have (a) splintering tension, (b) combined tension and shear, (c) shear, (d) brittle tension. [22]. Looking at the testing that was done the 0.125" thick samples more commonly broke due to tension failure of earlywood, compared to the 0.25" thick sample more frequently would break due to shearing along growth rings.

58
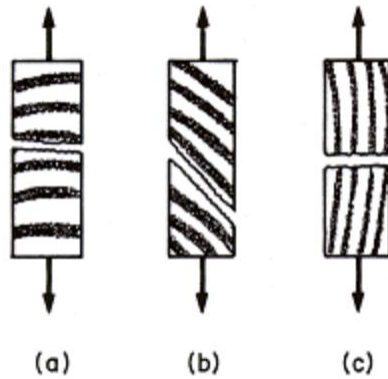
Figure 40: Failure Types for Force Perpendicular to the Grain [22]
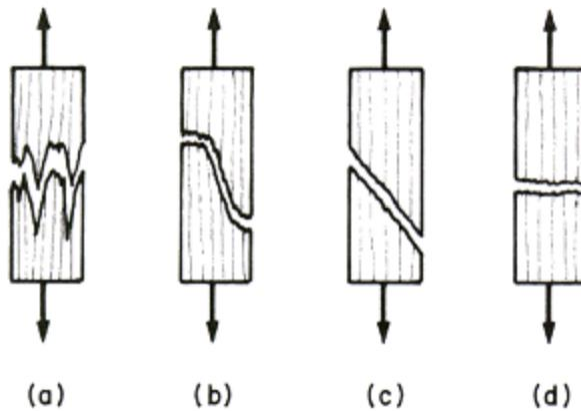
Figure 41: Failure Types for Force Parallel to the Grain [22]

Since there were almost 500 tests run, it was decided to select random samples to investigate the failure type. More specifically 3 test samples from each density per thickness. For example, in the 0.125" thick samples all the samples from groupings 9, 18, and 19 were selected to inspect. For 0.25" thick samples, 5, 27, and 36 were selected to inspect for failure types.

Noting with this that lower densities tended to fail more commonly like figure (a) and then the higher density had failure type typically like (b). This is most likely since denser balsa wood is from older trees so it makes sense that lighter-density balsa will have a failure type of tension failure in earlywood.

Visual inspection of the failure plane can be seen below in Figure 42, Figure 43, and Figure 44. Noting that balsa wood that is heavy and extra heavy have ray cells in the plane of failure and can also be seen on the side view of the sample. However, the extra light can be seen without visible rays at the cross-section of failure. Noting further that the extra heavy failed due to shearing along the ray cells, and the light density balsa wood fails to tension failure in the earlywood.
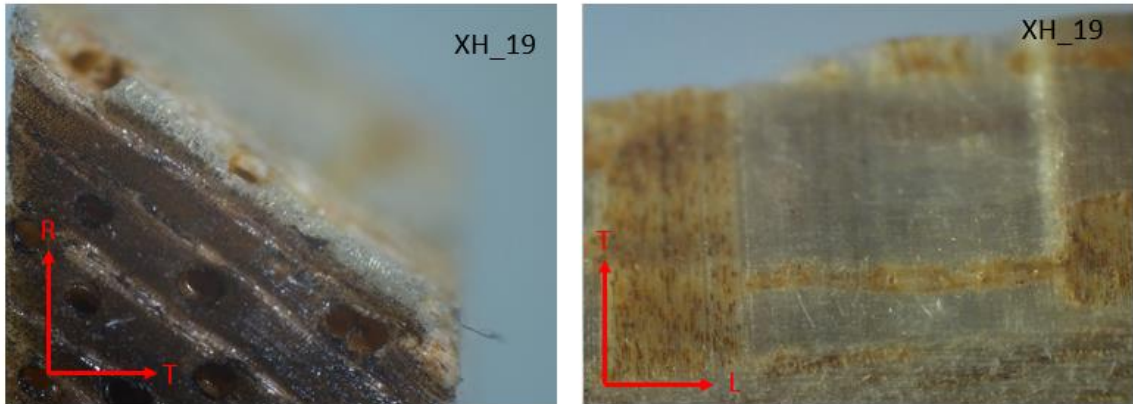
Figure 42: 0.125" Extra Heavy Sample 19, Visual Inspection of Failure planes
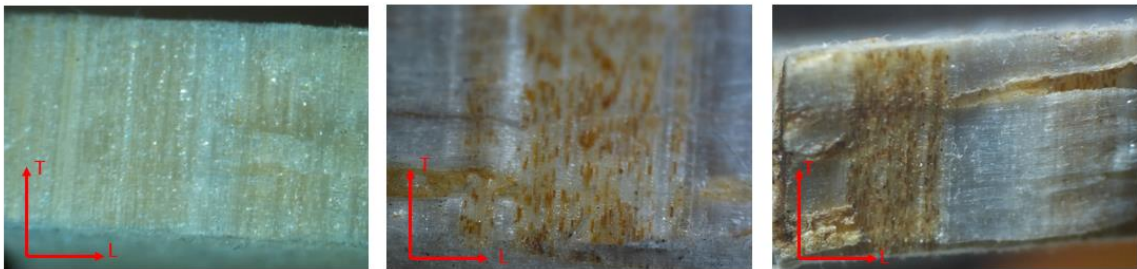
Figure 43: XL_9, H_9, and XH_9 Cross Section
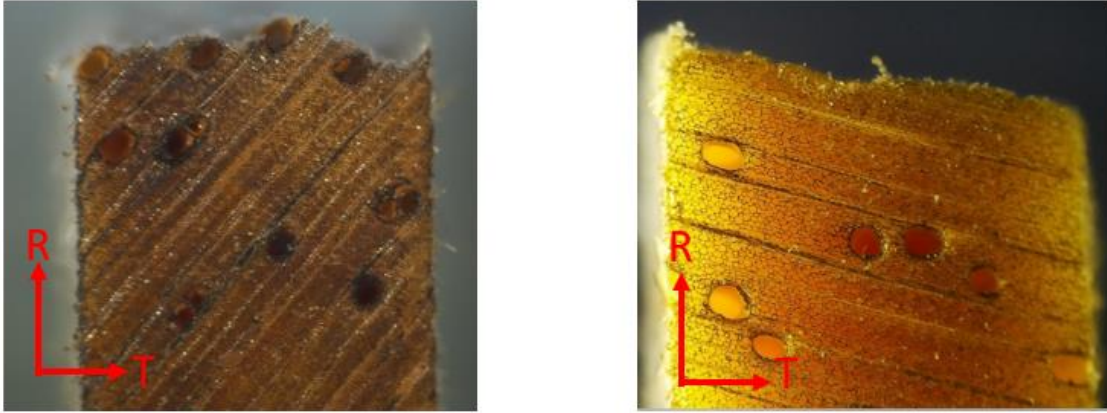
Figure 44: Side View, M_9, XL_9

Tensile Test Set #3

The previous 2 test groups have been conducted with the force perpendicular to the grain direction. However, when the force is parallel to the grain it can be expected to show a higher ultimate tensile strength. It was decided to add this last test set to see if results were remaining constant, as well as to complete the tensile properties for balsa wood in more than one axial direction. Due to this being an added test and not crucial for this paper, it was decided to only test extra light, medium, and extra heavy densities. That way there is still a large spread of densities acknowledged, but it shrinks the number of tests done. Additionally, the number of samples tested significantly decreased. It was decided to test each sup group a minimum of 3 times. So, this test group will have a significant decrease in the number of samples tested.

Initially, this test group was utilizing the same design for the test sample as before, this design can be seen above in, Figure 28: Tensile Test Sets 1 and 2 Sample Design. However, after initial testing, it was noted that most test samples failed due to bearing stress instead of tensile. This failure can be seen in Figure 45. With that, a redesign was needed.

Figure 45: Failure Due to Bearing Stress

Before the redesign was finalized, bearing stress and how to limit it was investigated. The definition of bearing stress is the compression of the points of contact between multiple bodies. There are a few ways to decrease the bearing stress, those being to either add more connection points or to increase the surface area where that connection is applied [23]. Below Figure 46, the diagram for bearing stress for the original tensile test design can be seen.
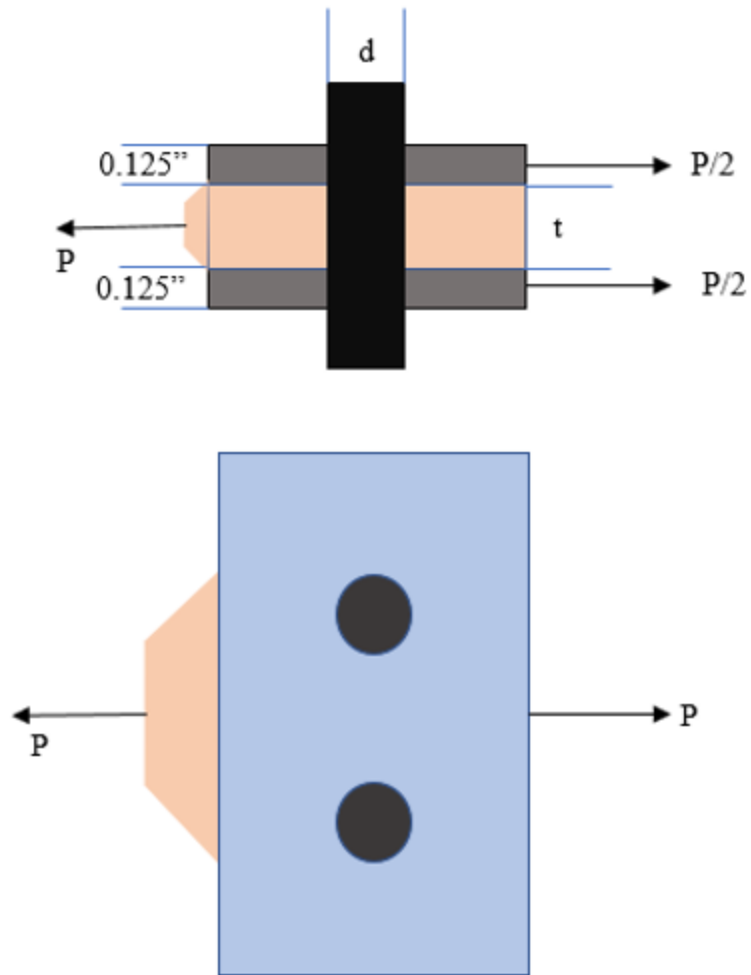
Figure 46: Diagram of Bearing Stress for Design #1

The bearing stress equation is shown below. With P, being the applied load, A_b; being the surface area of the contact point of the bolt; and n, being the number of bolts [24]. Therefore, if an

additional bolt hole was added that would reduce the bearing stress by around 150%. This design

can be seen in Figure 47.

$$\sigma_b = \frac{P}{A_b * n}$$
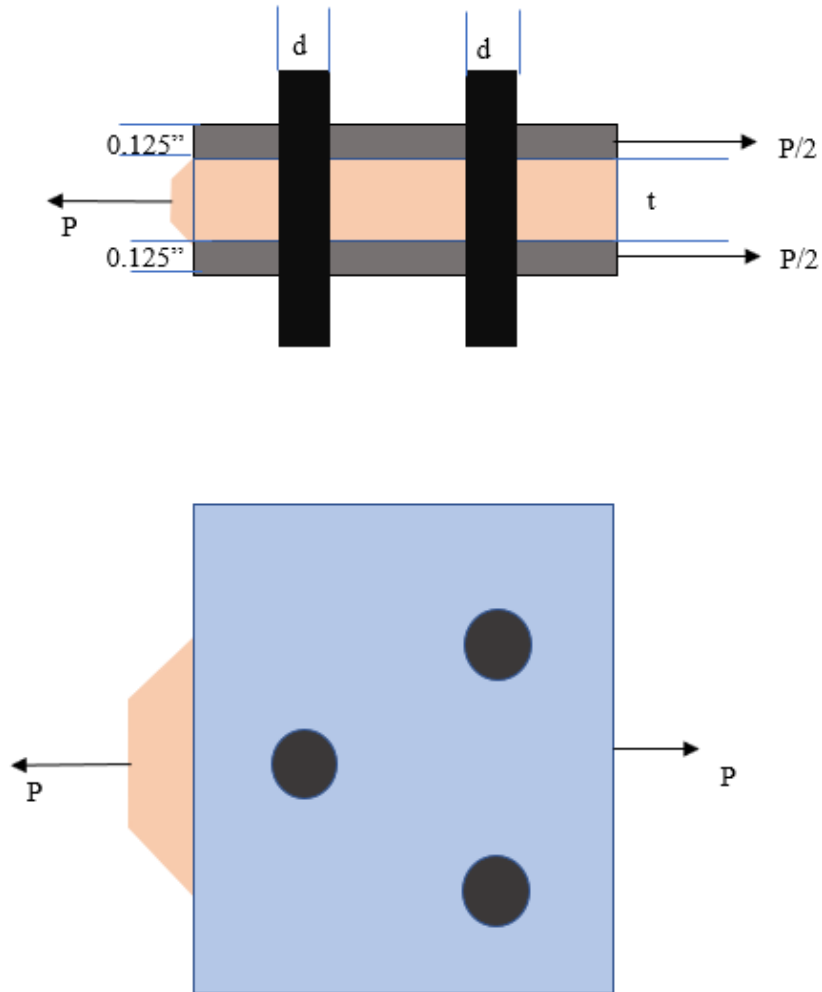
Figure 47: Updated Hole Pattern to Reduce Bearing Stress

After the modifications for bearing stress were implemented, a different change needed to

be made. The data acquisition method is the Vernier Structures & Materials Tester (VS&MT),

which is aluminum 80/20 so it is very modular which is beneficial when testing larger materials or

designs. [25] Initially, the 3D mounts were created and printed using ABS, this was fine for testing perpendicular to the grain direction due to the lower ultimate strength being recorded. However, yielding of the plastic mount was taking place, most prominently on the bottom mount. Due to this both top and bottom mounts were reprinted out of nylon and there was an increase in the infill on the designs. This modification was then able to withstand the increased forces that had to be applied. The new design can be seen in Figure 48, most notably the larger face for mount attachments, as well as a larger gauge area and a large difference in thickness between the gauge area and the shoulders.
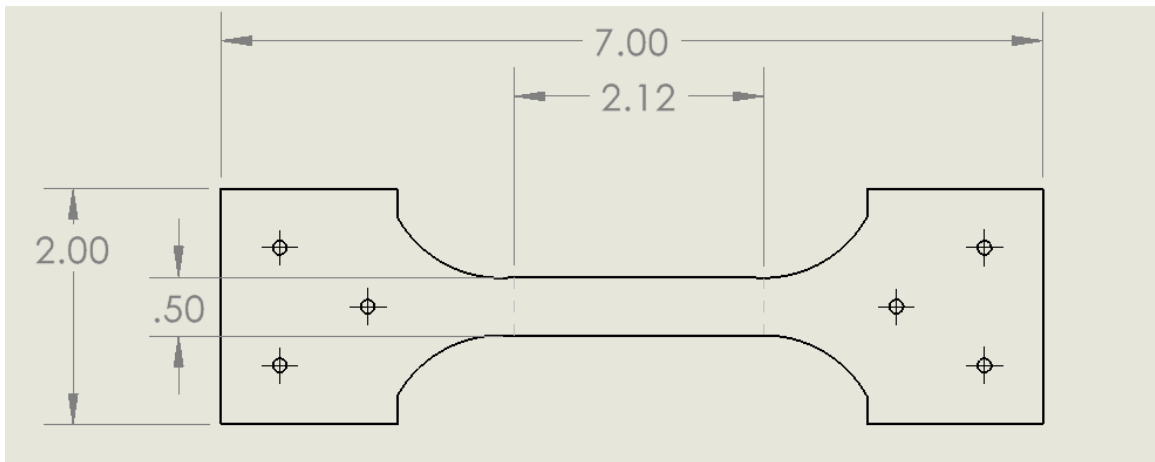
Figure 48: Updated Tensile Specimen for Testing Force Parallel to the Grain

Figure 49: Test Set #3, M_3a, 0.125."
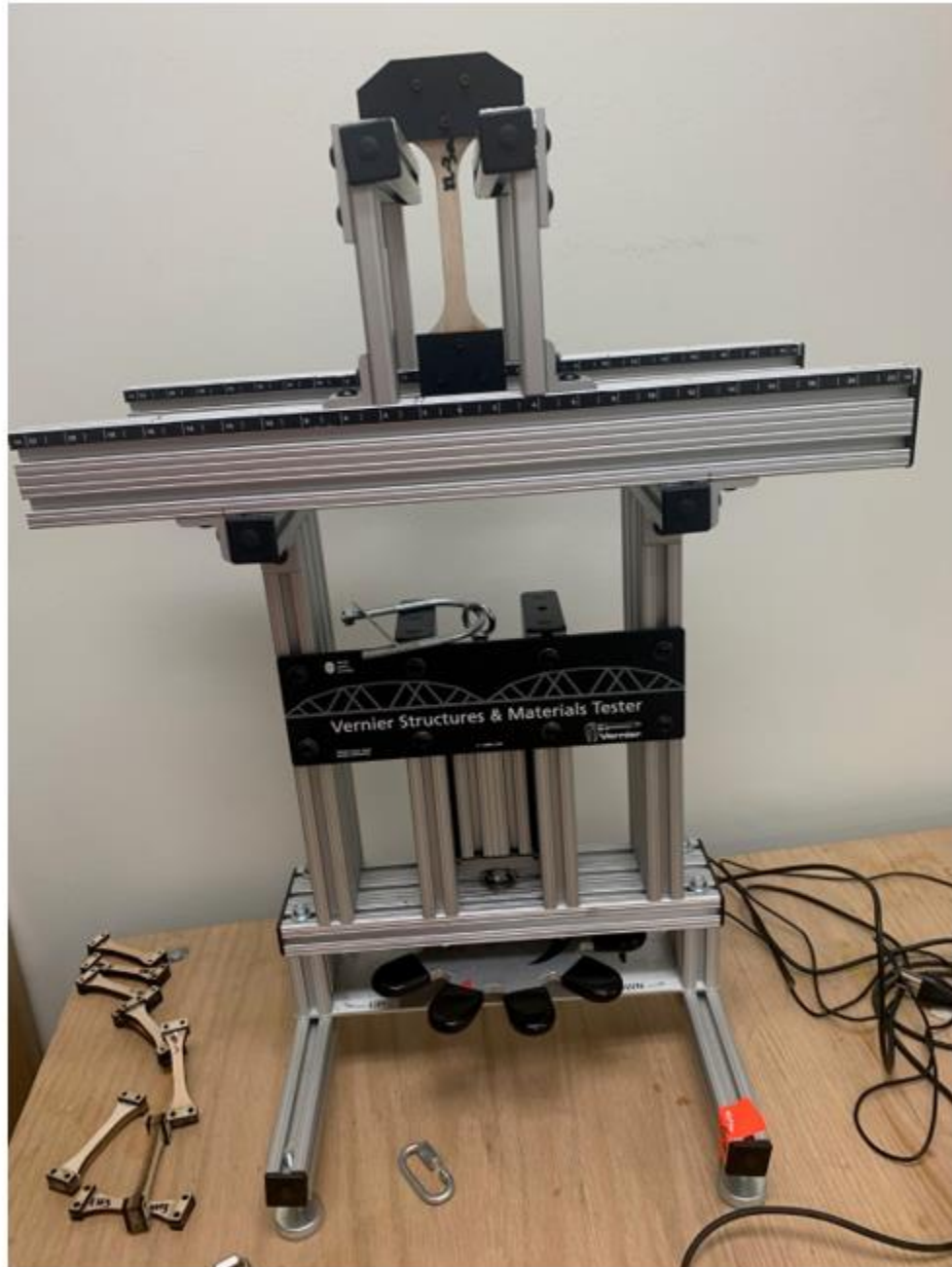
Figure 50: Test Set #3 Shown in the Modified VS&MT

Initially, the testing went on without issue. After testing the extra light and medium density 0.125" thick balsa samples, the testing for extra heavy began and there a stagnation in the force recorded started to be seen. Initially, it was not realized to be due to reaching the limitations of the load cell, it was believed to be due to a lack of displacement distance. So, a link was removed for the remainder of the testing to try to solve the displacement problem, and the last extra heavy sample failed within the range of the load cell, so the problem was thought to be solved.
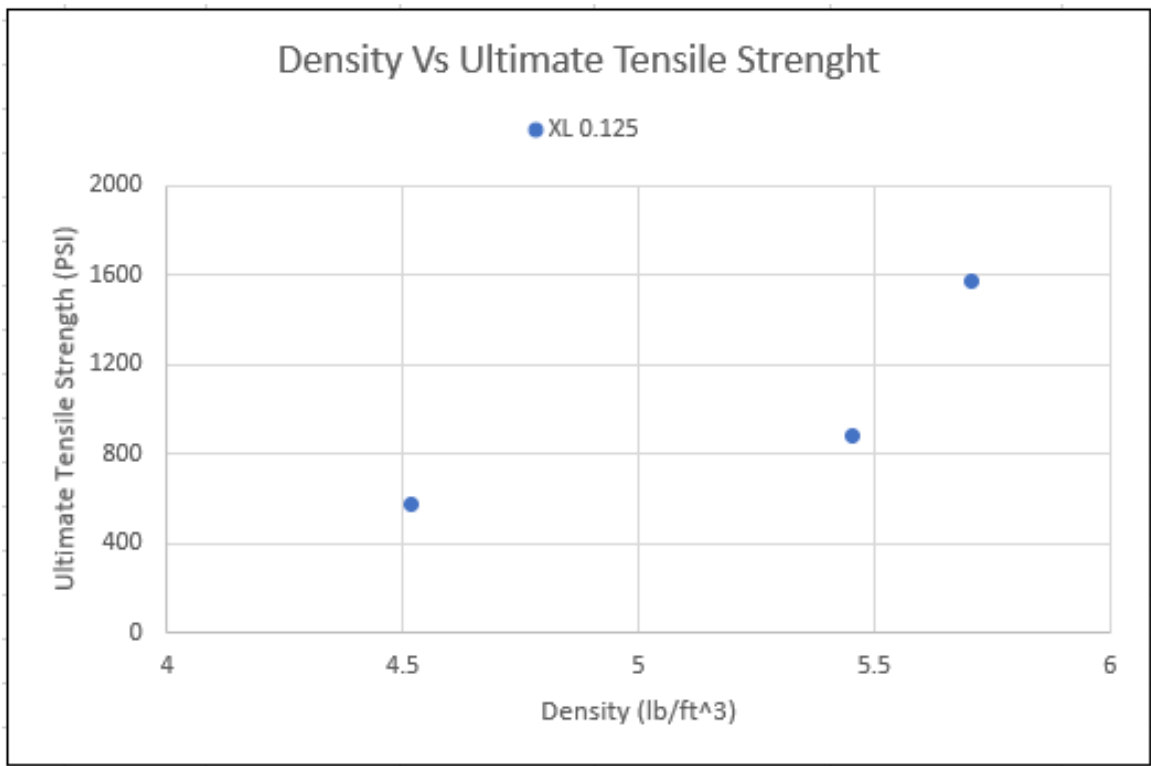
Figure 51: 0.125" Extra Light, Density Vs Ultimate Tensile Strength

However, after further testing and completing the extra light 0.25" without issues. Testing began for medium density 0.25" thick samples, and again the plateau in force at around 1100N was noticed, after this, it was discovered that the tests were reaching the top of the load cells limitations. The load cell has an operational range of 0 to 1000 N, and a safety range of 0 to 1,300 N before

damage [25]. To prevent any damage to the load cell it was decided not to move forward with the remainder of this test set. While the full scope of this testing was not able to continue due to the limitation of the data acquisition system, some data was able to be recorded.

Starting with the extra light density, no problems mechanically or with the load cell occurred during this testing. An average ultimate tensile strength can be seen at around 1009psi, but it is important to note that there is a standard deviation of over 400. This is theorized to be due to the reduced sample size not allowing for a large-scale view of this direction of testing. The 3 test results can be seen in Figure 51.

The medium grouping showed different results. The first test that was run for this density reached the maximum force for the load cell and plateaued. Initially, it was not noted that this plateau was due to reaching the limitation of the load cell but was thought to not have enough lateral distance to continue adding tension to the load cell. So, after the sample reached failure, adjustments were made. Fewer linkages were attached from the load cell to the 3D mount. Next, 2a was tested and it reached the maximum force for the load cell but the same stagnation in the force was not seen so it was not flagged as a problem initially. Then, in 3a a test force was recorded that was within the acceptable range for this load cell, which was found to be around 530 N. These results can be seen in Figure 52.
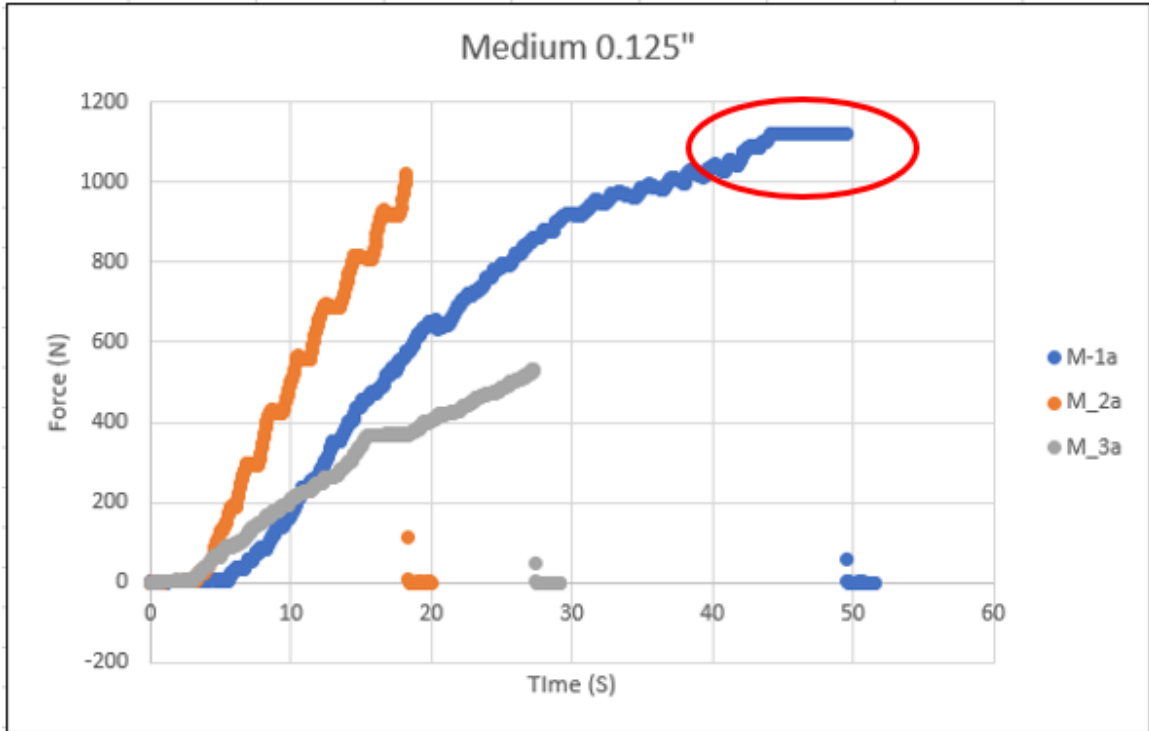
Figure 52: Medium 0.125" Density V. Force

Next was the extra heavy grouping. In Figure 53, the force verses time graph can be seen. All 3 test samples are shown. Both 1a and 2a increase and then hit a limiting force at around 1100 N, while 3a fails at around 700 N. For this test particularly, the ultimate tensile strength cannot be found since the test was limited by the load cell.
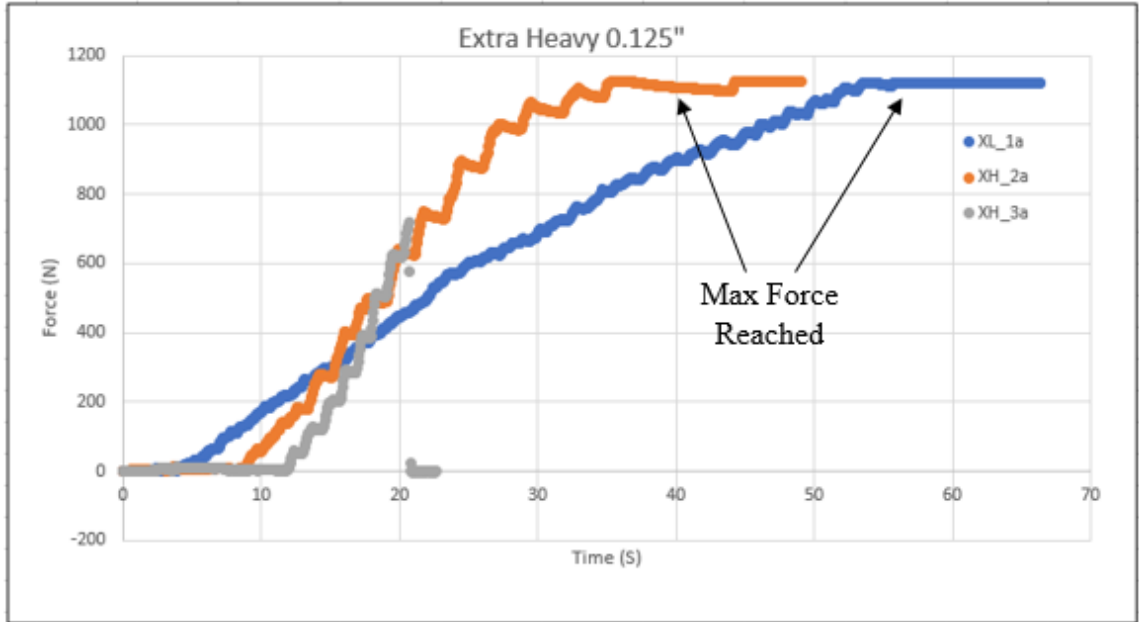
Figure 53: Extra Heavy, 0.125" Force Vs. Time

As a whole, the data for this test set can be seen below in Figure 54. With a red zone of where the load cell is in the maximum loading reached. From this figure, it is noted that the only density that had all 3 successful test sets was the extra light. With that, that is the only density classification that has the ultimate tensile strength that can be used. This can be seen in Table 14.
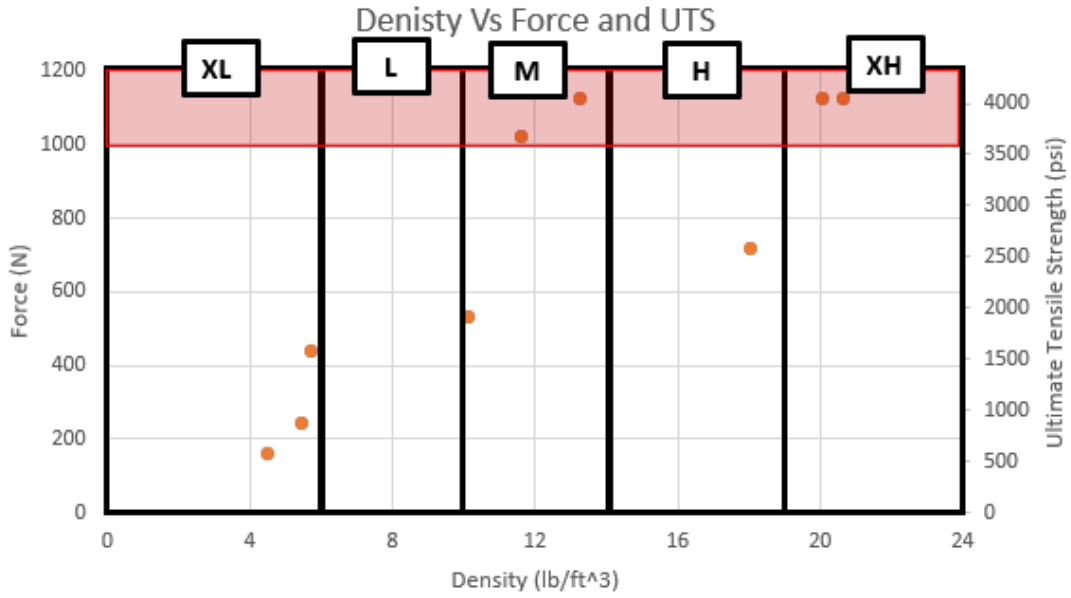
Figure 54: Test Set #3, 0.125" Samples, Density Verses Force and Ultimate Tensile

Strength

Table 14: Found Ultimate Tensile Strength Values (psi)

	Density				
	Extra Light	Light	Medium	Heavy	Extra Heavy
Direction	Ultimate Tensile Strength (PSI)				
Axial	1000	~	~	~	~
Radial	133	165	247	344	400

71

Uncertainty

With this research relying heavily on the measurements of humans and the accusation of data from the Vernier tester, it is important to understand that no device or human can perfectly record measurements. Therefore, it is important to understand the uncertainty that is associated with the measured values. It is hoped that with this analysis, a better view of the potential errors in the research can be found. With the experimentation that was done, there are a few sources for uncertainty before the experimentation starts. There is uncertainty in the laser that cuts the samples out, the human measurement of the thickness of the samples, as well as the scale to measure the weight of the samples. All of these will compound on one another when looking at the ultimate tensile strength and the density of each test sample. Additionally, there will be uncertainty in the VTSM and the recording of force.

Uncertainty Method Referenced in Kline

The uncertainty equation below shows W as the uncertainty with the subscript being the variable. With this equation the partial derivative of the equation, R, with respect to each variable of the equation, $X_1, X_2, X_3,$ and so on [26].

$$W_R = \sqrt{\left(\frac{\delta R}{\delta X_1}W_{X_1}\right)^2 + \left(\frac{\delta R}{\delta X_2}W_{X_2}\right)^2 + \cdots \left(\frac{\delta R}{\delta X_n}W_{X_n}\right)^2}$$

For this research, there are many uncertainty variables to investigate, with the most important being the uncertainty of the ultimate tensile strength of the balsa wood. To find that other

uncertainties had to be solved first, due to the propagation of uncertainties that can be seen in the equation above.

For the ultimate tensile strength, the force for breaking is noted as F and the cross-sectional area will be noted as A.

$$\sigma = \frac{F}{A}$$

The uncertainty of the cross-sectional area, U_A, has multiple variables so this value propagates. Due to this, the equation for the uncertainty of the area can be seen below.

$$A = w * t$$

$$U_A = \sqrt{\left(\frac{\delta A}{\delta w} U_w\right)^2 + \left(\frac{\delta A}{\delta t} U_t\right)^2}$$

After solving for the uncertainty terms for the cross-sectional area the ultimate tensile strength uncertainty could be found. With the uncertainty of the force recorded being noted as U_F.

$$U_\sigma = \sqrt{\left(\frac{\delta \sigma}{\delta F} U_F\right)^2 + \left(\frac{\delta \sigma}{\delta A} U_A\right)^2}$$

Using the equations above the uncertainty can be found for both the 0.125" and 0.25" thick balsa samples. Additionally, the percent uncertainty can be found.

$$\%U = \frac{U_\sigma}{\sigma} * 100$$

Table 15: 0.125" and 0.25" Thick Uncertainty Values

0.125 Thick Uncertainty					0.25 Thick Uncertainty			
Uncertainty of UTS					Uncertainty of UTS			
UTS (psi)	Force(lbf)	Uncertainty (psi)	%		UTS (psi)	Force(lbf)	Uncertainty (psi)	%
101.59	4	7.45	7.333		50.8	4	2.794	5.500
253.97	10	17.437	6.866		203	16	9.711	4.784
406.35	16	27.67	6.809		355.6	28	16.871	4.744
558.73	22	37.95	6.792		508	40	24.057	4.736

Below in Figure 55 and Figure 56, the percent uncertainty can be seen. It is noted that the thinner samples have a higher percent uncertainty. As well as the values for the percent uncertainty converge to around 6.8% for the 0.125" samples and 4.74% for the 0.25" samples.
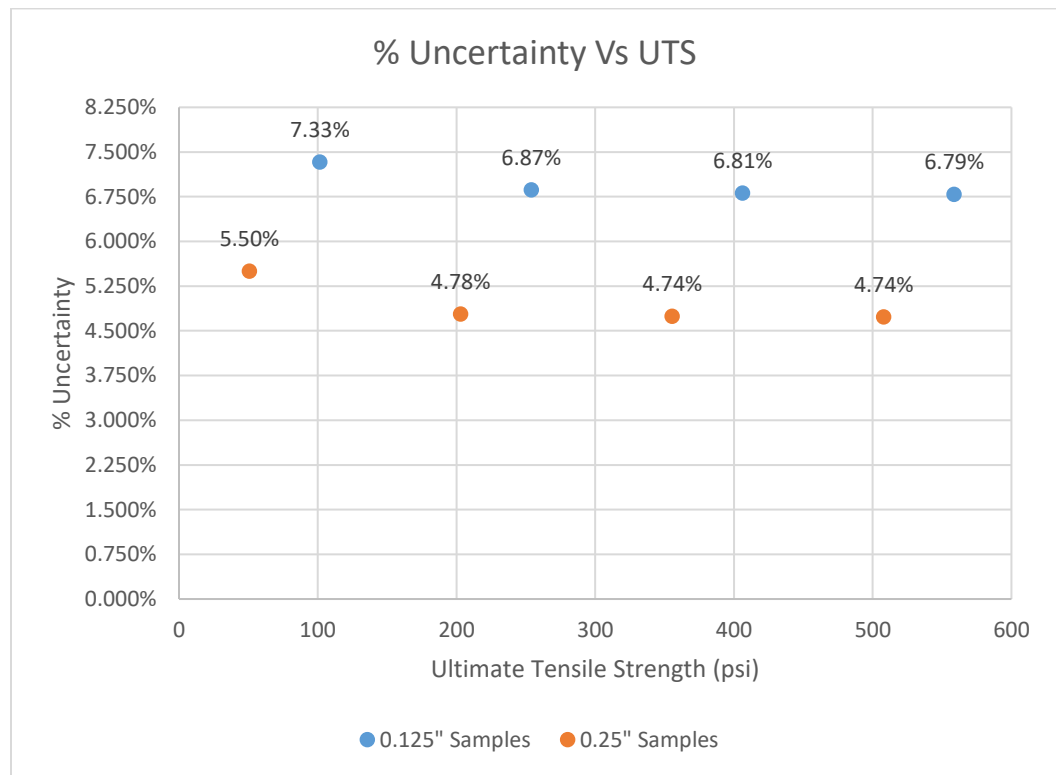
Figure 55: Percent Uncertainty Vs Ultimate Tensile Strength
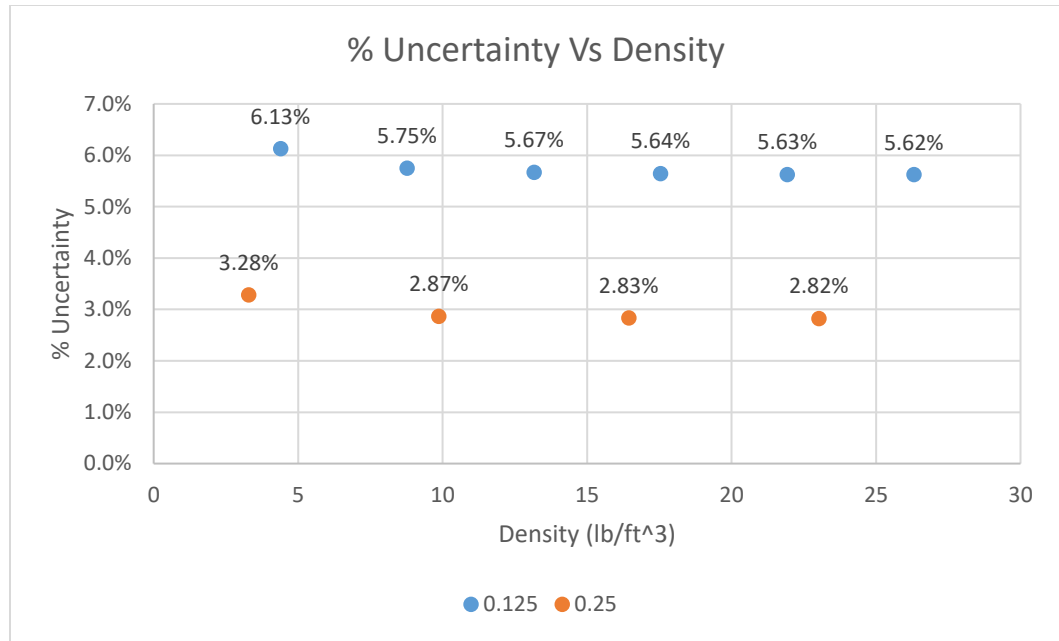
Figure 56: Percent Uncertainty Vs Density

From the data above, uncertainty bounds were found. Taking the equation for the uncertainty of ultimate tensile strength, and finding the uncertainty for the recorded values, an average upper and lower bound were input into the density verse ultimate tensile strength graph. This can be seen below in both Figure 57 and Figure 58. The first thing noticed is that as density increases, the recorded samples are more outside of the uncertainty bounds. For example, in the 0.125" uncertainty graph, after density reaches around $14 \frac{lb}{ft^3}$, or exceeds the medium density classification, a large number of the test points are outside the uncertainty bound. Similarly, the 0.25" uncertainty graph shows a trend at around $10\frac{lb}{ft^3}$, or light density, the data points are outside of the bounds.
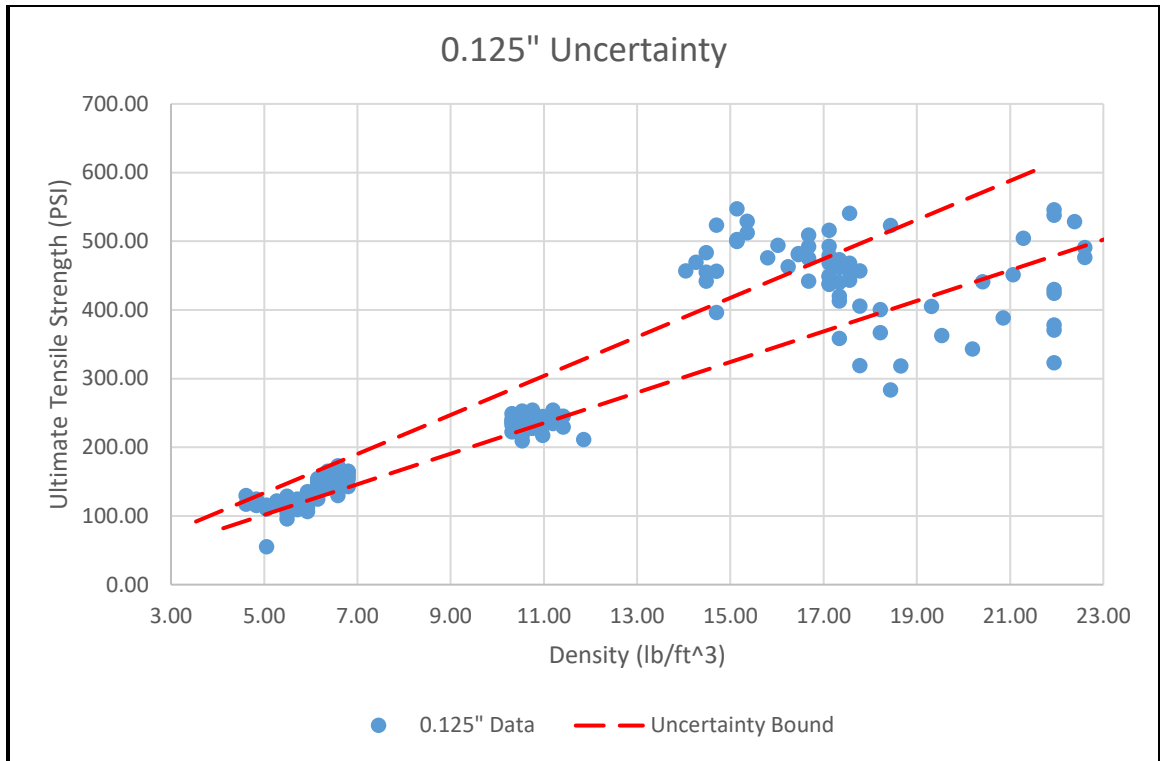
Figure 57: 0.125" Uncertainty of Ultimate Tensile Strength
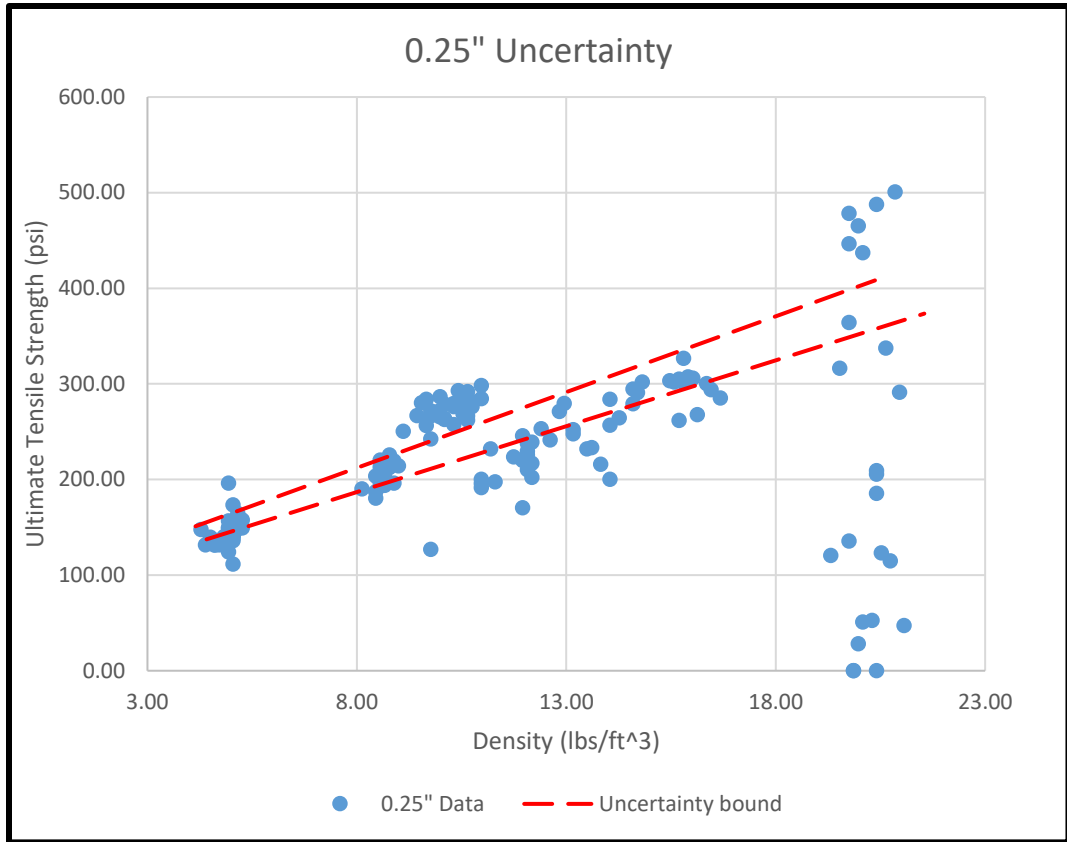
Figure 58: 0.25" Uncertainty of Ultimate Tensile Strength

With that, a closer look into the uncertainty of both the 0.125" and 0.25" thick is needed. First looking at the uncertainty for 0.125" thick balsa with a density range of extra light to medium density can be seen in Figure 59. Noticing how with the more limited data points, the data falls nicer into the uncertainty bounds that are seen above. While some data points are outside the boundaries of uncertainty, overall, the data fits nicely.
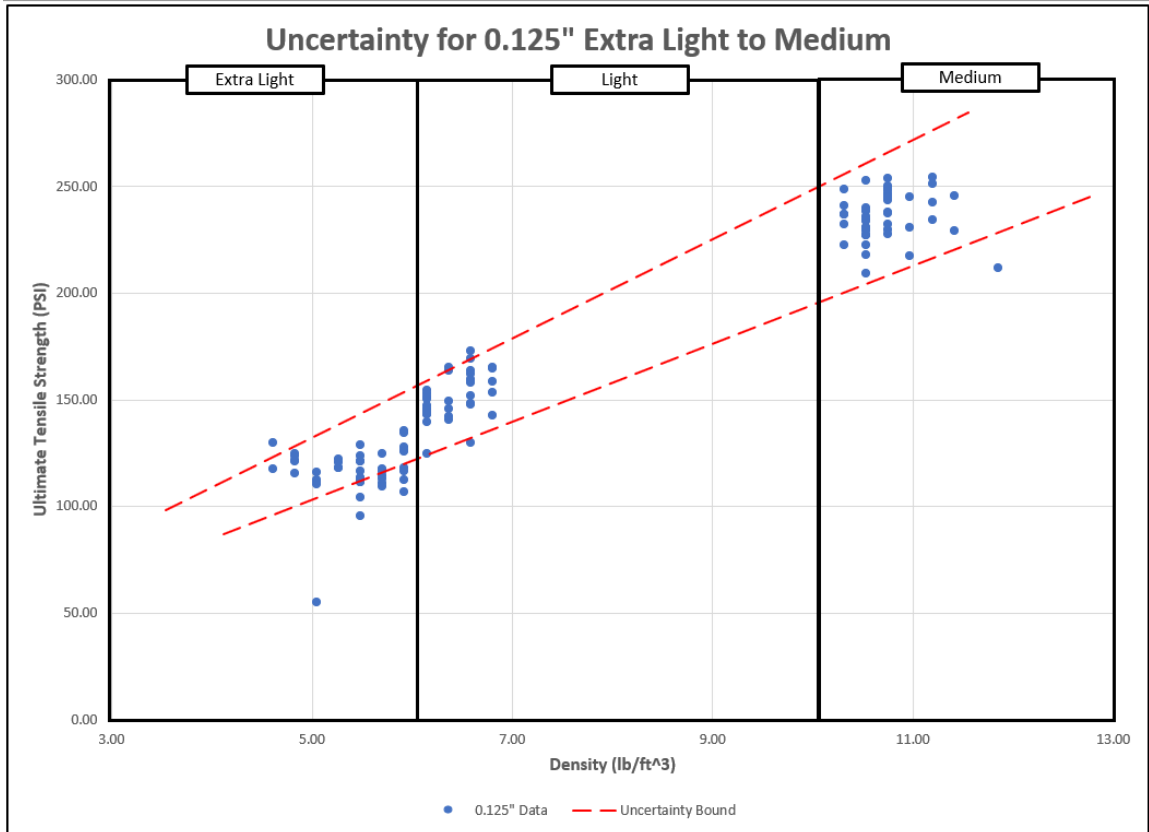
Figure 59: Uncertainty for 0.125" Extra Light to Medium Samples

Continuing to Figure 60, similar to the figure above but with fewer data points shown, the data itself fits the boundaries of uncertainty better. With the 0.25" data set, it shows that most of the test samples lie in between the bounds. Compared to Figure 58, where a large portion of the data points was outside of the uncertainty bounds, starting around medium density.
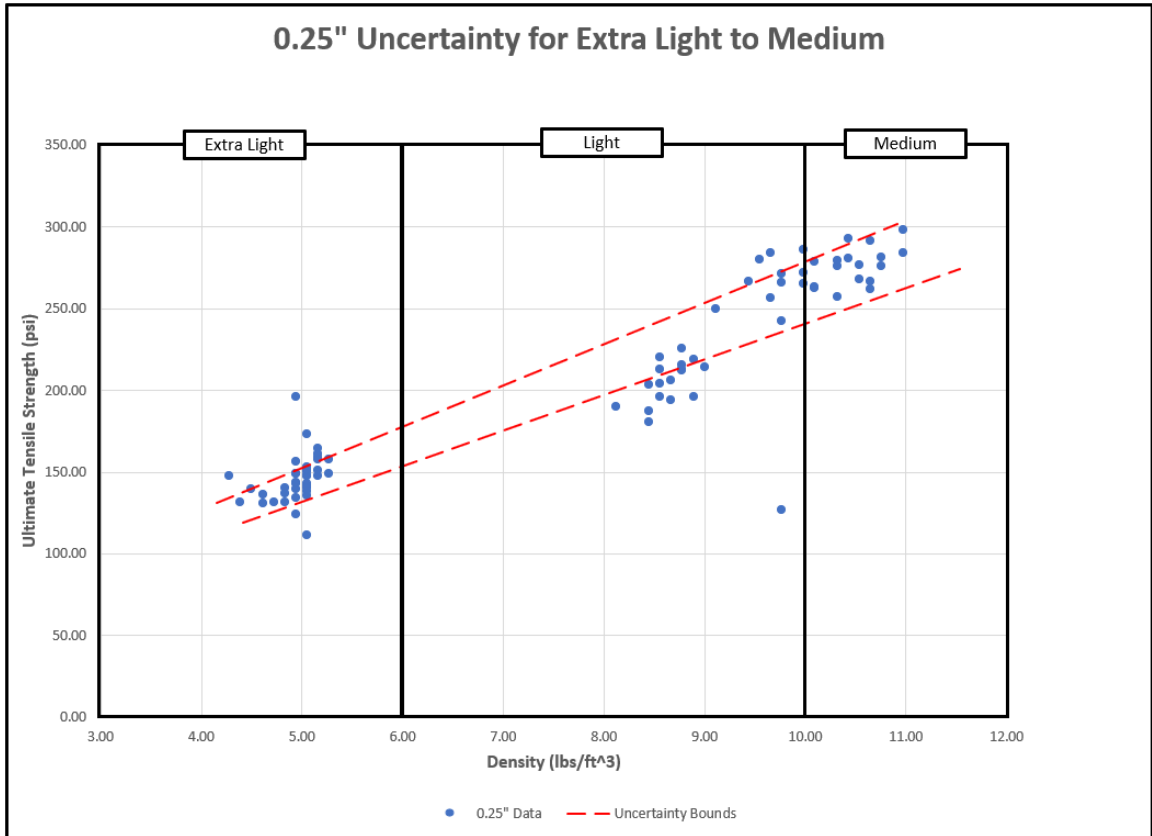
Figure 60: Uncertainty for 0.25" Extra Light to Medium Samples

Moving forward, the heavy to extra heavy data set will be labeled as not safe for aircraft use, due to most of the data that are heavy to extra heavy density being outside of the uncertainty bounds. This can be seen further below in Table 16, which shows each density classification and what aircraft structure would be the best for that density. With that, it can be seen that both heavy and extra heavy have been labeled "Not recommended for use in aircraft structure".

Table 16: Recommended Uses for each Density Classification

Density Classification	Recommended Uses
Extra Light	Core
Light	Shear Webs, Bulkheads, Ribs
Medium	Shear Webs, Bulkheads, Ribs
Heavy	Not Recommended for Use in Aircraft Structure
Extra Heavy	Not Recommended for Use in Aircraft Structure

Visual Test

This part of the testing was the hardest. After testing multiple samples and visually inspecting both before and after, the ability to start anticipating where failure would happen arose. However, not all samples can have failure location predicted. It was found that the accurately predicted failure locations were more noticeable, such as large knots on the side of the test subject, scorch marks where the laser was in contact with the side too long, or larger growth rings that display as extremely dark or light.

When trying to predict the failure location, it required more than a quick once-over. And the visual signs changed depending on the thickness of the sample. For instance, the thinner 1/8th samples were more likely to fracture at larger, traditionally whiter fibers whereas the larger ¼ inch samples would be more likely to show failure along a darker vessel.

Figure 61: XL_12, Laser Scorch

Figure 62: XL_12, Correctly Predicted Failure Location

While some of the samples that had accurate predictions of failure, failed outside of the gauge area and were not taken into consideration for ultimate tensile strength results, the findings were still valid for the visual inspection. For instance, test sample XL_12 seen in Figure 62, failed outside of that region due to what seem to be scorch marks from the laser. This test sample's results for ultimate tensile strength were disregarded but still show valuable results in this section.

Figure 63: XH_9, 0.25", Split.

Figure 64:XH_9, 0.25" Correct Failure Location

Below another failure type can be seen. In this sample, a dark, split can be seen in Figure 63. This is another instance of a very noticeable defect. Additionally, this sample failed at around 50 psi, so considerably less than the average value of 400 psi. The next specimen in Figure 65, can be seen with a similar dark line to sample XH_9. Noting that on one side it is a split and on the other side it looks to be a line of dark vessels. This test sample is also accurately predicted for failure location, and like the one before it had a lower breaking stress of 185psi. While that is higher than the specimen previously, it is still half the average value shown in Table 14: Found Ultimate Tensile Strength Values (psi).
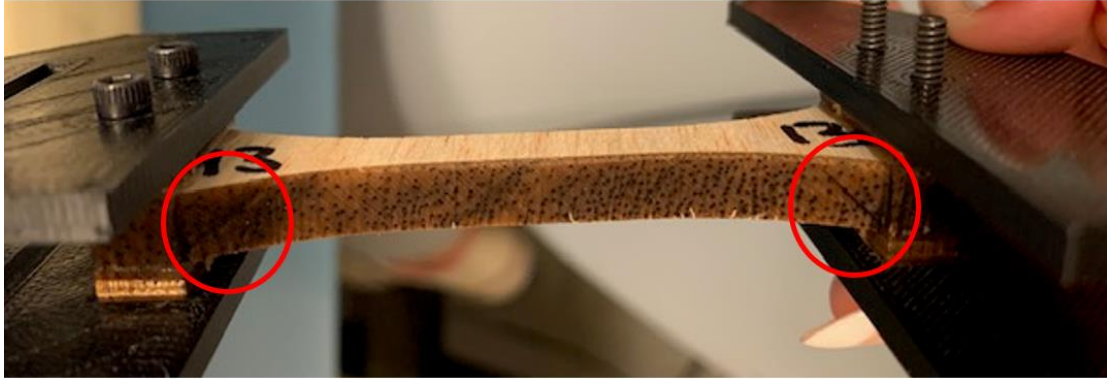
Figure 65: XH_13, 0.25" Split.

Figure 66: XH_13, Correct Failure Location Predicted

While the previous visual inspection tests were accurate, that wasn't always the case. Some classified defects were noted but failure did not occur in that location. Below in Figure 67, a small knot can be seen on the broad size of the specimen. While this is classified as a defect in most inspection articles, it can also be seen as harmless. For this sample, the knot was noted but was not the correct location of the failure. Additionally, there was no decrease in the ultimate tensile

strength like the previous results, M_19,0.125" had an ultimate tensile strength of 242 psi, which is very comparable to the recorded values that were found above. Adding to this point, test sample XL_6, 0.125" shows a dark knot. Again, this was noted and again this specimen did not fail in that location, nor did it lose any strength due to the defect. With an ultimate tensile strength of 112 psi, it is only a difference of around 16% to the average ultimate tensile strength for Extra light of 132 psi.

Figure 67: M_19, 0.25" Knot

Figure 68: XL_6, 0.125", Knot

Figure 69: XL_6, 0.125", Incorrect Prediction of Failure Location

While not every visual inspection resulted in correctly identifying a failure location, some trends were able to be found. Starting with 0.25" thick balsa samples were more likely to have defects of splits near the shoulder of the specimen. Alternately, 0.125" thick samples had defects

predominantly of knots or laser marks. Along with this, knots are not as detrimental to the strength of balsa wood in comparison to manufacturing-made scorches or the dark like of the rays, or fracture.

Something important to note is that while not every sample was predicted, the ones that were accurately predicted, traditionally had a lower ultimate tensile strength. This shows that quality control of balsa wood can be implemented if knowledge of what to look for is known.

CHAPTER V

DISCUSSION AND RECOMMENDATIONS

This final chapter will discuss all the testing that has taken place and the knowledge gained throughout the research done. The two main goals of this thesis were to investigate the microstructure of balsa shear webs in composite wing spars and how it might affect failure, as well as to find if there is the ability to predict failure based on visual inspection of balsa wood sheets. Additional objectives were to investigate the phenomenon found that thicker denser balsa fails at a lower rate than the thinner less dense sheets, create a test procedure for visual inspection, and compare findings to previous results.

With preliminary testing it was found that results were dependent on the grain direction, therefore test set 1 was inconclusive. Once grain direction was able to be accurately selected, further testing into the microstructural properties versus strength characteristics were able to be found. From these findings it was apparent that the microstructure plays a large role in the strength properties of balsa wood. It is apparent that ray cells have a high impact on the strength characteristics of balsa wood, specifically when loaded in the radial direction and as density increases. More specifically as the density increases and ray cells increase in size and frequency ultimate tensile strength becomes less predictable. Additionally, it is noted that there was some failure associated with vessels.

This is due to a similar occurrence with the increase and size and frequency of vessels with respect to density. This trend was seen in Figure 10: Zoomed-in View of Balsa Cross Section at Multiple Densities. Rays help to reinforce the radial and tangential direction and increase in ray cells can also increase Young's modulus [5]. Additionally, as density increases, the S2 layer of the cell increases, and the S2 layer impacts stiffness, which is what this thesis theorizes created the discrepancy between the thicker denser balsa and thinner less dense balsa sheets. It can be noted that as density increases so does Young's modulus which further shows this increase in stiffness as density increases [8]. Since the thinner less dense balsa sheets behave more ductile there is more compliance in the tensile testing than the thicker samples that have a sudden failure.

This thesis concludes that the abnormal scattering that is seen at higher level densities for balsa can be attributed to the microstructure of the balsa wood, more specifically an increase in the S2 layer and ray cells which causes the wood to become stiffer and fail less uniformly. From these findings it was decided to reduce the potential useful range of density from extra light through extra heavy to extra light through medium. This reduction in density range was due to the unpredictably in the ultimate tensile strength as density increase.

Moving on to the next goal, which was to investigate the ability to visually inspect and find failure locations in balsa wood. It can be seen in the section on visual testing that while not every sample was able to be accurately labeled and failure found, failure locations were able to still be found and analyzed. It can also be noted that the failure location that was found to fail at a considerably lower level. This means that there is potential to quality check and find failures that could cause a shear web to fail before expected.

The research done to understand the failure due to the microstructure as well as investigating methods for visually inspecting balsa wood was completed. This research will further help to understand balsa wood which is one of the main materials used for UAV shear webs and

other structural components. While the questions asked in the beginning were answered new questions were posed to further the knowledge of the use of balsa shear webs.

Recommendations

To Supplement this research, it is recommended to find a new testing apparatus. While the Vernier Materials & Structure Tester worked great for the scope of the first two tensile test sets, it was not capable of being used when testing for ultimate tensile strength for the force loaded in the axial direction. Additionally, if ever testing balsa wood that is thicker than 0.25" the same operational limit will be exceeded. Along with this, it would be useful to see the results from the tensile test loaded in the longitudinal direction to get a better understanding of balsa, as well as the traditionally loaded direction for tensile tests run on wood. Expanding on this, further testing utilizing different grain cuts (A and C grain) of balsa wood could be useful in further understanding balsa wood's strength characteristics.

Furthermore, it would be interesting to see a shear web visually inspected and marked for defects before bonding to spar caps to see if the visual inspection that was found above will translate to failure in shear webs. And in the future, it could be useful to expand upon the visual inspection process that was established in this research. Additionally, it is recommended that further testing takes place on different thicknesses of balsa wood and different layering methods. For example, does layering 2- 0.125" thick tensile tests show double the strength to 1 layer of 0.125" thick, as well as does the 2 layers have a higher value ultimate tensile strength value in comparison to the 0.25" thick balsa.

Along with further research recommendations, recommendations for the manufacturing of balsa shear webs were found. When going through the manufacturing process, it is important to keep the balsa wood as flat as possible before manufacturing to prevent wrapping. Along

procedures for manufacturing balsa wood, Table 17 has been created for future projects as the GSD lab at Oklahoma State University.

Manufacturing Procedures:

1. Verify that the balsa wood is secured with enough support to prevent bowing or movement during lasering.
2. Verify the correct power and speed setting for the laser are being used. (If using heavy or extra heavy increase power)
3. Do not utilize tabs during the laser process.
4. Promptly retrieve the cut sample from the bottom of the bed to prevent excessive scorching.

Table 17:Recommended Density and Grain Classification For each Structural Member

Structural Members	Density	Grain
Core	Extra Light-Light	A
Shear Webs	Light-Medium	B, C
Ribs	Light-Medium	B, C
Bulkheads	Light-Medium	B, C

In conclusion, the research presented in this paper found that microstructure plays a significant role in the strength properties of balsa wood with both rays and vessels affecting the ultimate tensile strength of balsa wood. Additionally, visual inspection can help to locate failure in balsa wood. It is hoped that this research will contribute to the understanding of balsa wood.

REFERENCES

Z. T. Watkins, "Modeling and Failure analysis of composite I-Beams for UAV wing spar desing," ShareOK, Stillwater, 2020.

1]

"The Wood Database," Eric Meier, [Online]. Available: https://www.wood-database.com/balsa/. [Accessed 9 January 2023].

2]

"Specialized Balsa Wood," Specializedbalsa, [Online]. Available: https://specializedbalsa.com/balsa_grain_classification.php. [Accessed 9 January 2023].

3]

M. Chilson, "All about Balsa," RCSCALEBUILDER, [Online]. Available: https://www.rcscalebuilder.com/tutorials/balsa/balsa_1.htm. [Accessed 9 January 2023].

4]

O. Shishkina, S. V. Lomov, I. Verpoest and L. Gorbatikh, "Structure–property relations for balsa wood as a function of denisty: modelling approah," *Arrchive of Applied Mechanics,* vol. 84, pp. 789-805, 2014.

5]

M. Borrega, P. Ahvenainen, R. Serimaa and L. Gibson, "Composition and structure of balsa (Ochroma Pyramidale) wood," *Wood Science Technology,* no. 49, pp. 403-420, 2015.

6]

M. Vural and G. Ravichanran, "Microstructural aspects and modeling of failure in naturally occuring porous composites," *Mechanics of Materials,* no. 35, pp. 523-536, 2003.

7]

M. Borrega and L. J. Gibson, "Mechanics of Balsa (Ochroma Pyramidale) wood,"

8] *Mechanics of Materials,* vol. 84, pp. 75-90, 2015.

G. Newas, M. Mayeed and A. Rasul, "Characterization of balsa wood mechanical

9] properties required for continuum damage mechanics analysis," *Materials: Design and Applications,* vol. 230, no. 1, pp. 206-218, 2014.

I. Cave and L. Hutt, "The Longitudinal Young's Modulus of Pinus Radiata," *Wood*

10] *Science and Technology,* vol. 3, pp. 40-48, 1969.

"Orthotropic Material, From Wikipedia," Wikimedia Foundation, 18 August 2022.

11] [Online]. Available: https://en.wikipedia.org/wiki/Orthotropic_material. [Accessed 9 January 2023].

D. W. Green, "Wood: Strength and Stiffness," in *Encyclopedia of Materials:*

12] *Science and Technology*, Madison, USDA Forest Services, 2001, pp. 9732-9736.

D. Wertheimer, "Branching out wood," 2019. [Online]. Available:

13] https://www.branchingoutwood.com/blog/wood-movement-and-moisture. [Accessed 30 January 2023].

K. E. Easterling, R. Harrysson, L. J. Gibson and M. F. Ashby, "On the Mecahnics

14] of Balsa and Other Woods," *Mathematical and Physical Sciences,* vol. 383, no. 1784, pp. 31-41, 1982.

A. Da Silva and S. Kyriakides, "Compressive response and failure of balsa wood,"

15] *International Journal of Solids and Structures,* vol. 44, pp. 8685-8717, 2007.

M. Kryl, L. Danys, R. Jaros, R. Martinek, P. Kodytek and P. Bilik, "Wood Recognition and Quality Imaging Inspection Systems," *Journal of Sensors,* vol. 2020, pp. 1-19, 2020.

[16]

O. Silven, M. Niskanen and H. Kauppinen, "Wood inspection with non-supervised clustering," *Machine Vision adn Applications ,* vol. 13, pp. 275-285, 2003.

[17]

L. J. Markwardt and W. G. Youngquist, "TENSION TEST METHODS FOR WOOD, WOOD-BASE MATERIALS,," United States Department of Agriculture Forest Service, Madison, 1962.

[18]

"Introduction to Tenisle Testing," in *Tensile Testing, Second Edition*, ASM Interantional, 2004, pp. 1-12.

[19]

"Questions Pro," QuesitonsPro Survey Software, 2023. [Online]. Available: https://www.questionpro.com/sample-size-calculator/. [Accessed 14 March 2023].

[20]

"National Balsa," National Balsa Wood2, [Online]. Available: https://www.nationalbalsa.com/. [Accessed 15 December 2022].

[21]

J. Bodin and B. Jayne, in *Mechanics of Wood and Wood Composites*, Krieger Publishing, 1993, pp. 5,291,297,299,305.

[22]

E. Poverly, "Revolutionized," Revolutionized, 24 FEBRUARY 2023. [Online]. Available: https://revolutionized.com/bearing-stress/#:~:text=How%20to%20Prevent%20Bearing%20Stress%20Failures%201%20Calc

[23]

ulate,4%20Monitor%20Stress%20Points%20With%20IoT%20Sensors%20. [Accessed 16 march 2023].

24] K. Chaudhri, "Engineering Gallery," Engineering Gallery, 11 August 2015. [Online]. Available: https://www.engineersgallery.com/bearing-stress/#:~:text=A%20localised%20compressive%20stress%20at%20the%20surface%20of,of%20riveted%20joints%2C%20cotter%20joints%2C%20knuckle%20joints%2C%20etc.. [Accessed 16 March 2023].

25] "Vernier Science Eduation," Vernier Science Eduation, [Online]. Available: https://www.vernier.com/product/vernier-structures-materials-tester/. [Accessed 2023 17 March].

26] S. J. Kline, "The Purposes of Uncertainty Analysis," *Journal of Fluids Engineering,* vol. 107, no. 2, pp. 153-160, 1985.

27] D. W. Bryer, R. C. Pankhurst and National Physical Laboratory, Pressure-Probe methods for determining wind speed and flow direction, London: H.M.S.O, 1971.

28] "Hankinson's Equation From Wikipedia," Wikimedia Foundation, [Online]. Available: https://en.wikipedia.org/wiki/Hankinson%27s_equation. [Accessed 9 january 2023].

APPENDICIES

Test set #1

label	thickness	weight (g)	area (in^2	vol(in^3)	lb/ft3	Max F	light /med	UTSs psi
a1	0.125	0.26	1.39	0.17375	5.70068	42.0609	XL	240.175
a2	0.125	0.27	1.39	0.17375	5.91994	39.4271	XL	225.135
a3	0.125	0.27	1.39	0.17375	5.91994	40.8144	XL	233.057
a4	0.125	0.27	1.39	0.17375	5.91994		XL	
a5	0.125	0.27	1.39	0.17375	5.91994		XL	
a6	0.125	0.28	1.39	0.17375	6.13919	42.0609	L	240.175
a7	0.125	0.27	1.39	0.17375	5.91994	37.7383	XL	215.491
a8	0.125	0.26	1.39	0.17375	5.70068		XL	
a9	0.125	0.25	1.39	0.17375	5.48142		XL	
a10	0.125	0.24	1.39	0.17375	5.26216		XL	
a11	0.125	0.26	1.39	0.17375	5.70068	36.7531	XL	209.866
a12	0.125	0.27	1.39	0.17375	5.91994	38.0398	XL	217.213
a13	0.125	0.27	1.39	0.17375	5.91994		XL	
a14	0.125	0.26	1.39	0.17375	5.70068	36.8134	XL	210.21
a15	0.125	0.25	1.39	0.17375	5.48142		XL	
a16	0.125	0.27	1.39	0.17375	5.91994	36.8134	XL	210.21
a17	0.125	0.25	1.39	0.17375	5.48142		XL	
a18	0.125	0.26	1.39	0.17375	5.70068	37.1753	XL	212.277
a19	0.125	0.23	1.39	0.17375	5.04291	39.206	XL	223.872
a20	0.125	0.23	1.39	0.17375	5.04291		XL	
a21	0.125	0.25	1.39	0.17375	5.48142	40.0303	XL	228.579
a22	0.125	0.24	1.39	0.17375	5.26216		XL	
a23	0.125	0.27	1.39	0.17375	5.91994		XL	
a24	0.125	0.25	1.39	0.17375	5.48142		XL	
a25	0.125	0.25	1.39	0.17375	5.48142	46.1424	XL	263.48
a26	0.125	0.24	1.39	0.17375	5.26216	37.5573	XL	214.458
a27	0.125	0.25	1.39	0.17375	5.48142	39.1456	XL	223.528
a28	0.125	0.25	1.39	0.17375	5.48142		XL	
a29	0.125	0.26	1.39	0.17375	5.70068	43.7096	XL	249.589
a30	0.125	0.27	1.39	0.17375	5.91994		XL	
a31	0.125	0.25	1.39	0.17375	5.48142	41.699	XL	238.108
a32	0.125	0.24	1.39	0.17375	5.26216	36.2102	XL	206.766
a33	0.125	0.24	1.39	0.17375	5.26216	42.0609	XL	240.175
a34	0.125	0.24	1.39	0.17375	5.26216	39.6684	XL	226.513
a35	0.125	0.24	1.39	0.17375	5.26216		XL	
a36	0.125	0.24	1.39	0.17375	5.26216	40.5128	XL	231.335

label	thickness	weight (g)	area (in^2)	vol(in^3)	density(lb/ft^3)	Max F	UTSs psi
a37	0.25	0.57	1.39	0.3475	1.64	54.1645	154.644
a38	0.25	0.56	1.39	0.3475	1.61	72.0584	205.733
a39	0.25	0.58	1.39	0.3475	1.67	72.4606	206.881
a40	0.25	0.6	1.39	0.3475	1.73	77.7483	221.978
a41	0.25	0.62	1.39	0.3475	1.78	83.4985	238.395
a42	0.25	0.58	1.39	0.3475	1.67	65.2427	186.273
a43	0.25	0.58	1.39	0.3475	1.67	73.0235	208.488
a44	0.25	0.53	1.39	0.3475	1.53	65.9665	188.339
a45	0.25	0.59	1.39	0.3475	1.70	74.5918	212.965
a46	0.25	0.58	1.39	0.3475	1.67	70.9325	202.518
a47	0.25	0.68	1.39	0.3475	1.96	101.111	288.68
a48	0.25	0.72	1.39	0.3475	2.07	109.716	313.248
a49	0.25	0.62	1.39	0.3475	1.78		
a50	0.25	0.67	1.39	0.3475	1.93	80.9451	231.105
a51	0.25	0.71	1.39	0.3475	2.04	107.344	306.475
a52	0.25	0.57	1.39	0.3475	1.64	74.6119	213.023
a53	0.25	0.68	1.39	0.3475	1.96	95.1597	271.689
a54	0.25	0.54	1.39	0.3475	1.55	66.2077	189.028
a55	0.25	0.58	1.39	0.3475	1.67	77.4467	221.117
a56	0.25	0.69	1.39	0.3475	1.99	82.3726	235.18
a57	0.25	0.57	1.39	0.3475	1.64	71.1135	203.035
a58	0.25	0.63	1.39	0.3475	1.81	86.6953	247.522
a59	0.25	0.56	1.39	0.3475	1.61	73.5463	209.98
a60	0.25	0.54	1.39	0.3475	1.55	67.4945	192.702
a61	0.25	0.64	1.39	0.3475	1.84	80.6837	230.358
a62	0.25	0.66	1.39	0.3475	1.90	62.9305	179.672
a63	0.25	0.58	1.39	0.3475	1.67		
a64	0.25	0.59	1.39	0.3475	1.70	83.9408	239.658
a65	0.25	0.58	1.39	0.3475	1.67	79.3166	226.455
a66	0.25	0.61	1.39	0.3475	1.76	103.202	294.65
a67	0.25	0.65	1.39	0.3475	1.87		
a68	0.25	0.59	1.39	0.3475	1.70	64.7802	184.953
a69	0.25	0.56	1.39	0.3475	1.61	72.36	206.594
a70	0.25	0.62	1.39	0.3475	1.78	70.6511	201.714
a71	0.25	0.67	1.39	0.3475	1.93		
a72	0.25	0.6	1.39	0.3475	1.73	75.9187	216.754
a73	0.25	0.63	1.39	0.3475	1.81	87.8614	250.851
a74	0.25	0.71	1.39	0.3475	2.04	112.33	320.711

label	thickness (in)	weight (g)	area (in^2)	vol(in^3)	density(lb/	Max F	stress
R_DB_1	0.25	0.57	1.39	0.3475	1.64	53.7624	153.496
R_DB_2	0.25	0.59	1.39	0.3475	1.70	56.356	160.901
R_DB_3	0.25	0.57	1.39	0.3475	1.64	55.1296	157.399
R_DB_4	0.25	0.56	1.39	0.3475	1.61	52.0333	148.559
R_DB_5	0.25	0.59	1.39	0.3475	1.70	54.8481	156.596
R_DB_6	0.25	0.57	1.39	0.3475	1.64	49.6609	141.786
R_DB_7	0.25	0.63	1.39	0.3475	1.81	57.9242	165.378
R_DB_8	0.25	0.61	1.39	0.3475	1.76	54.0439	154.3
R_DB_9	0.25	0.64	1.39	0.3475	1.84	48.3942	138.169
R_DB_10	0.25	0.62	1.39	0.3475	1.78	49.9021	142.475
R_DB_11	0.25	0.59	1.39	0.3475	1.70	56.1147	160.212
R_DB_12	0.25	0.62	1.39	0.3475	1.78	56.8184	162.221
R_DB_13	0.25	0.6	1.39	0.3475	1.73	55.3507	158.031
R_DB_14	0.25	0.57	1.39	0.3475	1.64	51.4502	146.895
R_DB_15	0.25	0.6	1.39	0.3475	1.73	55.1095	157.342
R_DB_16	0.25	0.58	1.39	0.3475	1.67	51.1889	146.148
R_DB_17	0.25	0.59	1.39	0.3475	1.70	51.7317	147.698
R_DB_18	0.25	0.62	1.39	0.3475	1.78	45.6196	130.248
R_DB_19	0.25	0.64	1.39	0.3475	1.84	56.9793	162.68
R_DB_20	0.25	0.63	1.39	0.3475	1.81	59.3919	169.569
R_DB_21	0.25	0.63	1.39	0.3475	1.81	55.4714	158.375
R_DB_22	0.25	0.61	1.39	0.3475	1.76	52.0735	148.674
R_DB_23	0.25	0.58	1.39	0.3475	1.67	55.592	158.72
R_DB_24	0.25	0.59	1.39	0.3475	1.70	51.8323	147.985
R_DB_25	0.25	0.64	1.39	0.3475	1.84	56.8385	162.279
R_DB_26	0.25	0.6	1.39	0.3475	1.73	46.0419	131.453

label	thickness	weight (g)	area (in^2)	vol(in^3)	density(lb/ft^3)	Max F
R_DB_1	0.125	0.4	1.39	0.17375	2.30	38.9044
R_DB_2	0.125	0.39	1.39	0.17375	2.24	38.9848
R_DB_3	0.125	0.33	1.39	0.17375	1.90	34.2399
R_DB_4	0.125	0.36	1.39	0.17375	2.07	32.5711
R_DB_5	0.125	0.33	1.39	0.17375	1.90	31.6463
R_DB_6	0.125	0.39	1.39	0.17375	2.24	37.2959
R_DB_7	0.125	0.41	1.39	0.17375	2.36	42.3625
R_DB_8	0.125	0.41	1.39	0.17375	2.36	39.8091
R_DB_9	0.125	0.39	1.39	0.17375	2.24	40.171
R_DB_10	0.125	0.34	1.39	0.17375	1.96	33.6166
R_DB_11	0.125	0.37	1.39	0.17375	2.13	31.3849
R_DB_12	0.125	0.42	1.39	0.17375	2.42	41.1964
R_DB_13	0.125	0.4	1.39	0.17375	2.30	42.5033
R_DB_14	0.125	0.34	1.39	0.17375	1.96	29.9775
R_DB_15	0.125	0.33	1.39	0.17375	1.90	29.696
R_DB_16	0.125	0.34	1.39	0.17375	1.96	36.17
R_DB_17	0.125	0.41	1.39	0.17375	2.36	37.9795
R_DB_18	0.125	0.37	1.39	0.17375	2.13	26.7405
R_DB_19	0.125	0.4	1.39	0.17375	2.30	38.1404
R_DB_20	0.125	0.4	1.39	0.17375	2.30	39.6885
R_DB_21	0.125	0.34	1.39	0.17375	1.96	38.824
R_DB_22	0.125	0.41	1.39	0.17375	2.36	39.8895
R_DB_23	0.125	0.4	1.39	0.17375	2.30	44.353
R_DB_24	0.125	0.34	1.39	0.17375	1.96	38.7435
R_DB_25	0.125	0.4	1.39	0.17375	2.30	39.6081

Test set #2 Data.

number	XS (in)	area (in^2)	Thickness (in)	Weight (g)	density (lb/ft^2)	Force lb	stress psi
XH_1	0.31496	1.3887	0.125	0.78	17.11804453	17.645755	448.203075
XH_2	0.31496	1.3887	0.125	0.79	17.33750664	17.320322	439.937046
XH_4	0.31496	1.3887	0.125	0.78	17.11804453	18.441259	468.40892
XH_5	0.31496	1.3887	0.125	0.78	17.11804453	19.39948	492.747789
XH_7	0.31496	1.3887	0.125	0.79	17.33750664	18.188144	461.97979
XH_8	0.31496	1.3887	0.125	0.79	17.33750664	16.542897	420.190422
XH_11	0.31496	1.3887	0.125	1	21.94621093	16.91353	429.604511
XH_12	0.31496	1.3887	0.125	0.97	21.28782461	19.851471	504.228379
XH_14	0.31496	1.3887	0.125	0.95	20.84890039	15.295402	388.503981
XH_15	0.31496	1.3887	0.125	0.93	20.40997617	17.37004	441.199911
XH_16	0.31496	1.3887	0.125	0.92	20.19051406	13.500997	342.926015
XH_17	0.31496	1.3887	0.125	0.83	18.21535508	15.769992	400.558606
XH_19	0.31496	1.3887	0.125	0.85	18.65427929	12.533736	318.357542
XH_20	0.31496	1.3887	0.125	0.89	19.53212773	14.282942	362.787447
XH_21	0.31496	1.3887	0.125	1	21.94621093	14.88409	378.056638
XH_23	0.31496	1.3887	0.125	1.03	22.60459726	19.327162	490.910888
XH_24	0.31496	1.3887	0.125	1	21.94621093	12.728093	323.294199
XH_25	0.31496	1.3887	0.125	0.81	17.77643086	17.989268	456.928328
XH_26	0.31496	1.3887	0.125	0.81	17.77643086	15.959829	405.380455
XH_27	0.31496	1.3887	0.125	0.81	17.77643086	12.547296	318.701961
XH_28	0.31496	1.3887	0.125	0.83	18.21535508	14.441139	366.805653
XH_31	0.31496	1.3887	0.125	0.8	17.55696875	18.4277	468.064504
XH_32	0.31496	1.3887	0.125	0.79	17.33750664	16.262662	413.072453
XH_33	0.31496	1.3887	0.125	0.8	17.55696875	17.91243	454.976625
XH_34	0.31496	1.3887	0.125	0.78	17.11804453	17.257043	438.329763
XH_35	0.31496	1.3887	0.125	1.02	22.38513515	20.814212	528.682049
XH_36	0.31496	1.3887	0.125	1	21.94621093	21.496719	546.017749
XH_37	0.31496	1.3887	0.125	1	21.94621093	14.590296	370.59425
XH_38	0.31496	1.3887	0.125	1	21.94621093	16.705614	424.32344
XH_40	0.31496	1.3887	0.125	1	21.94621093	21.184845	538.096134
XH_41	0.31496	1.3887	0.125	1.05	23.04352148	22.332902	567.25685
XH_42	0.31496	1.3887	0.125	0.76	16.67912031	14.979008	380.467564
XH_44	0.31496	1.3887	0.125	0.97	21.28782461	19.761073	501.932258
XH_45	0.31496	1.3887	0.125	0.97	21.28782461	20.818732	528.796855
XH_46	0.31496	1.3887	0.125	1	21.94621093	20.601777	523.286171

number	XS(in)	area (in^2)	Thickness (in)	Weight (g)	density (lb/ft^2)	Force (lb)	stress (psi)
XH_1	0.31496	1.3887	0.25	1.82	19.97105195	36.6248587	465.136636
XH_2	0.31496	1.3887	0.25	1.8	19.75158984	37.6553982	478.2245136
XH_3	0.31496	1.3887	0.25	1.86	20.40997617	16.4750983	209.234167
XH_5	0.31496	1.3887	0.25	1.9	20.84890039	39.4226833	500.669079
XH_7	0.31496	1.3887	0.25	1.8	19.75158984	10.6715334	135.5287448
XH_10	0.31496	1.3887	0.25	1.91	20.95863144	22.9204904	291.0908105
XH_11	0.31496	1.3887	0.25	1.8	19.75158984	35.1423281	446.3084596
XH_12	0.31496	1.3887	0.25	1.86	20.40997617	38.3831039	487.4663939
XH_13	0.31496	1.3887	0.25	1.86	20.40997617	14.5993354	185.4119306
XH_14	0.31496	1.3887	0.25	1.78	19.53212773	24.8911715	316.1185099
XH_15	0.31496	1.3887	0.25	1.83	20.080783	34.4055826	436.9517734
XH_16	0.31496	1.3887	0.25	1.76	19.31266562	9.4737571	120.3169558
XH_17	0.31496	1.3887	0.25	1.8	19.75158984	28.6743364	364.1648006
XH_18	0.31496	1.3887	0.25	1.86	20.40997617	16.1858241	205.5603767
XH_19	0.31496	1.3887	0.25	1.87	20.51970722	9.69071285	123.0722994
XH_22	0.31496	1.3887	0.25	1.89	20.73916933	9.04436564	114.8636733
XH_23	0.31496	1.3887	0.25	1.88	20.62943828	26.5680581	337.4150127

number	XS(in)	area (in^2)	Thickness (in)	Weight (g)	density (lb/ft^2)	Force (lb)	stress (psi)
H_9	0.31496	1.3887	0.125	0.69	15.14288554	2.51309518	63.83274518
H_10	0.31496	1.3887	0.125	0.75	16.4596582	18.9700887	481.8412169
H_11	0.31496	1.3887	0.125	0.66	14.48449922	17.9305094	455.43585
H_12	0.31496	1.3887	0.125	0.66	14.48449922	17.9124297	454.976625
H_13	0.31496	1.3887	0.125	0.78	17.11804453	20.3215421	516.1682004
H_14	0.31496	1.3887	0.125	0.76	16.67912031	18.6943743	474.8380573
H_15	0.31496	1.3887	0.125	0.78	17.11804453	18.8570911	478.971071
H_16	0.31496	1.3887	0.125	0.76	16.67912031	17.39716	441.8887474
H_17	0.31496	1.3887	0.125	0.66	14.48449922	17.39716	441.8887474
H_18	0.31496	1.3887	0.125	0.66	14.48449922	18.057067	458.6504187
H_19	0.31496	1.3887	0.125	0.76	16.67912031	19.3859206	492.4033678
H_20	0.31496	1.3887	0.125	0.65	14.26503711	18.4864584	469.5569819
H_21	0.31496	1.3887	0.125	0.66	14.48449922	16.3937399	416.4018255
H_22	0.31496	1.3887	0.125	0.64	14.045575	17.9802284	456.698716
H_23	0.31496	1.3887	0.125	0.69	15.14288554	19.7836728	502.5062936
H_24	0.31496	1.3887	0.125	0.73	16.02073398	19.4446794	493.8958437
H_25	0.31496	1.3887	0.125	0.79	17.33750664	18.6265755	473.1159646
H_26	0.31496	1.3887	0.125	0.67	14.70396133	15.6072755	396.4255907
H_27	0.31496	1.3887	0.125	0.75	16.4596582	18.9203699	480.5783561
H_28	0.31496	1.3887	0.125	0.76	16.67912031	20.0367876	508.935424
H_29	0.31496	1.3887	0.125	0.67	14.70396133	17.9621488	456.2394926
H_30	0.31496	1.3887	0.125	0.74	16.24019609	18.2288235	463.0130422
H_31	0.31496	1.3887	0.125	0.66	14.48449922	19.0378874	483.5633079
H_32	0.31496	1.3887	0.125	0.78	17.11804453	17.2073238	437.0668987
H_33	0.31496	1.3887	0.125	0.72	15.80127187	18.7350535	475.8713099
H_34	0.31496	1.3887	0.125	0.78	17.11804453	17.6864342	449.2363262
H_35	0.31496	1.3887	0.125	0.69	15.14288554	19.7294337	501.1286184
H_37	0.31496	1.3887	0.125	0.69	15.14288554	21.5509576	547.3954177
H_38	0.31496	1.3887	0.125	0.7	15.36234765	20.8322919	529.1412722
H_40	0.31496	1.3887	0.125	0.69	15.14288554	19.6706749	499.6361425
H_41	0.31496	1.3887	0.125	0.7	15.36234765	20.167865	512.264795
H_44	0.31496	1.3887	0.125	0.8	17.55696875	21.279763	540.5070622
H_45	0.31496	1.3887	0.125	0.67	14.70396133	20.6062965	523.4009768
H_47	0.31496	1.3887	0.125	0.84	18.43481718	20.5836967	522.8269425
H_49	0.31496	1.3887	0.125	0.8	17.55696875	17.4559188	443.381225

number	XS(in)	area (in^2)	Thickness (in)	Weight (g)	density (lb/ft^2)	Force (lb)	stress (psi)
H_1	0.31496	1.3887	0.25	1.09	11.96068496	13.4196388	340.8595082
H_3	0.31496	1.3887	0.25	1.09	11.96068496	19.3271617	490.9108902
H_4	0.31496	1.3887	0.25	1.11	12.18014707	15.9010697	403.887977
H_5	0.31496	1.3887	0.25	1.1	12.07041601	18.6943743	474.8380556
H_6	0.31496	1.3887	0.25	1.1	12.07041601	16.5564567	420.5348408
H_7	0.31496	1.3887	0.25	1.11	12.18014707	18.8164118	477.9378167
H_8	0.31496	1.3887	0.25	1.26	13.82611289	16.9813282	431.3265999
H_9	0.31496	1.3887	0.25	1.34	14.70396133	22.9069307	581.8372036
H_10	0.31496	1.3887	0.25	1.11	12.18014707	17.0762465	433.7375277
H_11	0.31496	1.3887	0.25	1.2	13.16772656	19.4989182	495.2735138
H_12	0.31496	1.3887	0.25	1.35	14.81369238	23.7521538	603.3059142
H_13	0.31496	1.3887	0.25	1.1	12.07041601	18.0796664	459.2244461
H_14	0.31496	1.3887	0.25	1.52	16.67912031	22.4504199	570.2418053
H_15	0.31496	1.3887	0.25	1.23	13.49691972	18.2695028	464.0463
H_16	0.31496	1.3887	0.25	1.3	14.26503711	20.8006525	528.3376296
H_17	0.31496	1.3887	0.25	1.5	16.4596582	23.1284064	587.4626965
H_18	0.31496	1.3887	0.25	1.33	14.59423027	21.9758292	558.1871768
H_19	0.31496	1.3887	0.25	1.44	15.80127187	23.7114748	602.2726651
H_20	0.31496	1.3887	0.25	1.28	14.045575	15.7631189	400.3840202
H_22	0.31496	1.3887	0.25	1.33	14.59423027	23.1916851	589.06998
H_23	0.31496	1.3887	0.25	1.41	15.47207871	23.8696717	606.2908729
H_24	0.31496	1.3887	0.25	1.43	15.69154082	24.000749	609.6202439
H_25	0.31496	1.3887	0.25	1.44	15.80127187	25.7137952	653.1317048
H_26	0.31496	1.3887	0.25	1.24	13.60665078	18.3599009	466.342415
H_27	0.31496	1.3887	0.25	1.46	16.02073398	24.0911473	611.9163641
H_28	0.31496	1.3887	0.25	1.42	15.58180976	23.7702336	603.765141
H_29	0.31496	1.3887	0.25	1	10.97310547	15.0739261	382.878488
H_30	0.31496	1.3887	0.25	1.02	11.19256758	18.2695028	464.0462982
H_31	0.31496	1.3887	0.25	1	10.97310547	15.4219593	391.7185496
H_32	0.31496	1.3887	0.25	1.03	11.30229863	15.5349569	394.5886955
H_33	0.31496	1.3887	0.25	1.43	15.69154082	20.6017765	523.2861693
H_34	0.31496	1.3887	0.25	1.28	14.045575	20.2085443	513.298051
H_36	0.31496	1.3887	0.25	1.28	14.045575	22.3509818	567.7160734
H_37	0.31496	1.3887	0.25	1.13	12.39960918	19.9102302	505.7208588
H_38	0.31496	1.3887	0.25	1.07	11.74122285	17.5915162	446.8254053
H_39	0.31496	1.3887	0.25	1.18	12.94826445	22.0119885	559.1056269
H_40	0.31496	1.3887	0.25	1.06	11.6314918	15.4581184	392.6369928
H_41	0.31496	1.3887	0.25	1.17	12.8385334	21.3475617	542.2291515
H_42	0.31496	1.3887	0.25	1.1	12.07041601	17.7587529	451.0732247
H_43	0.31496	1.3887	0.25	1.2	13.16772656	19.8379115	503.8839602
H_44	0.31496	1.3887	0.25	1.09	11.96068496	17.3112816	439.707433
H_45	0.31496	1.3887	0.25	1.47	16.13046504	21.0854069	535.570406
H_46	0.31496	1.3887	0.25	1	10.97310547	15.7609524	400.3289926
H_47	0.31496	1.3887	0.25	1.15	12.61907129	18.9972083	482.5300554
H_48	0.31496	1.3887	0.25	1.45	15.91100293	24.1905853	614.442096
H_49	0.31496	1.3887	0.25	1.49	16.34992715	23.6436761	600.5505741

numbe	XS(in)	area (in²)	Thickness	Weight l	density (lb/ft)	Max F ()	Stress (p)
1	0.315	1.3887	0.125	0.48	10.53418125	8.9313679	226.8572
2	0.315	1.3887	0.125	0.47	10.31471914	8.7550914	222.37977
4	0.315	1.3887	0.125	0.49	10.75364336	9.0398457	229.61254
5	0.315	1.3887	0.125	0.48	10.53418125	9.3833589	238.33779
6	0.315	1.3887	0.125	0.49	10.75364336	9.1347638	232.02347
7	0.315	1.3887	0.125	0.49	10.75364336	9.5867549	243.50406
8	0.315	1.3887	0.125	0.5	10.97310547	8.5652551	217.55792
9	0.315	1.3887	0.125	0.49	10.75364336	9.8082305	249.12955
10	0.315	1.3887	0.125	0.49	10.75364336	9.6997527	246.37421
11	0.315	1.3887	0.125	0.49	10.75364336	9.3697992	237.99338
12	0.315	1.3887	0.125	0.49	10.75364336	9.6274342	244.53732
13	0.315	1.3887	0.125	0.47	10.31471914	9.4692372	240.51911
14	0.315	1.3887	0.125	0.48	10.53418125	8.2398216	209.29189
15	0.315	1.3887	0.125	0.48	10.53418125	8.1268238	206.42174
16	0.315	1.3887	0.125	0.48	10.53418125	9.0217661	229.15332
17	0.315	1.3887	0.125	0.5	10.97310547	9.080525	230.6458
18	0.315	1.3887	0.125	0.48	10.53418125	9.071485	230.41618
19	0.315	1.3887	0.125	0.51	11.19256758	9.5415557	242.356
20	0.315	1.3887	0.125	0.49	10.75364336	8.9630072	227.66084
21	0.315	1.3887	0.125	0.51	11.19256758	9.229682	234.43439
22	0.315	1.3887	0.125	0.52	11.41202969	9.0308059	229.38293
23	0.315	1.3887	0.125	0.54	11.8509539	8.3256999	211.4732
24	0.315	1.3887	0.125	0.49	10.75364336	9.3426797	237.30454
25	0.315	1.3887	0.125	0.48	10.53418125	8.7686512	222.72419
26	0.315	1.3887	0.125	0.49	10.75364336	9.7765911	248.32591
27	0.315	1.3887	0.125	0.52	11.41202969	9.6590735	245.34096
28	0.315	1.3887	0.125	0.48	10.53418125	8.9449276	227.20162
29	0.315	1.3887	0.125	0.47	10.31471914	9.3200802	236.73051
30	0.315	1.3887	0.125	0.47	10.31471914	9.4873167	240.97833
31	0.315	1.3887	0.125	0.49	10.75364336	9.6590734	245.34095
32	0.315	1.3887	0.125	0.48	10.53418125	9.4375977	239.71546
33	0.315	1.3887	0.125	0.47	10.31471914	9.3200802	236.73051
34	0.315	1.3887	0.125	0.49	10.75364336	9.9980666	253.9514
35	0.315	1.3887	0.125	0.48	10.53418125	9.0850449	230.7606
36	0.315	1.3887	0.125	0.47	10.31471914	9.9528675	252.80334
37	0.315	1.3887	0.125	0.47	10.31471914	9.930268	252.22931
38	0.315	1.3887	0.125	0.48	10.53418125	9.9573874	252.91815
39	0.315	1.3887	0.125	0.51	11.19256758	9.8805492	250.96645
40	0.315	1.3887	0.125	0.48	10.53418125	9.2070824	233.86036
41	0.315	1.3887	0.125	0.5	10.97310547	9.6409939	244.88173
42	0.315	1.3887	0.125	0.48	10.53418125	9.2161222	234.08997
43	0.315	1.3887	0.125	0.48	10.53418125	8.5697751	217.67272
44	0.315	1.3887	0.125	0.48	10.53418125	9.2839209	235.81206
45	0.315	1.3887	0.125	0.47	10.31471914	9.1438036	232.25308
46	0.315	1.3887	0.125	0.48	10.53418125	9.4195182	239.25624
47	0.315	1.3887	0.125	0.49	10.75364336	9.8398697	249.93319
48	0.315	1.3887	0.125	0.47	10.31471914	9.7946707	248.78513
49	0.315	1.3887	0.125	0.51	11.19256758	10.007107	254.18101
50	0.315	1.3887	0.125	0.48	10.53418125	8.4432175	214.45815

number	XS (in)	area (in^2)	Thickness (in)	Weight (g)	density (lb/ft^2)	Max F (lbs)	Stress (psi)
M_1	0.31496	1.3887	0.25	0.92	10.09525703	20.68	262.68
M_2	0.31496	1.3887	0.25	0.96	10.53418125	21.81	276.97
M_3	0.31496	1.3887	0.25	0.89	9.766063866	20.96	266.18
M_4	0.31496	1.3887	0.25	0.83	9.107677538	19.70	250.16
M_5	0.31496	1.3887	0.25	0.86	9.436870702	20.99	266.58
M_6	0.31496	1.3887	0.25	0.94	10.31471914	21.72	275.88
M_8	0.31496	1.3887	0.25	0.87	9.546601756	22.05	280.01
M_10	0.31496	1.3887	0.25	0.92	10.09525703	21.94	278.69
M_11	0.31496	1.3887	0.25	0.94	10.31471914	20.25	257.22
M_12	0.31496	1.3887	0.25	0.92	10.09525703	20.76	263.65
M_13	0.31496	1.3887	0.25	0.89	9.766063866	21.39	271.63
M_14	0.31496	1.3887	0.25	0.91	9.985525975	20.89	265.32
M_16	0.31496	1.3887	0.25	0.96	10.53418125	21.13	268.36
M_17	0.31496	1.3887	0.25	0.91	9.985525975	22.56	286.50
M_19	0.31496	1.3887	0.25	0.97	10.6439123	20.98	266.41
M_23	0.31496	1.3887	0.25	0.94	10.31471914	22.01	279.55
M_25	0.31496	1.3887	0.25	0.98	10.75364336	21.73	275.94
M_26	0.31496	1.3887	0.25	0.95	10.42445019	23.05	292.70
M_27	0.31496	1.3887	0.25	0.88	9.656332811	20.19	256.36
M_28	0.31496	1.3887	0.25	0.88	9.656332811	22.35	283.86
M_29	0.31496	1.3887	0.25	1	10.97310547	23.49	298.27
M_33	0.31496	1.3887	0.25	0.91	9.985525975	21.43	272.15
M_40	0.31496	1.3887	0.25	0.97	10.6439123	20.63	261.99
M_42	0.31496	1.3887	0.25	1	10.97310547	22.39	284.32
M_45	0.31496	1.3887	0.25	0.95	10.42445019	22.12	280.87
M_46	0.31496	1.3887	0.25	0.97	10.6439123	22.97	291.72
M_47	0.31496	1.3887	0.25	0.98	10.75364336	22.16	281.45
M_48	0.31496	1.3887	0.25	0.89	9.766063866	19.08	242.36

number	XS(in)	area (in^2)	Thickness (in)	Weight (g)	density (lb/ft^2)	Force (lb)	stress (psi)
L_1	0.31496	1.3887	0.125	0.3	6.58386328	6.3821384	162.1066408
L_2	0.31496	1.3887	0.125	0.3	6.58386328	6.2329814	158.318043
L_3	0.31496	1.3887	0.125	0.3	6.58386328	6.4408973	163.5991184
L_4	0.31496	1.3887	0.125	0.31	6.80332539	6.504176	165.2064002
L_5	0.31496	1.3887	0.125	0.3	6.58386328	6.80701	172.8983999
L_6	0.31496	1.3887	0.125	0.31	6.80332539	6.2420212	158.5476547
L_7	0.31496	1.3887	0.125	0.31	6.80332539	5.6227935	142.8192393
L_8	0.31496	1.3887	0.125	0.28	6.144939062	5.9256275	150.5112391
L_9	0.31496	1.3887	0.125	0.28	6.144939062	6.0115058	152.6925517
L_10	0.31496	1.3887	0.125	0.28	6.144939062	5.4871961	139.3750607
L_11	0.31496	1.3887	0.125	0.3	6.58386328	6.6668927	169.3394138
L_12	0.31496	1.3887	0.125	0.28	6.144939062	5.9617867	151.4296858
L_13	0.31496	1.3887	0.125	0.28	6.144939062	5.6996319	144.7709403
L_14	0.31496	1.3887	0.125	0.28	6.144939062	5.6408731	143.2784644
L_15	0.31496	1.3887	0.125	0.28	6.144939062	5.7945501	147.1818681
L_16	0.31496	1.3887	0.125	0.28	6.144939062	5.7357912	145.6893887
L_17	0.31496	1.3887	0.125	0.29	6.364401171	5.7448311	145.9190021
L_18	0.31496	1.3887	0.125	0.29	6.364401171	6.5086959	165.3212077
L_20	0.31496	1.3887	0.125	0.28	6.144939062	6.0793043	154.4146376
L_21	0.31496	1.3887	0.125	0.29	6.364401171	6.4499371	163.8287301
L_22	0.31496	1.3887	0.125	0.3	6.58386328	6.2103819	157.7440155
L_23	0.31496	1.3887	0.125	0.3	6.58386328	5.8216696	147.8707031
L_24	0.31496	1.3887	0.125	0.3	6.58386328	5.9798664	151.8889091
L_25	0.31496	1.3887	0.125	0.29	6.364401171	5.5233555	140.2935092
L_26	0.31496	1.3887	0.125	0.29	6.364401171	5.8668687	149.0187632
L_27	0.31496	1.3887	0.125	0.29	6.364401171	5.5866343	141.9007943
L_28	0.31496	1.3887	0.125	0.26	5.706014843	4.6012938	116.8730958
L_29	0.31496	1.3887	0.125	0.26	5.706014843	4.5108955	114.5769739
L_31	0.31496	1.3887	0.125	0.27	5.925476952	4.9493268	125.7131522
L_32	0.31496	1.3887	0.125	0.25	5.486552734	4.3798182	111.2476046
L_34	0.31496	1.3887	0.125	0.31	6.80332539	6.0386252	153.3813868
L_35	0.31496	1.3887	0.125	0.27	5.925476952	5.3335193	135.4716605
L_36	0.31496	1.3887	0.125	0.31	6.80332539	5.9798664	151.8889109
L_37	0.31496	1.3887	0.125	0.31	6.80332539	6.4815764	164.6323692
L_39	0.31496	1.3887	0.125	0.3	6.58386328	5.8352293	148.2151206
L_40	0.31496	1.3887	0.125	0.26	5.706014843	4.6193735	117.3323209
L_42	0.31496	1.3887	0.125	0.3	6.58386328	6.2872203	159.6957148
L_43	0.31496	1.3887	0.125	0.28	6.144939062	5.6318335	143.0488562

number	XS(in)	area (in^2)	Thickness (in)	Weight (g)	density (lb/ft^2)	Force (lb)	stress (psi)
L_18	0.31496	1.3887	0.25	0.82	8.997946483	16.8502508	427.9972254
L_19	0.31496	1.3887	0.25	0.8	8.778484374	16.7327331	425.0122719
L_20	0.31496	1.3887	0.25	0.81	8.888215428	17.2525229	438.2149571
L_23	0.31496	1.3887	0.25	0.78	8.559022264	17.3338812	440.2814639
L_24	0.31496	1.3887	0.25	0.79	8.668753319	15.2637623	387.7003384
L_26	0.31496	1.3887	0.25	0.8	8.778484374	17.7587529	451.0732247
L_30	0.31496	1.3887	0.25	0.8	8.778484374	16.9542088	430.6377649
L_33	0.31496	1.3887	0.25	0.77	8.44929121	16.0231072	406.9877381
L_34	0.31496	1.3887	0.25	0.8	8.778484374	16.791492	426.5047495
L_38	0.31496	1.3887	0.25	0.79	8.668753319	16.2265032	412.154006
L_41	0.31496	1.3887	0.25	0.74	8.120098046	14.9609283	380.0083386
L_42	0.31496	1.3887	0.25	0.78	8.559022264	16.7598526	425.7011087
L_43	0.31496	1.3887	0.25	0.78	8.559022264	16.0954258	408.8246333
L_45	0.31496	1.3887	0.25	0.77	8.44929121	14.7349327	374.2680398
L_46	0.31496	1.3887	0.25	0.78	8.559022264	15.4671582	392.8666045
L_47	0.31496	1.3887	0.25	0.77	8.44929121	14.2061033	360.8357447
L_49	0.31496	1.3887	0.25	0.81	8.888215428	15.4355189	392.0629637

number	XS (in)	area (in²)	Thickness	Weight	density (lb/ft)	Max F	stress (p)
XL_1	0.31496	1.3887	0.125	0.23	5.047628515	4.556095	115.72504
XL_2	0.31496	1.3887	0.125	0.22	4.828166406	4.913168	124.79471
XL_3	0.31496	1.3887	0.125	0.23	5.047628515	4.569654	116.06945
XL_4	0.31496	1.3887	0.125	0.21	4.608704296	5.103004	129.61655
XL_5	0.31496	1.3887	0.125	0.21	4.608704296	4.619373	117.33232
XL_6	0.31496	1.3887	0.125	0.23	5.047628515	4.420497	112.28086
XL_7	0.31496	1.3887	0.125	0.22	4.828166406	4.542535	115.38062
XL_8	0.31496	1.3887	0.125	0.24	5.267090624	4.646493	118.02115
XL_9	0.31496	1.3887	0.125	0.22	4.828166406	4.76853	121.12092
XL_10	0.31496	1.3887	0.125	0.22	4.828166406	4.78209	121.46533
XL_11	0.31496	1.3887	0.125	0.23	5.047628515	4.379818	111.2476
XL_12	0.31496	1.3887	0.125	0.23	5.047628515	2.174102	55.222299
XL_13	0.31496	1.3887	0.125	0.23	5.047628515	4.465696	113.42892
XL_14	0.31496	1.3887	0.125	0.23	5.047628515	4.343659	110.32916
XL_15	0.31496	1.3887	0.125	0.22	4.828166406	4.872488	123.76145
XL_16	0.31496	1.3887	0.125	0.27	5.925476952	4.976446	126.40199
XL_17	0.31496	1.3887	0.125	0.25	5.486552734	4.104104	104.24444
XL_18	0.31496	1.3887	0.125	0.26	5.706014843	4.899608	124.45029
XL_19	0.31496	1.3887	0.125	0.27	5.925476952	5.030685	127.77966
XL_20	0.31496	1.3887	0.125	0.24	5.267090624	4.80469	122.03936
XL_21	0.31496	1.3887	0.125	0.24	5.267090624	4.646493	118.02115
XL_22	0.31496	1.3887	0.125	0.25	5.486552734	4.77305	121.23572
XL_23	0.31496	1.3887	0.125	0.25	5.486552734	3.76555	95.645156
XL_24	0.31496	1.3887	0.125	0.25	5.486552734	4.434057	112.62527
XL_25	0.31496	1.3887	0.125	0.24	5.267090624	4.750451	120.66169
XL_26	0.31496	1.3887	0.125	0.27	5.925476952	4.940287	125.48354
XL_27	0.31496	1.3887	0.125	0.27	5.925476952	4.199022	106.65537
XL_28	0.31496	1.3887	0.125	0.26	5.706014843	4.447617	112.96969
XL_29	0.31496	1.3887	0.125	0.25	5.486552734	5.075884	128.92772
XL_31	0.31496	1.3887	0.125	0.3	6.58386328	5.116564	129.96097
XL_32	0.31496	1.3887	0.125	0.25	5.486552734	4.77305	121.23572
XL_33	0.31496	1.3887	0.125	0.25	5.486552734	4.470216	113.54372
XL_34	0.31496	1.3887	0.125	0.26	5.706014843	4.583214	116.41387
XL_36	0.31496	1.3887	0.125	0.25	5.486552734	4.438577	112.74008
XL_37	0.31496	1.3887	0.125	0.28	6.144939062	4.908648	124.6799
XL_38	0.31496	1.3887	0.125	0.27	5.925476952	4.429537	112.51047
XL_39	0.31496	1.3887	0.125	0.26	5.706014843	4.357219	110.67357
XL_40	0.31496	1.3887	0.125	0.25	5.486552734	4.863449	123.53184
XL_41	0.31496	1.3887	0.125	0.25	5.486552734	4.379818	111.2476
XL_42	0.31496	1.3887	0.125	0.27	5.925476952	4.651013	118.13596
XL_43	0.31496	1.3887	0.125	0.25	5.486552734	4.447617	112.96969
XL_44	0.31496	1.3887	0.125	0.27	5.925476952	4.583214	116.41387
XL_45	0.31496	1.3887	0.125	0.25	5.486552734	4.583214	116.41387
XL_46	0.31496	1.3887	0.125	0.25	5.486552734	4.406938	111.93644
XL_47	0.31496	1.3887	0.125	0.26	5.706014843	4.30298	109.2959
XL_48	0.31496	1.3887	0.125	0.26	5.706014843	4.596774	116.75829
XL_49	0.31496	1.3887	0.125	0.27	5.925476952	5.29284	134.4384

number	XS (in)	area (in^2)	Thickness (in)	Weight (g)	density (lb/ft^2)	Force lb	Stress (psi)
XL_1	0.31496	1.3887	0.25	0.45	4.93789746	11.76083	149.3628621
XL_2	0.31496	1.3887	0.25	0.46	5.047628515	12.04559	152.9792503
XL_3	0.31496	1.3887	0.25	0.47	5.15735957	11.65687	148.0425924
XL_4	0.31496	1.3887	0.25	0.47	5.15735957	12.51114	158.8917553
XL_6	0.31496	1.3887	0.25	0.5	5.486552734	13.93943	177.0310967
XL_9	0.31496	1.3887	0.25	0.46	5.047628515	11.08737	140.8098186
XL_11	0.31496	1.3887	0.25	0.46	5.047628515	11.81959	150.1091009
XL_12	0.31496	1.3887	0.25	0.45	4.93789746	10.58566	134.4380877
XL_13	0.31496	1.3887	0.25	0.46	5.047628515	10.68961	135.7583565
XL_14	0.31496	1.3887	0.25	0.44	4.828166406	10.78905	137.0212233
XL_15	0.31496	1.3887	0.25	0.46	5.047628515	12.00491	152.4626223
XL_16	0.31496	1.3887	0.25	0.46	5.047628515	11.87835	150.8553397
XL_17	0.31496	1.3887	0.25	0.4	4.389242187	10.36418	131.625342
XL_18	0.31496	1.3887	0.25	0.45	4.93789746	10.49526	133.2900284
XL_19	0.31496	1.3887	0.25	0.46	5.047628515	11.23652	142.7041166
XL_20	0.31496	1.3887	0.25	0.46	5.047628515	11.61619	147.5259661
XL_21	0.31496	1.3887	0.25	0.46	5.047628515	10.88849	138.2840867
XL_22	0.31496	1.3887	0.25	0.46	5.047628515	11.07833	140.6950127
XL_23	0.31496	1.3887	0.25	0.45	4.93789746	9.763031	123.9907469
XL_24	0.31496	1.3887	0.25	0.46	5.047628515	11.12352	141.2690428
XL_25	0.31496	1.3887	0.25	0.42	4.608704296	10.31898	131.051312
XL_26	0.31496	1.3887	0.25	0.48	5.267090624	11.73823	149.0758475
XL_27	0.31496	1.3887	0.25	0.45	4.93789746	15.431	195.9740789
XL_28	0.31496	1.3887	0.25	0.46	5.047628515	8.768651	111.3620918
XL_29	0.31496	1.3887	0.25	0.47	5.15735957	11.90999	151.2571602
XL_30	0.31496	1.3887	0.25	0.47	5.15735957	12.93149	164.2302337
XL_31	0.31496	1.3887	0.25	0.45	4.93789746	11.75631	149.3054592
XL_32	0.31496	1.3887	0.25	0.44	4.828166406	11.04217	140.2357902
XL_33	0.31496	1.3887	0.25	0.45	4.93789746	12.31678	156.4234289
XL_34	0.31496	1.3887	0.25	0.44	4.828166406	10.37774	131.7975525
XL_35	0.31496	1.3887	0.25	0.46	5.047628515	13.63659	173.1850976
XL_38	0.31496	1.3887	0.25	0.46	5.047628515	11.65235	147.9851903
XL_39	0.31496	1.3887	0.25	0.42	4.608704296	10.70769	135.9879691
XL_40	0.31496	1.3887	0.25	0.41	4.498973242	10.98793	139.5469518
XL_41	0.31496	1.3887	0.25	0.45	4.93789746	11.33596	143.9669826
XL_42	0.31496	1.3887	0.25	0.47	5.15735957	12.71453	161.4748901
XL_44	0.31496	1.3887	0.25	0.45	4.93789746	11.2772	143.2207429
XL_45	0.31496	1.3887	0.25	0.47	5.15735957	12.4343	157.9159048
XL_46	0.31496	1.3887	0.25	0.43	4.718435351	10.3461	131.3957304
XL_47	0.31496	1.3887	0.25	0.48	5.267090624	12.40718	157.5714873
XL_48	0.31496	1.3887	0.25	0.45	4.93789746	10.97437	139.3747447
XL_49	0.31496	1.3887	0.25	0.39	4.279511132	11.62975	147.6981766

The test set 2 samples out of the gage area.

0.25"	
Fail Outside of Gage Area	
Density	Number
XL	5
	7
	8
	10
	36
	37
	43
L	1
	2
	3
	5
	6
	7
	8
	9
	11
	12
	13
	14
	15
	16
	17
	21
	22
	25
	27
	28
	29
	33
	34
	35
	36
	37
	39
	40
	44
	48

0.125"	
Fail Outside of Gage Area	
Density	Number
XL	12
	23
	35
L	19
	38
	41
	44
	45
M	3
H	1
	2
	3
	4
	5
	6
	7
	8
	42
	43
	46
	48
XH	3
	6
	9
	10
	13
	18
	22
	29
	30
	39
	43

M	7
	9
	15
	18
	20
	21
	22
	24
	30
	31
	32
	41
	43
	44
	43
	44
	49
	50
H	2
	21
	35
XH	4
	6
	8
	9
	20
	21
	24

Test Set #3

number	XS (in)	area (in^2)	Thickness (in)	Weight (g)	density (lb/ft^2)	Force lb	Stress (psi)
XL_1	0.5	8.437	0.125	1.58	5.707383067	98.37587404	1574.013985
XL_2	0.5	8.437	0.125	1.51	5.454524324	54.86269712	877.8031539
XL_3	0.5	8.437	0.125	1.25	4.515334705	35.98755138	575.8008221
M_1	0.5	8.437	0.125	3.67	13.25702269	252.6358951	4042.174322
M_2	0.5	8.437	0.125	3.22	11.6315022	229.2950781	3668.721249
M_3	0.5	8.437	0.125	2.8	10.11434974	119.8092892	1916.948627
XH_1	0.5	8.437	0.125	5.55	20.04808609	252.3466211	4037.545938
XH_2	0.5	8.437	0.125	5.71	20.62604893	252.7579326	4044.126921
XH_3	0.5	8.437	0.125	5	18.06133882	161.1574294	2578.51887

Average UTS at Each Density		
Thickness	Density	Avg. UTS (PSI)
0.125"	XL	111
	L	134
	M	231
	H	407
	XH	378
0.25"	XL	147
	L	356
	M	253
	H	473
	XH	340

Uncertainty

$w := 0.315 \text{in} \qquad t := .25 \text{in} \qquad F := 23.491 \text{lbf} \qquad$ Variables

$A1(w,t) := w \cdot t \qquad$ Cross sectional area

$\sigma(F,A1) := \dfrac{F}{A1} \qquad$ Ultimate tensile strength

$U_F := \dfrac{.225}{2} \text{lbf}$

$U_w := 0.012 \text{in} \qquad$ <mark>Uncertainties of measured variables</mark>

$U_t := 0.007 \text{in}$

$a_1 := A1(w,t) = 0.079 \cdot \text{in}^2$

$U_A := \sqrt{\left[\dfrac{d}{dw}\left[(A1(w,t)) \cdot U_w\right]\right]^2 + \left[\dfrac{d}{dt}\left[(A1(w,t)) \cdot U_t\right]\right]^2} = 3.723 \times 10^{-3} \cdot \text{in}^2$

$U_\sigma := \sqrt{\left[\dfrac{d}{dF}\left[(\sigma(F,a_1)) \cdot U_F\right]\right]^2 + \left[\dfrac{d}{da_1}\left[(\sigma(F,a_1)) \cdot U_A\right]\right]^2} = 14.175 \cdot \text{psi}$

$a := 1.39 \text{in}^2 \quad W := 1.45 \text{gm}$

$Vol(a,t) := a \cdot t$

$\rho(W, Vol) := \dfrac{W}{Vol}$

$U_W := \dfrac{0.01}{2} \text{gm}$

$U_a := 0.0039 \text{in}^2$

$volume := Vol(a,t) = 0.347 \cdot \text{in}^3$

$$U_{Vol} := \sqrt{\left[\frac{d}{da}\left[(Vol(a,t)) \cdot U_a\right]\right]^2 + \left[\frac{d}{dt}\left[(Vol(a,t)) \cdot U_t\right]\right]^2} = 9.779 \times 10^{-3} \cdot \text{in}^3$$

$$U_\rho := \sqrt{\left[\frac{d}{dW}\left[(\rho(W, volume)) \cdot U_W\right]\right]^2 + \left[\frac{d}{dvolume}\left[(\rho(W, volume)) \cdot U_{Vol}\right]\right]^2} = 0.451 \cdot \frac{\text{lb}}{\text{ft}^3}$$

VITA

Taylor Michelle Matlock

Candidate for the Degree of

Master of Science

Thesis: EXPERIMENTAL INVESTIGATION INTO MICROSTRUCTURES OF AIRCRAFT GRADE BALSA SHEAR WEBS

Major Field: Mechanical and Aerospace Engineering

Biographical:

Education:

Completed the requirements for the Master of Science in Mechanical and Aerospace Engineering Oklahoma State University, Stillwater, Oklahoma in May 2023.

Completed the requirements for the Bachelor of Science Mechanical Engineering at Oklahoma State University, Stillwater, Oklahoma in 2020.

Completed the requirements for the Bachelor of Science Aerospace Engineering at Oklahoma State University, Stillwater, Oklahoma in 2020.

Experience:

Professional Memberships: